

**GROUNDWATER RESOURCES
OF ATOLL ISLANDS:
OBSERVATIONS, MODELING,
AND MANAGEMENT**

by

**Ryan T. Bailey
John W. Jenson
Donald Rubinstein
Arne E. Olsen**

WERI

**WATER AND ENVIRONMENTAL RESEARCH INSTITUTE
OF THE WESTERN PACIFIC
UNIVERSITY OF GUAM**

**Technical Report No. 119
April 2008**

Groundwater Resources of Atoll Islands: Observations, Modeling, and Management

by

Ryan T. Bailey¹
John W. Jenson¹
Donald Rubinstein²
Arne E. Olsen¹

¹Water and Environmental Research Institute of the Western Pacific
University of Guam, UOG Station, Mangilao, Guam 96923

²Micronesian Area Research Center
University of Guam, UOG Station, Mangilao, Guam 96923

Technical Report No. 119
April 2008

The work reported herein was funded by the Department of Interior via the Water Resources Research Institute Program of the U.S. Geological Survey (Award No. 01HQPA0010), administered through the Water and Environmental Research Institute of the Western Pacific at the University of Guam. The content of this report does not necessarily reflect the views and policies of the Department of the Interior, nor does the mention of trade names or commercial products constitute their endorsement by the United States Government.

ABSTRACT

Atolls are composed of ring-shaped coral reefs and islands, enclosing or nearly enclosing a shallow lagoon. The small size, low elevation, unique geology, and isolation of atoll islands make island inhabitants vulnerable to water shortage during times of prolonged drought or the aftermath of damaging tropical storms. Under normal conditions freshwater demand is met by rooftop rain catchments, although under drought conditions the demand is supplemented by groundwater from hand-dug wells. However, the location, quality and quantity of the groundwater from the freshwater lens are not known in advance for most atoll islands, thus making effective long-term water resources planning difficult. In this study, a modified version of the USGS numerical model SUTRA was used to analyze the dimensions of the freshwater lens on atoll islands under varying geologic and climatic conditions.

Results from steady-state simulations show that the depth to the discontinuity between the upper and lower aquifer, presence of the reef flat plate, island width, recharge rate, and hydraulic conductivity of the upper aquifer all govern the thickness and volume of the lens. The discontinuity between the upper and lower aquifers acts as a limiting feature of the growth of the lens, while the reef flat plate acts as a confining layer, extending the lens under the plate on the ocean side of the island. An increase in island width and recharge increases the thickness of the lens to the depth of the discontinuity. The position of the island in reference to the prevailing winds has a large influence, as comparisons between numerical simulation results and observed lens thicknesses demonstrate that the hydraulic conductivity of the upper aquifer is 50 m day^{-1} and 400 m day^{-1} for islands located on the leeward and windward portions of the atoll, respectively.

Results from all simulations enabled the development of an algebraic model that predicts the depth of the freshwater lens for atoll islands as a function of recharge, island width, hydraulic conductivity of the upper aquifer, depth to the discontinuity, the existence of the reef flat plate, and time. The algebraic model may be valuable prediction tool for water resources managers of atoll islands.

TABLE OF CONTENTS

| | |
|---|------------|
| ABSTRACT | I |
| TABLE OF CONTENTS..... | II |
| LIST OF FIGURES | III |
| LIST OF TABLES | V |
| ACKNOWLEDGEMENTS..... | VI |
| INTRODUCTION..... | 1 |
| ATOLLS AND FRESHWATER | 1 |
| PROBLEM STATEMENT | 2 |
| OBJECTIVES AND METHODS | 4 |
| ATOLL ISLAND HYDROGEOLOGY..... | 5 |
| REVIEW OF HYDROGEOLOGY STUDIES | 5 |
| FACTORS INFLUENCING THE THICKNESS OF THE FRESHWATER LENS..... | 9 |
| STEADY-STATE SIMULATIONS | 17 |
| NUMERICAL MODEL..... | 17 |
| SIMULATIONS AND RESULTS | 20 |
| SENSITIVITY ANALYSIS | 32 |
| TRANSIENT SIMULATIONS | 33 |
| TRANSIENT CONDITIONS | 33 |
| TIME-VARIABLE BOUNDARY CONDITIONS..... | 33 |
| INFLUENCE OF THE REEF FLAT PLATE ON SIMULATION RESULTS | 35 |
| SIMULATIONS AND RESULTS | 36 |
| APPLICATIONS..... | 42 |
| ALGEBRAIC MODEL FOR STEADY-STATE CONDITIONS | 42 |
| ALGEBRAIC MODEL FOR TRANSIENT CONDITIONS..... | 55 |
| PRACTICAL APPLICATIONS..... | 59 |
| CONCLUSIONS AND RECOMMENDATIONS | 62 |
| INSIGHTS INTO ATOLL ISLAND HYDROGEOLOGY | 62 |
| ALGEBRAIC MODEL | 62 |
| CAUTIONS | 62 |
| FUTURE STUDIES..... | 63 |
| REFERENCES | 64 |
| APPENDICES | 69 |
| APPENDIX A | 70 |
| APPENDIX B..... | 76 |
| APPENDIX C..... | 78 |

LIST OF FIGURES

| | |
|--|----|
| Figure 1. Map of (A) Pingelap Atoll, Pohnpei State, FSM, and (B) Ulithi Atoll, Yap State, FSM..... | 1 |
| Figure 2. Roof catchments on Falalop Island, Ulithi Atoll, Yap State, FSM | 2 |
| Figure 3. Hand-dug wells on Ulithi (A and B) and Pingelap (C and D)..... | 3 |
| Figure 4. Conceptual model of atoll island hydrogeology, after Ayers and Vacher (1986)..... | 5 |
| Figure 5. Recharge Model (after Falkland 1994). | 8 |
| Figure 6. Direction of prevailing winds on Pingelap Atoll, Pohnpei State, Federated States of Micronesia 11 | |
| Figure 7. Observed maximum depths of the freshwater lens of atoll islands | 12 |
| Figure 9. Variation in surface deposits between leeward (A and C) and windward (B and D) sides..... | 14 |
| Figure 10. Well on Mogmog Island, Ulithi Atoll showing reef flat plate | 15 |
| Figure 11. Monthly Rainfall values for the island of Pohnpei, Federated States of Micronesia | 16 |
| Figure 12. Finite element mesh of atoll cross-section, with accompanying boundary conditions | 17 |
| Figure 13. Enlarged view of atoll island subsurface..... | 18 |
| Figure 14. Climatic and geologic factors studied using the numerical model..... | 20 |
| Figure 15. Typical freshwater lens delineation | 21 |
| Figure 16. View groundwater velocity vectors..... | 21 |
| Figure 17. Lens geometry for a 600-m island for differing recharges rates | 22 |
| Figure 18. Results from the rainfall experiment..... | 23 |
| Figure 19. Relationship between depth of lens and island width for single and dual aquifer system | 23 |
| Figure 20. Lens geometry for differing hydraulic conductivity values | 24 |
| Figure 21. Relationship between the hydraulic conductivity of the Holocene sediments and the maximum depth of the freshwater lens | 24 |
| Figure 22. Results from the Holocene hydraulic conductivity experiment | 25 |
| Figure 23. Observed depths compared to depths found from the hydraulic conductivity study..... | 26 |
| Figure 24. Lens geometries for differing Thurber Discontinuity depths | 27 |
| Figure 25. Results from the Thurber Discontinuity depth..... | 27 |
| Figure 26. Simulation results for the reef flat plate experiment | 28 |
| Figure 27. The freshwater lens configuration when a reef flat plate is present | 29 |
| Figure 28. The direction and magnitude of the groundwater flow with a reef flat plate | 29 |

| | |
|--|----|
| Figure 29. Effect of extension of reef flat plate on the freshwater lens..... | 30 |
| Figure 30. The thickness of the lens as the reef flat plate hydraulic conductivity is varied | 31 |
| Figure 31. Sensitivity analysis of the parameters analyzed in the steady-state simulations | 32 |
| Figure 32. Daily recharge for Yap, 2000..... | 35 |
| Figure 33. Effect on freshwater lens of including the reef flat plate in transient simulations | 35 |
| Figure 34. Thickness of the lens as it responds to regular seasonal rainfall variation | 37 |
| Figure 35. Comparison of lens behavior between leeward islands located in the Western Caroline region (Yap) and the Eastern Caroline region (Pohnpei). | 37 |
| Figure 36. Monthly rainfall during the El Niño event of 1997-1999 in the Western Caroline region..... | 38 |
| Figure 37. Thickness of the lens as it responds to an El Niño even | 39 |
| Figure 38. Comparison of lens thickness during the 1997-1998 El Niño event between Western Caroline islands (using Yap data) and Eastern Caroline islands (using Pohnpei data)..... | 39 |
| Figure 39. Comparison of the lens depth through time for average seasonal weather patterns and an El Niño event..... | 40 |
| Figure 40. Contamination and recovery of the freshwater lens from a washover event..... | 41 |
| Figure 41. Recovery of the freshwater lens after a two-day washover event | 41 |
| Figure 42. Relationship between the recharge rate and the corresponding maximum depth of the lens | 43 |
| Figure 43 Hyperbolic fit to recharge/maximum lens depth relationship | 44 |
| Figure 44 Graphical definition of terms in hyperbolic equation. | 44 |
| Figure 45. Curve-fitting to produce trends of (A) B parameter and (B) Y parameter | 46 |
| Figure 46. Curves for B and Y parameters of the Algebraic Model..... | 46 |
| Figure 47. (A) Trend between the hydraulic conductivity of the Holocene sediments and the associated hydraulic conductivity factor, for an island width of 500 m, and (B) for each island width..... | 48 |
| Figure 48. Relationship between the width of the island and the hydraulic conductivity factor | 48 |
| Figure 49. Relationship between the width of the island and the reef flat plate factor..... | 49 |
| Figure 50. Comparison between the sensitivity of the parameters in the algebraic and numerical models.. | 50 |
| Figure 51. Comparison of SUTRA simulation results with the algebraic model results..... | 51 |
| Figure 52. Comparison between observed lens maximum depths and results from the algebraic model..... | 52 |
| Figure 53. Comparison of observed lens depths on atoll islands, results from the algebraic model, and results from published analytical and empirical models | 54 |

| | |
|---|----|
| Figure 54. Fluctuation of the lens during an El Niño event for a 400-m island within the Yap region..... | 58 |
| Figure 55. Freshwater Lens Tool for Water Resource Managers..... | 60 |
| Figure 56. Comparison of recharge rates curves to the observed lens depths for leeward and windward islands. | 61 |

LIST OF TABLES

| | |
|---|----|
| Table 1. Water Resources Survey of Households, Falalop, Ulithi Atoll (taken August 2006)..... | 2 |
| Table 2. Observed maximum lens thickness of atoll islands across Pacific and Indian Oceans | 6 |
| Table 3. Characteristics included in numerical modeling studies of atoll islands | 7 |
| Table 4. Mesh Attributes | 18 |
| Table 5. Model Input Parameters | 19 |
| Table 6. Geological and Climatic Parameters for each baseline simulation series..... | 20 |
| Table 7. Maximum thickness of Freshwater Lens for various island widths and recharge rates..... | 22 |
| Table 8. Influence of Reef Plate on Lens Thickness, for varying island widths | 28 |
| Table 9. Approximate cross-sectional area of the freshwater lens | 29 |
| Table 10. Extension of the reef flat plate under island | 30 |
| Table 11. Parameter Values for Daily Recharge Model (after Falkland 1994) | 33 |
| Table 12. Daily recharge calculations for May 2000 | 34 |
| Table 13. Summary of transient simulations | 36 |
| Table 14. Hydraulic head at the middle of the island and the associated discharge velocity | 43 |
| Table 15. Hydraulic Conductivity of Holocene Deposits and associated Depth to the Freshwater/Seawater Interface (Island Width = 500 m)..... | 47 |
| Table 16. Results of simulations, showing the maximum depth of the lens for conditions with and without a reef flat plate | 49 |
| Table 17. Values of the terms used in the algebraic model, for both leeward and windward islands. | 51 |
| Table 18. Monthly outputs for a 400-m leeward island within the West Caroline region..... | 56 |
| Table 19. Monthly lens thickness during an El Niño event for a 400-m leeward island..... | 57 |

ACKNOWLEDGEMENTS

We wish to thank Stephen Anthony, U.S. Geological Survey, for generously providing data on Ulithi Atoll, and Stephen Gingerich, U.S. Geological Survey, for advice on modeling techniques. Recognition is also extended to Chip Guard of the National Weather Service, Guam, for monthly average rainfall values. Finally, we are deeply grateful to the people from Ulithi and Pingelap Atolls, especially John Rulmal, Iganathio Hapithey, chairman of Council of Tamol, Mario Sukulbech, Chief Yaach, the chief of Fasseraï island, and Peter of Ulithi Atoll, and Jack Yakana, Lt. Governor of Pohnpei State, Semensin K. James, Anthon Edward, and Ellis Ernest of Pingelap Atoll for helping with travel logistics, accommodations, and field assistance.

INTRODUCTION

Atolls and Freshwater

Atolls have been a subject of scientific interest ever since the voyages of Captain James Cook during the late eighteenth century and the observations of Charles Darwin during the mid-nineteenth century (Vacher, 1997). Bryan (1953) lists 425 atolls throughout the oceans of the world, of which 285 are located in the Pacific Basin (Falkland, 1991, p. 2). These unique geologic features are commonly composed of a ring of closely spaced, small, coral islands, enclosing or nearly enclosing a shallow lagoon (Figure 1).

Typical maximum elevations of atoll islands range from two to three meters (Wheatcraft and Buddemeier, 1981). They vary in size from 100 to 1500 m in width and up to several thousand meters in length. The lagoon can range from a few to over 1000 square kilometers surface area, and from a few meters to about 100 meters in depth (Purdy and Winterer, 2001). The subsurface geology of atoll islands is unique, consisting of a surficial aquifer of Holocene age resting upon a highly permeable Pleistocene limestone aquifer. This dual-aquifer complex rests upon a submerged volcanic base that descends to the ocean floor (Emery et al., 1954). A shallow freshwater lens resides in the Holocene sediments, and is separated from the underlying seawater by a zone of mixing.

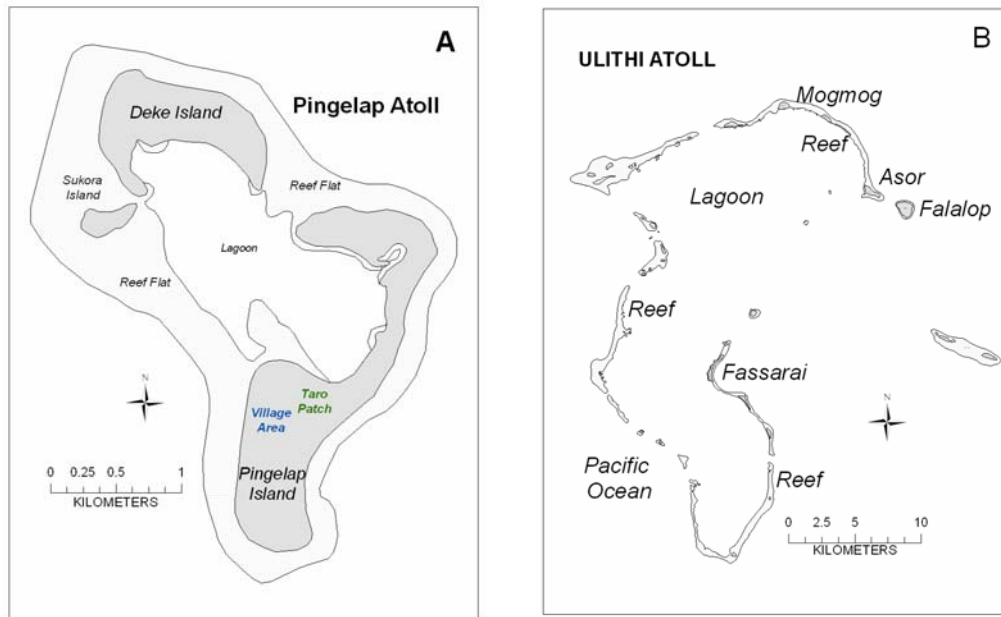


Figure 1. Map of (A) Pingelap Atoll, Pohnpei State, FSM, and (B) Ulithi Atoll, Yap State, FSM, showing quasi-circular string of small coral islands surrounding a lagoon. The difference in size of the two atolls demonstrates the wide variety of atoll configurations. The reef flat is a major component of the atoll system, as seen on Pingelap Atoll. (GIS data from Danko Tabarosi).

Problem Statement

The management of the freshwater resources is critical to the inhabitability of atoll islands. Under normal conditions, water for drinking and cooking is supplied from roof catchments (Figure 2), while water for bathing and washing clothes is supplied from hand-dug wells (Figure 3) (Table 1).

Table 1. Water Resources Survey of Households, Falalop, Ulithi Atoll (taken August 2006)

| House | Number of people | Drinking | Cooking | Wash dishes | Wash clothes | Bathing |
|-------|------------------|-----------|-----------|-------------|--------------|------------|
| 1 | 3 | rainwater | rainwater | well | well | well |
| 2 | 4 families | rainwater | rainwater | well | well | well |
| 3 | N/A | rainwater | rainwater | well | well | well |
| 4 | 11 | rainwater | rainwater | Govt. well | Govt. well | Govt. well |
| 5 | 5 | rainwater | rainwater | well | well | well |
| 6 | N/A | rainwater | rainwater | Govt. well | Govt. well | Govt. well |
| 7 | 7 | rainwater | rainwater | Govt. well | Govt. well | Govt. well |
| 8 | 9 | rainwater | rainwater | Govt. well | Govt. well | Govt. well |
| 9 | 11 | rainwater | rainwater | Govt. well | Govt. well | Govt. well |
| 10 | 12 | rainwater | rainwater | Govt. well | Govt. well | Govt. well |

However, during times of water stress, such as periods of prolonged drought or recovery from damaging storms, groundwater may be the sole source of water. As such, knowledge of the quantity and quality of groundwater is essential for effective water management and emergency preparedness. Information regarding groundwater, however, is not readily available for the vast majority of atoll islands around the world. The variation of the geology across atolls complicates groundwater management. Although atoll islands exhibit unifying geologic features, the combination and extent of these features make each island unique. Atolls also span geographic zones of differing rainfall and drought patterns. These differences combine to create unique groundwater conditions for each atoll island.



Figure 2. Roof catchments on Falalop Island, Ulithi Atoll, Yap State, FSM. Most households have their own catchment tank. The water from the tanks is used for drinking, cooking, and washing dishes. The tanks vary in construction material and size. Older tanks (a) are made from concrete, while newer ones (b) are made from fiber glass.



A



B



C



D

Figure 3. Hand-dug wells on Ulithi (A and B) and Pingelap (C and D). The depth to water in the wells ranges from 2 to 3 m, and also fluctuates with the rise and fall of the tides. The water within the wells is used mainly for bathing and washing clothes, and is extracted by either a rope and bucket or a small electric pump. Normally a well is shared by several households. Most wells are lined with concrete or rocks.

Objectives and Methods

The objective of this report is to investigate the impact of certain climatic and geologic factors on the freshwater lens, and, using the results, develop an algebraic model which can be used to estimate the thickness of the freshwater lens on atoll islands. This was accomplished through:

- Quantification of the influence of geologic and climatic factors on the thickness and volume of the freshwater lens.
- Quantification of the fluctuation of the thickness of the lens through regular seasonal rainfall variation as well as drought conditions.
- Creation of an algebraic model which enables water resources managers to more confidently predict the thickness of the lens during times of both average and extreme climatic conditions.

ATOLL ISLAND HYDROGEOLOGY

The geology of atoll islands is unique, consisting of a surficial, Holocene aquifer resting upon a Pleistocene aquifer. For hydrologic purposes this pattern has been termed as the dual-aquifer conceptual model of atoll island hydrogeology (Ayers and Vacher, 1986) (Figure 4).

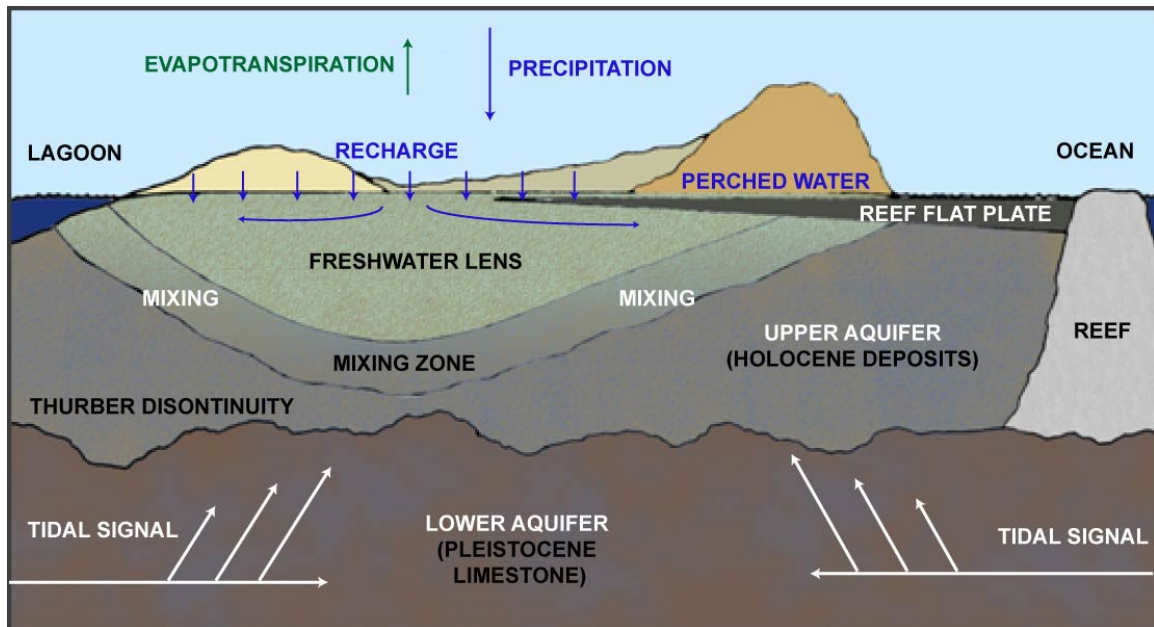


Figure 4. Conceptual model of atoll island hydrogeology, after Ayers and Vacher (1986)

Review of Hydrogeology Studies

This model was based upon the observation that tidal signals propagated vertically from more permeable Pleistocene limestone into the overlying, low-permeable Holocene deposits (Buddemeier and Holladay 1977; Vacher 1997), wherein the freshwater lens resides (Table 2). The hydraulic conductivity of the Holocene aquifer depends on the position of the island in reference to the prevailing winds (Anthony 1997; Spennemann 2006) and has been estimated to be one to two orders of magnitude less than that of the Pleistocene aquifer (Hunt and Peterson, 1980; Oberdorfer and Buddemeier, 1983; Woodroffe and Falkland, 1997). The higher hydraulic conductivity of the Pleistocene aquifer truncates the freshwater lens at or near the upper bound of the Pleistocene aquifer. This truncation is especially prevalent for leeward islands, which tend to be larger and have less-permeable Holocene deposits. The boundary between the aquifers has been termed the “Thurber Discontinuity” (Vacher 1997), a solution discontinuity (Thurber et al., 1965) located approximately 15-25 m below sea level (Wheatcraft and Buddemeier, 1981; Hamlin and Anthony, 1987). A complicating factor to the dual aquifer conceptual model is the reef flat plate, a semi-permeable slab of reef rock which acts as a confining layer to the Holocene aquifer, forcing freshwater to discharge from fractures in the plate or at the reef (Cox, 1951; Buddemeier and Holladay, 1977; Ayers and Vacher, 1986).

Table 2. Observed maximum lens thickness of atoll islands across Pacific and Indian Oceans

| Island / Location | Atoll | Region | Source | Location on Atoll | Width m | Max Thickness m |
|-------------------|--------------|----------|--------------------------------------|-------------------|---------|-----------------|
| Cantonment | Diego Garcia | CI | <i>PRC Toups, 1983</i> | Leeward | 2200 | 20 |
| AO NW | Diego Garcia | CI | <i>PRC Toups, 1983</i> | Leeward | 1150 | 15 |
| AO SE | Diego Garcia | CI | <i>PRC Toups, 1983</i> | Leeward | 1300 | 20 |
| Home Island | Cocos | EI | <i>Falkland, 1994</i> | Offset | 775 | 8 |
| WI Northern | Cocos | EI | <i>Falkland, 1994</i> | Leeward | 800 | 14 |
| WI 1 | Cocos | EI | <i>Falkland, 1994</i> | Leeward | 800 | 15 |
| WI 6 | Cocos | EI | <i>Falkland, 1994</i> | Leeward | 500 | 15 |
| WI 8 | Cocos | EI | <i>Falkland, 1994</i> | Leeward | 400 | 12 |
| WI 22 | Cocos | EI | <i>Falkland, 1994</i> | Leeward | 270 | 7 |
| South Island | Cocos | EI | <i>Falkland, 1994</i> | Windward | 1000 | 11 |
| Falalop | Ulithi | FSM | <i>Anthony, 1997</i> | Offset | 950 | 5 |
| Khalap | Mwoakilloa | FSM | <i>Anthony, 1996a</i> | Windward | 425 | 6 |
| Ngatik | Sapwuahfik | FSM | <i>Anthony, 1996b</i> | Leeward | 900 | 20 |
| Deke | Pingelap | FSM | <i>Ayes and Vacher, 1986</i> | Windward | 400 | 4 |
| Pingelap | Pingelap | FSM | <i>Anthony, 1996c</i> | Leeward | 750 | 16 |
| Laura | Majuro | MI | <i>Hamlin and Anthony, 1987</i> | Leeward | 1200 | 14 to 22 |
| Kwajelein | Kwajelein | MI | <i>Hunt and Peterson, 1980</i> | Offset | 600 | 10 to 18 |
| Roi-Namur | Kwajelein | MI | <i>Gingerich, 1992</i> | Windward | 750 | 5 to 7 |
| Eneu | Bikini | MI | <i>Peterson, 1997</i> | Offset | 400 | 5 to 10 |
| Bikini | Bikini | MI | <i>Peterson, 1997</i> | Windward | 600 | < 2 |
| Enjebi | Enewetak | MI | <i>Buddemeier and Holladay, 1977</i> | Windward | 1000 | < 2 |
| Matabou | Nonouti | GI | <i>Falkland, 2003</i> | Offset | 375 | 5 |
| Buariki | Tarawa | GI | <i>Jacobson and Taylor, 1981</i> | Offset | 1200 | 29 |
| Buota | Tarawa | GI | <i>Lloyd et al, 1980</i> | Offset | 650 | 23 |
| Bonriki | Tarawa | GI | <i>Falkland, 1992</i> | Windward | 1200 | 23 |
| NZ 4 | Christmas | Kiribati | <i>Falkland, 1983</i> | Leeward | 1500 | 14 |
| NZ 2 | Christmas | Kiribati | <i>Falkland, 1983</i> | Leeward | 1500 | 17 |

AO = Air Operations

WI = West Island

Cocos = Cocos (Keeling) Islands

CI = Central Indian Ocean

EI = Eastern Indian Ocean

FSM = Federated States of Micronesia

MI = Marshall Islands

GI = Gilbert Islands

As with most hydrologic investigations, attempts to quantify atoll islet water quantity have generally followed one of two paths, analytical or numeric. Fetter (1972) and Chapman (1985) proposed analytical solutions for determining the depth of the seawater/freshwater interface beneath oceanic islands. Oberdorfer and Buddemeier (1988), using the estimated lens thickness from eight small coral islets, found an exponential relationship between the ratio of the lens thickness and the annual rainfall, and the logarithm of the island width. This relationship neglects the influence of the hydraulic conductivity of the Holocene and Pleistocene aquifers (Falkland 1994). Numerical modeling of atoll island hydrogeology (Table 3) began with the work of Lam (1974). His study, along with atoll modeling studies during the next decade (Lloyd et al., 1980; Falkland, 1983) assumed a single homogeneous, isotropic aquifer and uniformly horizontal and single-phase flow. These were followed by Herman and Wheatcraft (1984), who divided the aquifer into upper and lower units and modeled the vertical propagation of the tidal signal, placing the Thurber Discontinuity at a depth of 15 m. During the past twenty years several investigators (Hogan 1988; Griggs, 1989; Oberdorfer et al., 1990; Underwood, 1990; Underwood et al., 1992; Griggs and Peterson, 1993; Peterson and Gingerich, 1995) have used SUTRA (Voss, 1984) to investigate water quantity issues upon atoll islets.

Table 3. Characteristics included in numerical modeling studies of atoll islands

| Investigators | Island | Model Type | Dupuit Assumpt. | Dual Aquifer | Density Depend. | Tides | Anisotropic K |
|--|--------------------|-------------------------|-----------------|--------------|-----------------|-------|---------------|
| <i>Lam, 1974</i> | Swains Island | F.D. | x | | | x | |
| <i>Lloyd et al., 1980</i> | Buota, Tarawa | F.D. | x | | | | |
| <i>Falkland, 1983</i> | Christmas Island | F.D. | x | | | | |
| <i>Herman and Wheatcraft, 1984</i> | Enjebi, Enewetak | F.E. <i>FEMWATER</i> | | x | | x | |
| <i>Hogan, Oberdorfer et al., 1988, 1990</i> | Enjebi, Enewetak | F.E. <i>SUTRA</i> | | x | x | x | |
| <i>Griggs, Griggs and Peterson, 1989, 1993</i> | Laura, Majuro | F.E. <i>SUTRA</i> | | x | x | | |
| <i>Underwood, Underwood et al., 1990, 1992</i> | Generic | F.E. <i>SUTRA</i> | | x | x | x | x |
| <i>Peterson and Gingerich, 1995</i> | Generic, Roi-Namur | F.E. <i>SUTRA</i> | | x | x | x | x |
| <i>Ghassemi et al., 1998</i> | Home Island, Cocos | F.E. <i>SALTFLOW</i> | | x | x | | x |
| <i>Lee, 2003</i> | Generic | F.E. <i>TOUGH2</i> | | | x | | |

F.E. = Finite Element Method

x = included in the modeling study

F.D. = Finite Difference Method

x** = Reef Flat Plate extended from reef to ocean shoreline

Recharge for the modeling studies are normally estimated as half of the annual rainfall (Hamlin and Anthony, 1987), or else the recharge rates are varied over a range of a couple of meters to analyze the influence of recharge on the thickness of the freshwater lens (Underwood et al., 1992; Peterson and Gingerich, 1995).

Monthly recharge has been modeled using the method described by Penman (1950) and Lloyd *et al.* (1966) (Lloyd et al., 1980; Falkland, 1994; Ghassemi, 1998). The model implemented by Falkland (1994) in his study of the Cocos (Keeling) Islands is depicted in Figure 5, in which the main parameters are maximum interception storage of the vegetation canopy, thickness of the soil zone, and the field capacity and wilting point of the soil are the parameters used in the model. Typical values for these parameters are 1 mm day⁻¹, 500 mm, 75 mm, and 25 mm, respectively. Potential evapotranspiration is calculated using the Thornwaite (1948) method. This method was developed for continental climates, and thus has its shortcomings when applied to a tropical climate (Ward, 1971). However, as explained by Lloyd et al. (1980) the Thornwaite method produces large errors only when applied to geographic regions with highly variable climate conditions, which is not the case for Micronesia.

Ghassemi et al. (1998) used the recharge model described by Falkland (1994) to estimate the mean annual recharge at 44% of the mean annual rainfall. Griggs (1989), Griggs and Peterson (1993) and Peterson and Ginerich (1995) calculated monthly recharge rates to analyze various scenarios of groundwater development. No one has yet attempted daily recharge.

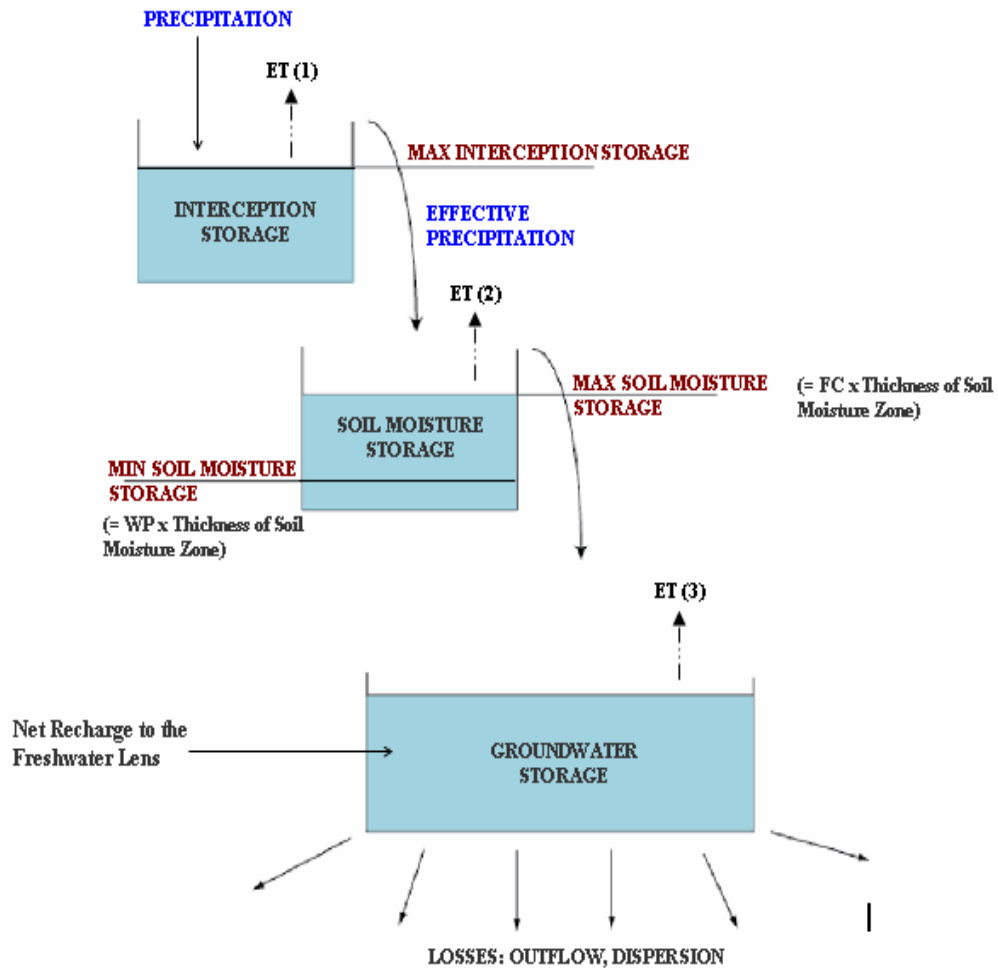


Figure 5. Recharge Model (after Falkland 1994). The portion of the precipitation which is taken up by vegetation interception and soil moisture is left to recharge the freshwater lens. Evapotranspiration occurs at every step, as (1) intercepted rainfall on vegetation is evaporated, (2) moisture from the soil is transpired by roots, and (3) water from the lens is transpired by deep-reaching coconut roots. The storage of the freshwater in the soil zone can never exceed the max soil storage, which is the Field Capacity (FC) of the soil multiplied by the determined thickness of the soil zone, and can never drop below the min soil storage, which is the Wilting Point (WP) multiplied by the soil zone thickness.

The recharge model (Figure 5), however, does not account for sinks from the lens. Coconut trees, abundant on atoll islands, have roots which reach far enough below the ground surface to transpire water directly from the lens (Falkland 1994). This groundwater sink becomes especially important during periods of drought. However, this transpiration value is assumed to be included within the Thornwaite calculation, and there is no provision in the method for extraction from the lens on days when no recharge occurs. Extraction from the lens by coconut roots has not yet been implemented in a numerical modeling study. Pumping from the lens has been modeled through a reduction in the recharge rate (Griggs and Peterson, 1993; Peterson and Gingerich, 1995), as specified by Mather (1975).

Factors Influencing the Thickness of the Freshwater Lens

Through the review of the literature and field work on Ulithi Atoll and Pingelap Atoll, six geologic and climatic factors have been identified which govern the thickness of the freshwater lens. These factors are width of the island, the recharge to the freshwater lens, the hydraulic conductivity of the upper aquifer, the depth to the contact between the upper and lower aquifers, the presence of the reef flat plate, and time-dependent weather conditions.

Recharge

The portion of precipitation which eventually recharges the freshwater lens is given by the following water balance model for atoll islands (Lloyd et al., 1980):

$$R = P - I - ET \pm \Delta ST \quad (4)$$

where:

| | | |
|-----------|---|--|
| <i>R</i> | = | Recharge to the freshwater lens |
| <i>P</i> | = | Total Precipitation |
| <i>I</i> | = | Intercepted Precipitation |
| <i>ET</i> | = | Evapotranspiration (evaporation from the surface, transpiration from the root zone, and extraction from the lens by deep-reaching coconut roots) |
| <i>ST</i> | = | Change in storage |

A small portion of the total precipitation does not reach the ground surface of the island, as it is intercepted by vegetation and subsequently evaporated (Lloyd et al., 1980). The rainwater which reaches the ground surface, the “effective rainfall”, infiltrates the surface and enters the soil zone. A portion of the water is taken up by the roots of plants, another portion may be used to increase the soil moisture if the field capacity of the soil has not yet been reached, and the remainder percolates down to recharge the freshwater lens. The top of the lens is normally only about 2-3 meters below the ground surface, enabling a portion of the coconut roots to extract water directly from the lens (Falkland, 1994). Surface runoff, normally included in a water balance model, is not usually observed on atoll islands except during extremely intense rainfall (Lloyd *et al.*, 1980; Falkland, 1994). Runoff can also occur on islands where a concrete airstrip has been built (Gingerich, 1992; Peterson, 1997).

The intercepted rainfall is thought to be approximately 15% of the total rainfall (Lloyd et al., 1980). The above water balance model becomes important when considering time-dependent recharge. For steady-state conditions the change in soil moisture and groundwater storage can be ignored. Several investigators (Griggs and Peterson, 1993) have reduced the above water balance model to the following relationship for long-term conditions:

$$R = P - ET \quad (5)$$

where the terms are the same as in equation (4). Hamlin and Anthony (1987), in their water resources study of the Laura Area, Majuro Atoll, estimated that 50% of the mean annual rainfall recharges the freshwater lens. Ghassemi et al. (1998), in their modeling study of Home Island, Cocos (Keeling) Islands, calculated an annual recharge which was 44% of the mean annual rainfall for the period 1953-1987.

Hydraulic Conductivity of the Holocene deposits

The hydraulic conductivity of the porous media reflects the ease with which water may pass through the pores, and directly influences the thickness of the freshwater lens. Aquifers with a low hydraulic conductivity are able to prevent the freshwater from quickly flowing out of the system, and thus have a much thicker lens than that with a high hydraulic conductivity. As reported by Spennemann (2006), islands on the leeward side of an atoll tend to be larger and have finer sediments, while those exposed to the prevailing wave action tend to be smaller and have more coarse-grained sediments (Figure 6). As explained by Anthony (1997), the low-permeability sediments, coupled with the larger surface area of leeward islands, produces a freshwater lens which is much thicker than those of windward islands (Figure 7). This pattern is especially striking when observing islands on the same atoll, for example Deke and Pingelap Islands, Pingelap Atoll, which have a lens thickness of 4 and 16 m, respectively, or Roi-Namur and Kwajelein Islands, Kwajelein Atoll, which have a lens thickness of 5 and 16 m, respectively (see Table 2). As a consequence of this pattern, leeward islands tend to be the inhabited islands of an atoll (Spennemann, 2006).

These trends are seen in a plot of the observed lens depths against island width (Figure 7). The trend for the leeward islands exhibits a linear relationship between lens thickness and island width for small to medium-size islands, followed by a diminishing of the rate of increase as the thickness of the lens approaches the depth to the Thurber Discontinuity. This limiting feature of the lens growth is especially apparent for large islands such as the Cantonment area of Diego Garcia atoll (Hunt, 1997). A quasi-linear relationship between island width and lens thickness exists for windward islands. This relationship is not straightforward, as several windward islands, such as Enjebi, Enetwetak Atoll, and Bikini, Bikini Atoll, do not have permanent lenses. Bonriki, Tarawa Atoll, is also off the trend with a thickness of 23 m, even though the Thurber Discontinuity is located at a depth of 17 m (Falkland and Woodroffe, 1997). As explained by Falkland and Woodroffe (1997), the Thurber Discontinuity acts to limit the depth of the lens except in the central region of the large islands of the atoll. The large islands include Buariki and Buota (Table 2; Figure 7), which are offset from the prevailing winds and are neither directly windward nor leeward. There is no apparent trend for islands offset from the prevailing winds (Figure 7).

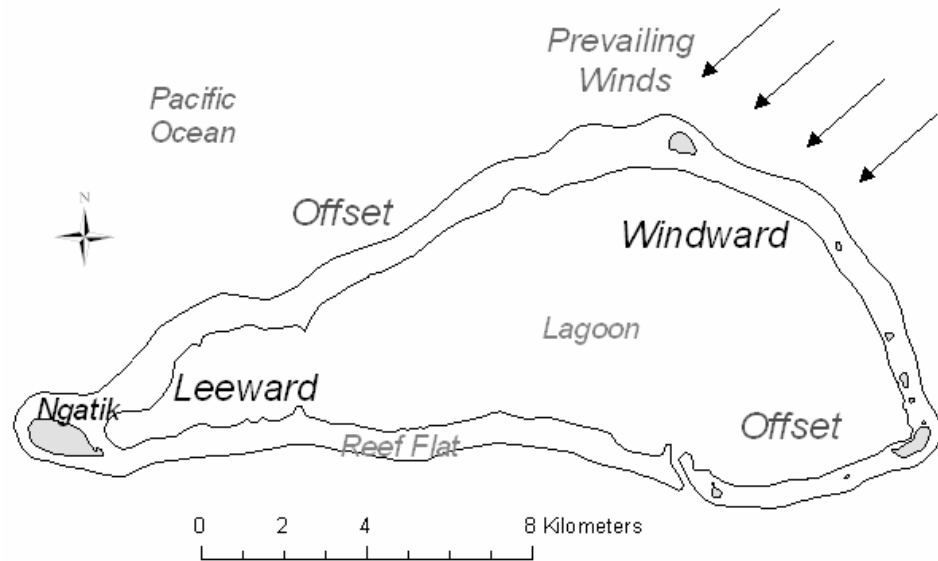
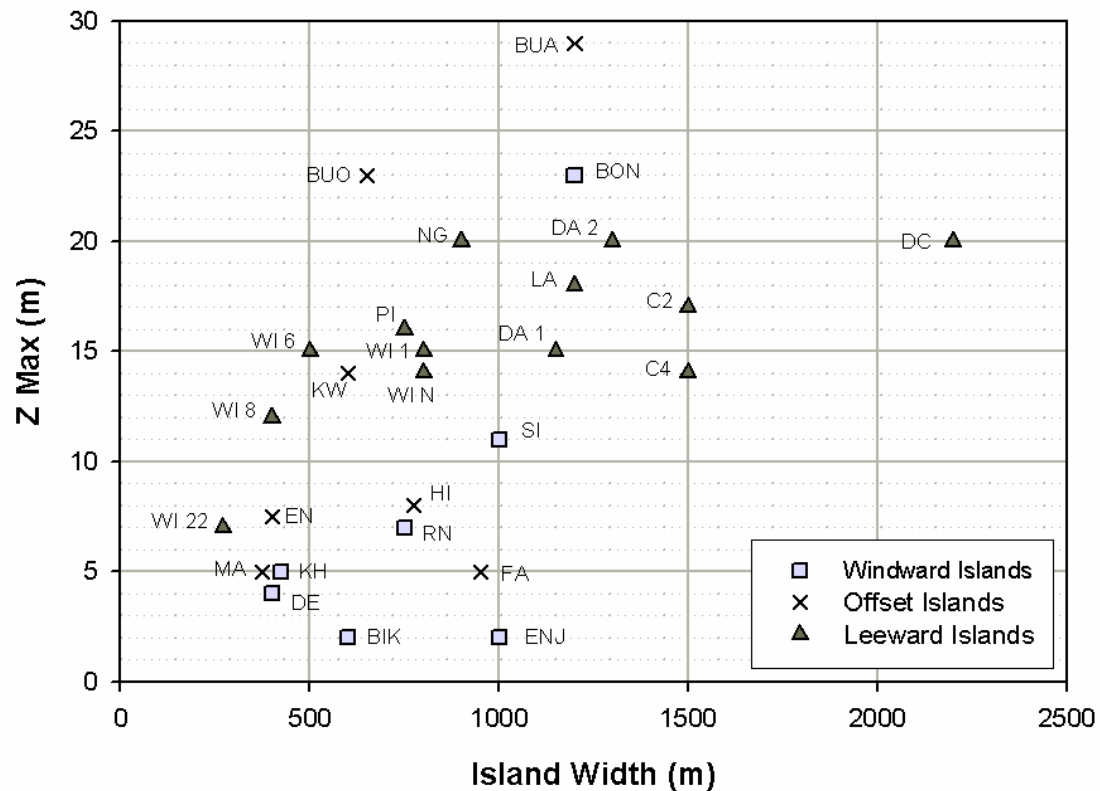


Figure 6. Direction of prevailing winds on Pingelap Atoll, Pohnpei State, Federated States of Micronesia. All Pacific island groups in the Northern Hemisphere experience the same north-easterly trade wind. The windward side of atolls is exposed to the high-energy waves associated with the prevailing winds. These waves produce a build-up of coarse sediments on the surface and subsurface, and thus affect the development of the aquifer. Aquifers with high hydraulic conductivity develop within islands located on the windward side of atolls while islands on the leeward side have aquifers with low hydraulic conductivity. Deke Island, on the windward side, has no residents, and is used only for farming. The village is located on the leeward side of Pingelap Island. The wells are located throughout the leeward portion of Pingelap Island, in and around the village and taro patch. Map after Anthony (1996a).



a Hunt and Peterson 1980
b Buddemeier and Holladay 1977
c Lloyd et al. 1980
d Jacobson and Taylor 1981
e Falkland 1983
f Ayers and Vacher 1986

g Hamlin and Anthony 1987
h Falkland 1994
i Gingerich 1992
j Falkland 1992
k Anthony 1996a
l Anthony 1996b

m Anthony 1996c
n Hunt 1997
o Anthony 1997
p Peterson 1997
q Falkland 2003

Figure 7 Observed maximum depths of the freshwater lens of atoll islands across the Pacific and Indian Oceans, according to their position within the atoll.

A trend of sediment size also exists between the windward and leeward sides of a single atoll island (Cox, 1951; Hamlin and Anthony, 1987). A large contrast exists between the surface sediments deposited on the leeward side of an island and the ocean side of an island, reflecting the difference in force between the high-energy windward waves and the low-energy leeward waves (Figure 8). Rocks and coarse-grained sediments build up on the ocean side and fine-grained sediments on the lagoon side, with a central depression in the middle. This central depression is close to sea level and underlying freshwater lens, and has traditionally been a prime location for farming. This pattern has been reported by many investigators (Lloyd et al., 1980; Ayers and Vacher, 1986; Hamlin and Anthony, 1987), beginning with Cox (1951) when studying the hydrology of Arno Atoll, Marshall Islands.

Thurber Discontinuity

As seen in the conceptual model of the island hydrogeology (Figure 4), the aquifer of atoll islands is divided into an upper aquifer and a lower aquifer. The upper aquifer is comprised of 15-25 m of unconsolidated deposits of Holocene age (Lloyd et al., 1980; Wheatcraft and Buddemeier, 1981; Hamlin and Anthony, 1987; Anthony, 1997), and rests upon the much more porous and permeable Pleistocene limestone. The vertical variation in hydraulic conductivity between the Holocene deposits and the Pleistocene limestone is quite drastic, as the hydraulic conductivity of the lower aquifer can be one to two orders of magnitude higher than that of the upper aquifer (Hunt and Peterson, 1980; Oberdorfer and Buddemeier, 1983; Anthony, 1987; Peterson, 1997). The high hydraulic conductivity of the lower aquifer allows the seawater to readily mix with the freshwater, thus serving to truncate the lens at the contact between the two aquifers (Hamlin and Anthony, 1987; Falkland, 1994; White, 1996; Falkland and Woodroffe, 1997; Hunt, 1997; Peterson, 1997). It is the limiting factor of the growth of the freshwater lens. This same effect can be seen in Figure 7.

Reef Flat Plate

An old reef flat plate (Figure 9) extends from the reef on the ocean side to the interior of the island see (Figure 4), and has been observed on numerous atolls (Cox, 1951; Buddemeier and Holladay, 1977; Oberdorfer and Buddemeier, 1983; Ayers and Vacher, 1986; Anthony, 1997). This feature was observed on Ulithi and Pingelap Atolls during this study. The reef plate acts as a confining layer to the freshwater, forcing the water to flow under the plate to be discharged at the reef, as well as along fractures in the plate. As shown in Figure 9, residents of atoll islands sometimes punch through the plate to access the water.

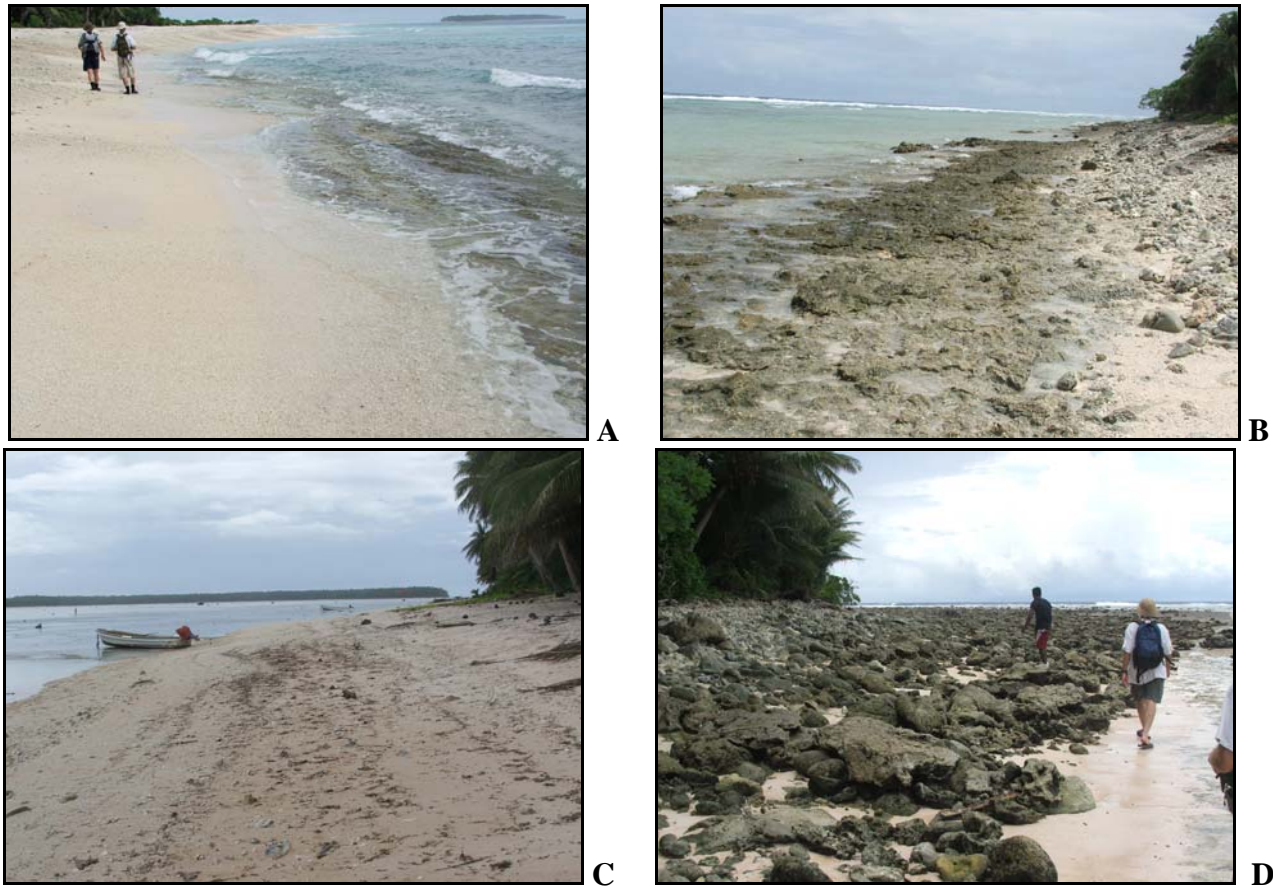


Figure 8. Variation in surface deposits between leeward (A and C) and windward (B and D) sides. Images a and b were taken January 2007 on Mogmog island, Ulithi Atoll, Yap State, FSM, and c and d were taken July 2007 on Pingelap Island, Pingelap Atoll, Pohnpei state, FSM. The contrast in sediment size between the leeward and windward sides, and the associated heterogeneous nature of the aquifer, produces a freshwater lens which is slightly thicker on the leeward side of the island (Ayers and Vacher 1986).



A



B

Figure 9. (A) Well on Mogmog Island, Ulithi Atoll showing reef flat plate, and (B) Close-up view of reef flat plate. The reef flat plate, located at mean sea level and extending across much of the island, is a confining layer to the freshwater. Residents of atoll islands are thus required to punch through the plate to reach the freshwater if they dig wells on the ocean side of the island.

Time-Dependent Weather Conditions

The lens is rarely in steady-state. Rather, it is constantly responding to the seasonal pattern of precipitation (Figure 10). In general the freshwater lens is the thickest during the wet season and thinnest during the dry season (Ayers and Vacher 1986). At times this regular seasonal variation is interrupted by extreme weather conditions such as El Niños, which occur on average every 2 to 7 years in the Pacific Basin, with a major event, such as in 1997-1998 occurring about every 15 years. Typically in Micronesia a drought occurs during the year following an El Niño (see Figure 10). The negative consequences of a drought on the freshwater lens are two-fold: not only do droughts deplete the freshwater lens through lack of recharge, but the residents use more groundwater since there is not enough rainfall to maintain the roof catchment supply.

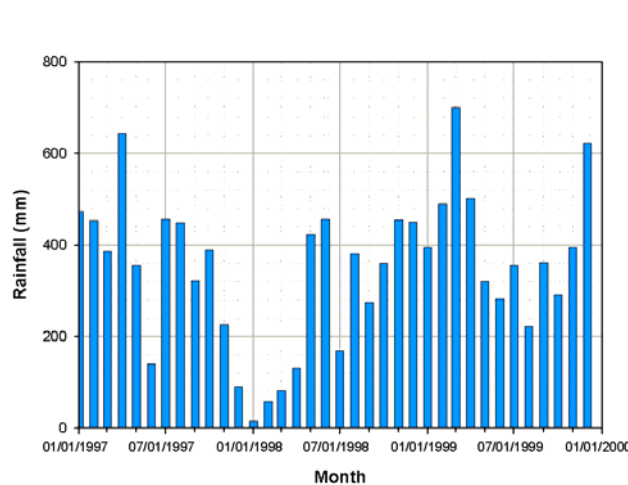


Figure 10. Monthly Rainfall values for the island of Pohnpei, Federated States of Micronesia. Notice the fluctuation of the rainfall between winter (wet season) and summer (dry season), as well as the low precipitation values during the last few months of 1997 (the El Niño year) and the beginning months of 1998.

Washover events are another extreme weather episode which strongly affects the freshwater lens. These events can be deadly, as high waves wash over parts of the island. Washover events occur periodically on small, low-lying islands (Lessa, 1964) as the high surf during tropical storms and typhoons is carried across the island's surface, inundating the interior of the island and leaving standing sea water, which subsequently infiltrates down through the soil and mixes with and contaminates the freshwater lens. A washover occurred on the island of Falalop, Ulithi Atoll during Typhoon Ophelia (Lessa, 1964), when waves pushed seawater into the central depression of the island, and the low central basin of the island was inundated by several feet of seawater, which subsequently drained to the water table. The height of the surge was initially about 3 to 4 feet, and then dropped to about two feet. Lack of sufficient water resources following a washover event can also prove deadly, as standing seawater left from the waves infiltrates the ground surface, percolates through the soil, and contaminates the freshwater (Lessa, 1964). The time needed for a complete recovery of the lens in such an event for atoll islands is unknown, but is examined hypothetically in the *Transient Simulations* section.

STEADY-STATE SIMULATIONS

Numerical Model

The USGS numerical model SUTRA (Saturated Unsaturated Transport) (Voss, 1984) was used to simulate the physics of the groundwater system. SUTRA approximates the solutions of the differential equations governing fluid density-dependent groundwater flow and solute transport, providing fluid pressure and solute concentrations at specified points in the problem domain. The original code was modified by Souza and Voss (1987) to include water-table storage.

Mesh Design

This study employed generic atoll island models, for which a simple two-dimensional mesh was constructed to represent the cross section of the island from the lagoon to the reef on the ocean side, as shown in Figure 4. A typical mesh is shown in Figure 12, with vertical exaggeration. Figure 13 shows an enlarged illustration of the island subsurface region. The nodes across the top of the mesh on the ocean side represent the island subsurface at sea-level.

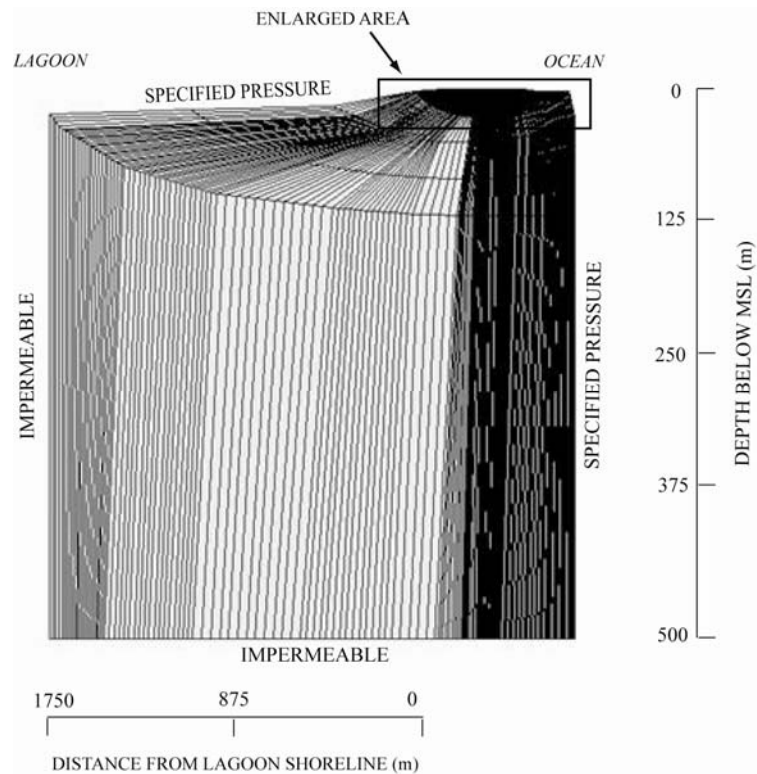


Figure 11. Finite element mesh of atoll cross-section, with accompanying boundary conditions

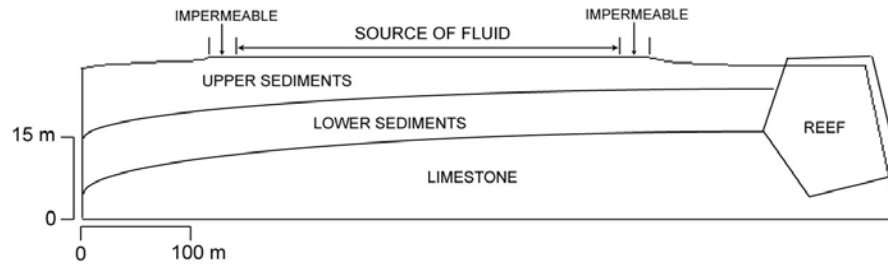


Figure 12. Enlarged view of atoll island subsurface, with boundary conditions and geologic units (after Griggs and Peterson 1993)

Following previous modeling studies (Underwood et al., 1992; Peterson and Gingerich, 1995) and conventional finite-element mesh design procedures, the mesh was more finely discretized in areas of expected high concentration gradients in order to promote numerical stability. In the atoll groundwater system these gradients occur as the seawater grades to freshwater across the transition zone. Thus the mesh was finely discretized in the region simulating the island subsurface as well as at the edge of each shoreline. The mesh is also refined at the interception of the groundwater divide and the freshwater/seawater mixing zone. Fine discretization was also necessary in the region designated as the reef flat plate, since the permeability of these elements would be much lower than in surrounding elements. Eight meshes (Table 4) were used, each having a different island width. ArgusONE (Argus Holdings Ltd. © 1992-1999) was used to design the meshes and prepare the input files for SUTRA. The results were viewed using Model Viewer (v. 1.1, United States Geological Survey, 2003).

Table 4. Mesh Attributes

| Island Width (m) | Nodes | Elements |
|------------------|-------|----------|
| 150 | 3726 | 3600 |
| 200 | 4600 | 4455 |
| 300 | 5040 | 4875 |
| 400 | 8055 | 7832 |
| 500 | 9540 | 9284 |
| 600 | 11408 | 11115 |
| 800 | 14688 | 14335 |
| 1100 | 18850 | 18424 |

Boundary and Initial Conditions

Boundary conditions were applied to simulate the influence of seawater pressure and recharge. Fluid pressure was specified at each point along the contact between the seawater and the reef on the ocean side, and between the seawater and the lagoon basement (Figures 12 and 13). Water flowing inward at these boundaries was assumed to have a salt concentration of $0.0357 \text{ kg kg}^{-1}$, equivalent to that of seawater. The top of the island, representing the water table (Figure 13), was assigned as a recharge boundary, where freshwater enters the island subsurface. Water entering the simulation at this boundary is assumed to have a concentration of salt found in typical rainwater in the Pacific (Anthony, 1987). The annual rate of recharge was taken to be half of the annual rainfall, following Griggs and Peterson (1993). The bottom of the mesh and the boundary simulating the limit of the lagoon were assigned as no-flow boundaries, where water can neither leave nor enter the system.

Model Parameters

SUTRA requires several parameters to specify the properties of the aquifer materials and waters in the aquifers. The values assigned to these parameters (Table 5) follow those found in other atoll modeling studies (Underwood et al., 1992; Griggs and Peterson, 1993; Peterson and Gingerich, 1995). The placement of hydraulic conductivity zones and their accompanying values followed the pattern observed by Hamlin and Anthony (1987) on Laura Island, Majuro Atoll, where the Holocene aquifer was divided into two zones of slightly differing permeability (see Figure 13). The top zone, called the Upper Sediment by Anthony, is slightly more permeable than the Lower Sediment section (Hamlin and Anthony 1987) and extends to a depth of 5 and 10 m below sea level on the ocean side and lagoon side, respectively, while the Lower Sediment section extends to depths of 13-18 m, which represent the Thurber Discontinuity. Porosity of the Holocene sediments was taken as $0.20 \text{ m}^3 \text{ m}^{-3}$, whereas the porosity of the Pleistocene limestone was set at $0.30 \text{ m}^3 \text{ m}^{-3}$.

Table 5. Model Input Parameters

| PARAMETER | VALUE | UNIT | SOURCE |
|--------------------------------------|------------------------|----------------------------------|---------------------------------|
| Freshwater Properties | | | |
| Compressibility of Water | 4.47×10^{-10} | $\text{m}^2 \text{N}^{-1}$ | Freeze and Cherry, 1979 |
| Fluid Viscosity | 1.00×10^{-3} | $\text{kg m}^{-1} \text{s}^{-1}$ | CRC |
| Density of Freshwater | 1000 | kg m^{-3} | Peterson and Gingerich, 1995 |
| Rainwater Specified Concentration | 2.00×10^{-5} | $\text{kg salt kg water}^{-1}$ | Hamlin and Anthony, 1987 |
| Seawater Properties | | | |
| Density of Seawater | 1025 | kg m^{-3} | Peterson and Gingerich, 1995 |
| Solute Mass Fraction, seawater, C | 0.0357 | $\text{kg salt kg water}^{-1}$ | Griggs and Peterson, 1993 |
| General Aquifer Properties | | | |
| Compressibility of Porous Matrix | 1.00×10^{-9} | $\text{m}^2 \text{N}^{-1}$ | Peterson and Gingerich, 1995 |
| Specific Yield | 0.18 | $\text{m}^3 \text{m}^{-3}$ | Griggs and Peterson, 1993 |
| Holocene Aquifer | | | |
| Holocene Porosity | 0.2 | $\text{m}^3 \text{m}^{-3}$ | Anthony, 1987 |
| Upper Deposits Thickness | 5 to 10 | m | Anthony, 1987 |
| Upper Deposits horizontal K | 50 | m day^{-1} | Griggs and Peterson, 1993 |
| Upper Deposits vertical K | 10 | m day^{-1} | Griggs and Peterson, 1993 |
| Lower Deposits Thickness | 8 | m | Anthony, 1987 |
| Lower Deposits horizontal K | 60 | m day^{-1} | Underwood <i>et al.</i> , 1992 |
| Lower Deposits vertical K | 12 | m day^{-1} | Underwood <i>et al.</i> , 1992 |
| Pleistocene Aquifer | | | |
| Pleistocene thickness | 485 | m | |
| Pleistocene Porosity | 0.3 | $\text{m}^3 \text{m}^{-3}$ | Swartz, 1962 |
| Pleistocene horizontal K | 5000 | m day^{-1} | Oberdorfer <i>et al.</i> , 1990 |
| Pleistocene vertical K | 1000 | m day^{-1} | Oberdorfer <i>et al.</i> , 1990 |
| Transport | | | |
| Horizontal longitudinal dispersivity | 6 | m | Underwood <i>et al.</i> , 1992 |
| Vertical longitudinal dispersivity | 0.5 | m | Underwood <i>et al.</i> , 1992 |
| Transverse dispersivity | 0.05 | m | Underwood <i>et al.</i> , 1992 |
| Molecular Diffusivity | 1.48×10^{-9} | $\text{m}^2 \text{s}^{-1}$ | CRC |

Simulations and Results

Four baseline sensitivity test series (Table 6) were run to quantify the influence of the following four factors on the geometry and behavior of the freshwater lens (Figure 14): recharge, hydraulic conductivity of the Holocene sediments, depth to the Thurber Discontinuity, the reef flat plate, and island width. For each factor value a simulation was run for each island width to determine the effect of a fifth factor, the island width, on the thickness of the lens.

The bottom of the freshwater lens was designated where the solute mass concentration was 0.00089 kg salt / kg water (0.89 ppt), which corresponds to a chloride (Cl) content of 500 mg/l. This value is lower than the World Health Organization recommended standard of 600 mg/l for potable water (WHO, 1972), in order to provide a safety margin for the eventual water resources application of the results (Lloyd et al., 1980). Each simulation was run to 60,000 1-hour time steps, or just under 7 simulated years, in order to reach a steady-state condition. The result from a typical simulation is seen in Figure 15, showing the freshwater lens surrounded by the underlying seawater. The direction and magnitude of the flow of freshwater follow a typical flow pattern (Figure 16), in which the freshwater, in blue, and the mixed seawater, grading to red, are both conducted to and discharged at the shoreline.

Table 6. Geological and Climatic Parameters for each baseline simulation series

| Test Series | Recharge, m yr ⁻¹ | K, m day ⁻¹ | Depth to TD, m | RFP |
|-----------------|------------------------------|------------------------|----------------|------------------|
| (1) Recharge | 0.25 to 2.75 | 50-60 | 17.5 | Not included |
| (2) K | 2 | 50 to 400 | 17.5 | Not included |
| (3) Depth to TD | 2 | 50-60 | 8 to 18 | Not included |
| (4) RFP | 2 | 50-60 | 17.5 | Presence* |

K = Hydraulic Conductivity of Holocene Deposits

RFP = Reef Flat Plate

TD = Thurber Discontinuity

Presence* = Comparing simulations with and without the presence of the reef flat plate

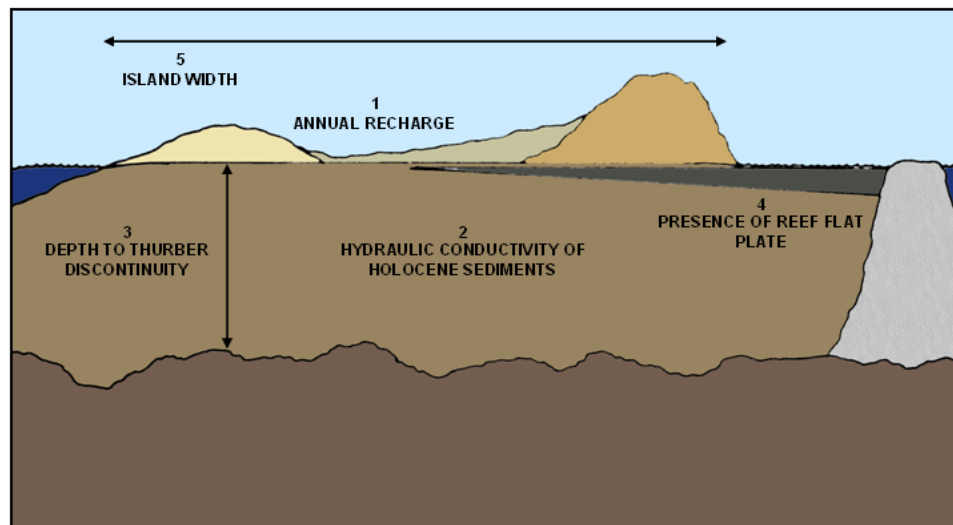


Figure 13. Climatic and geologic factors studied using the numerical model

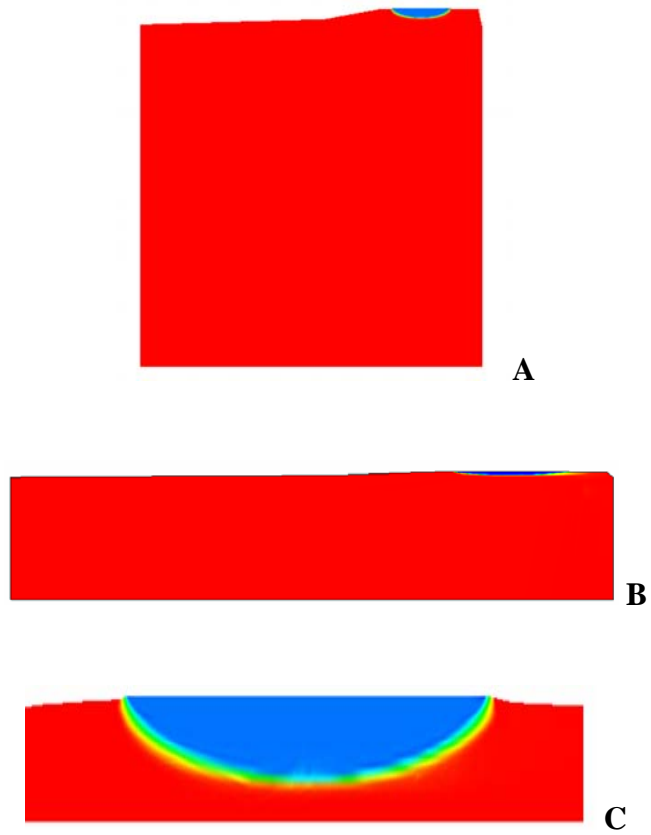


Figure 14. Typical freshwater lens delineation, (A) with vertical exaggeration and (B) without vertical exaggeration, and (C) an enlarged view of the island subsurface

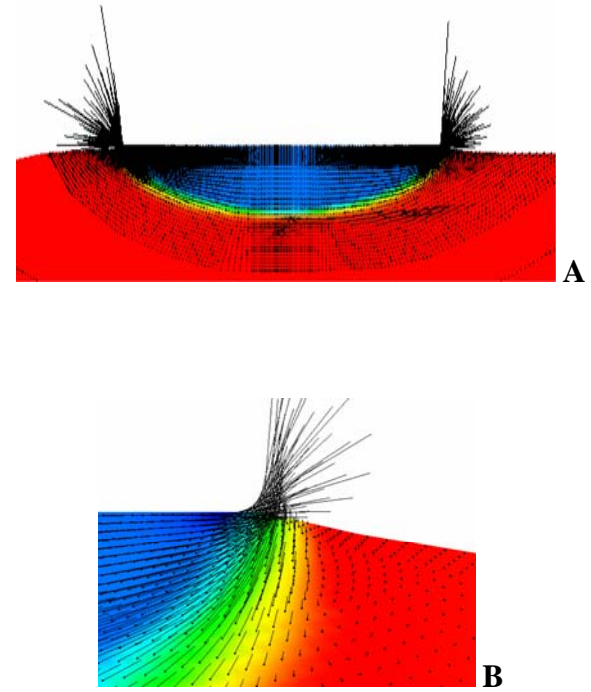


Figure 15. (A) View of velocity vectors, with the black circles as the tail, of the groundwater flow, and (B) Enlarged view of the direction and magnitude of groundwater flow at the coastline.

Recharge

Seven recharge values, ranging from 1.25 to 2.75 mm yr⁻¹, were examined. Recharge was assumed to be half of precipitation, and the annual precipitation rates experienced in the Federated States of Micronesia range from about 3 to 5.50 m yr⁻¹. Eight simulations were run for each rainfall rate, one for each island width (Table 7), for a total of 56 simulations. Table 7 shows the thickness of the lens with the associated island width and recharge rate.

Table 7. Maximum thickness of Freshwater Lens for various island widths and recharge rates

| Island Width | Recharge Rate | | | | | | |
|--------------|---------------|--------|--------|--------|--------|--------|--------|
| | 1.25 | 1.50 | 1.75 | 2.00 | 2.25 | 2.50 | 2.75 |
| 150 | 3.140 | 3.30 | 3.710 | 4.000 | 4.200 | 4.600 | 4.800 |
| 200 | 4.000 | 4.60 | 5.200 | 5.500 | 5.800 | 6.400 | 6.600 |
| 300 | 6.700 | 7.60 | 7.900 | 8.500 | 9.400 | 9.850 | 10.300 |
| 400 | 9.000 | 10.000 | 11.000 | 12.000 | 12.500 | 13.000 | 13.000 |
| 500 | 11.364 | 12.273 | 13.182 | 13.410 | 13.637 | 14.091 | 14.091 |
| 600 | 13.333 | 14.167 | 14.167 | 14.792 | 14.900 | 15.000 | 15.400 |
| 800 | 15.000 | 15.000 | 15.827 | 15.978 | 16.072 | 16.100 | 16.562 |
| 1100 | 15.833 | 16.000 | 16.000 | 16.111 | 16.500 | 16.667 | 16.713 |

Figure 17 shows the geometry of the lens for recharge rates ranging from 1.25 to 2.75 m yr⁻¹ for an island width of 600 m. There is an increase in lens thickness with an increase in recharge rate. Of particular interest, however, is the shape of the lens as the recharge rate is increased. A relatively low rate, 1.25 m yr⁻¹, produces an elliptical lens shape, whereas for higher rates, 2.00 m yr⁻¹, and 2.75 m yr⁻¹, the bottom of the lens is truncated as the lens intercepts the discontinuity between the upper and lower aquifers.

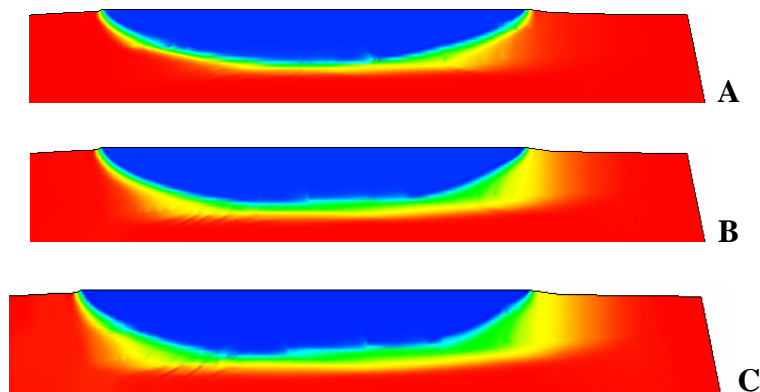


Figure 16. Lens geometry for a 600-m island for recharges rates of (A) 1.25 m yr⁻¹, (B) 2 m yr⁻¹, and (C) 2.75 m yr⁻¹

Results for the recharge simulations (Figure 18) show that for a given recharge rate, increasing the island width will increase the thickness of the freshwater lens. This increase is limited to the depth of the Thurber discontinuity. This is compared with the trend for a single aquifer system (Figure 19), wherein there is no discontinuity, and thus

no limiting growth factor of the lens. Recharge for all simulations was set at 2 m yr^{-1} , and the hydraulic conductivity of the single aquifer and the upper aquifer in the dual aquifer was 50 m day^{-1} . The difference between the two aquifer systems becomes significant when island width exceeds 500 m , as the discontinuity begins to affect the lens in the dual aquifer system.

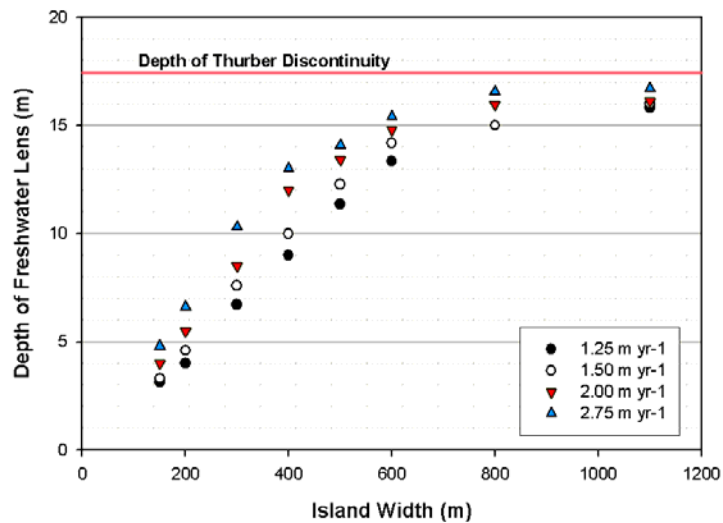


Figure 17. Results from the rainfall experiment, showing the increase of lens thickness with increasing rainfall rates

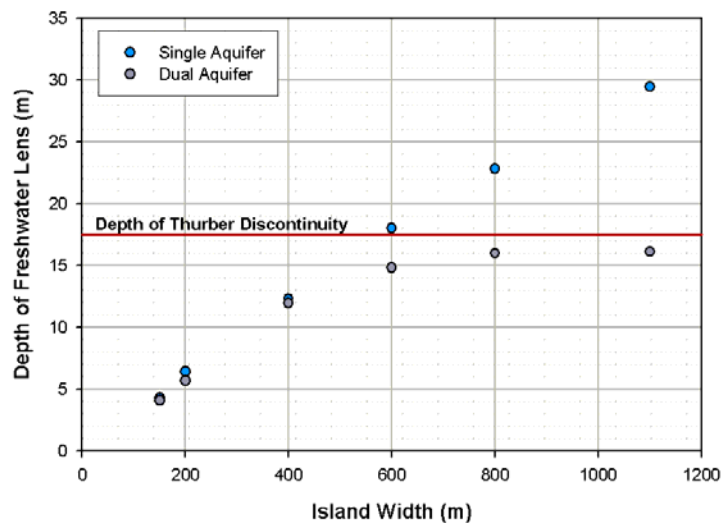


Figure 18. Relationship between depth of lens and island width for single and dual aquifer system, for a 600 m wide island. The dual aquifer system exhibits a limiting growth factor.

Hydraulic Conductivity of Holocene Deposits

Seven hydraulic conductivity values were examined (25, 50, 100, 200, 300, 400, and 500 m day⁻¹). Eight simulations, one for each island width, were run for each value of hydraulic conductivity, making a total of 56 simulations. Figure 20 shows the effect of the hydraulic conductivity of the Holocene sediments on the geometry of the lens. Low values of hydraulic conductivity ($K = 25 \text{ m day}^{-1}$) enable the lens to thicken until it is truncated by the Thurber Discontinuity, while high values of hydraulic conductivity ($K = 100 \text{ m day}^{-1}$ and 400 m day^{-1}) produce a shallow lens that is not affected by the highly permeable limestone aquifer. This pattern is explained further in Figure 21, as a plot of lens thickness vs. hydraulic conductivity shows a sharp decrease in the thickness of the lens as the hydraulic conductivity is increased.

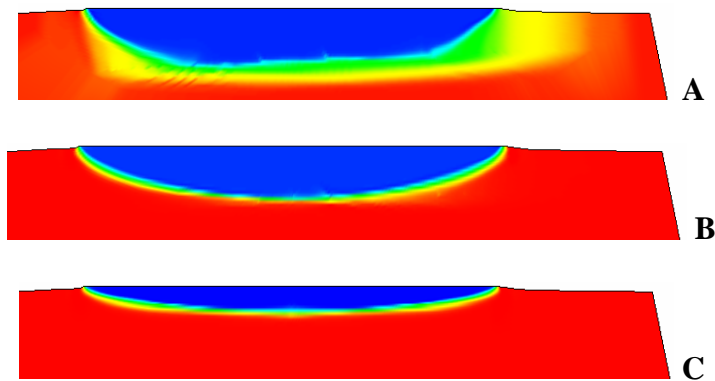


Figure 19 Lens geometry for hydraulic conductivity values of (A) 25 m day⁻¹, (B) 100 m day⁻¹, and (C) 400 m day⁻¹

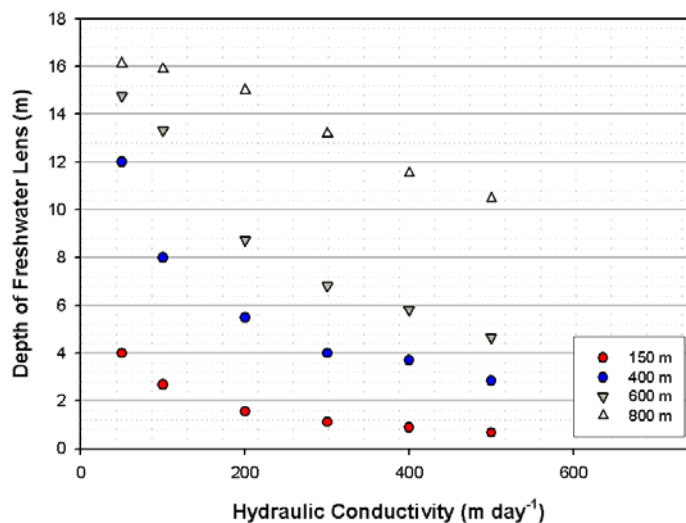


Figure 20 Relationship between the hydraulic conductivity of the Holocene sediments and the maximum depth of the freshwater lens. An increase in the hydraulic conductivity produces a decrease in the lens depth.

A different set of plots is presented in Figure 22, with the thickness of the lens plotted vs. island width, for varying values of hydraulic conductivity. The trend of the plot of low hydraulic conductivity ($K = 50 \text{ m day}^{-1}$) mirrors that from the recharge study (see Figure 18), as the Thurber Discontinuity limits the thickness of the lens for large islands. For high values of hydraulic conductivity, however, the discontinuity is never reached, and there exists a linear relationship between lens thickness and island width.

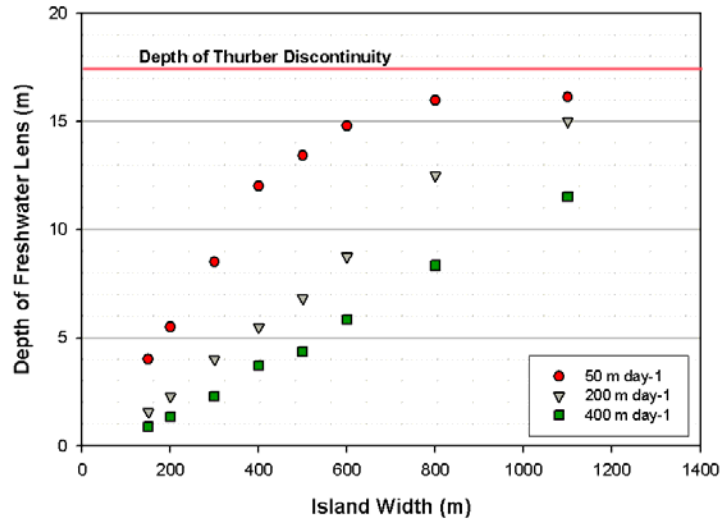


Figure 21. Results from the Holocene hydraulic conductivity experiment, showing the increase of lens thickness with decreasing hydraulic conductivity

Figure 23 shows plots of the calculated depth of the lens for $K = 50$ and 400 m day^{-1} on the same graph as the observed lens depths from atoll islands across the Pacific and Indian Oceans (see Figure 7). The graph shows that the SUTRA results for these two hydraulic conductivity values plot nicely against the observed values: hydraulic conductivity values of 50 m day^{-1} produce lens depths similar to those observed on islands located on the leeward portion of the atoll, and values of 400 m day^{-1} produce lens depths similar to those observed on windward islands. From these results we conclude that, in a very general sense, the Holocene sediments on leeward islands have a hydraulic conductivity close to 50 m day^{-1} , and those on windward islands have a hydraulic conductivity close to 400 m day^{-1} . Islands located at other locations on the atoll are assumed to have a hydraulic conductivity between these two end-member values.

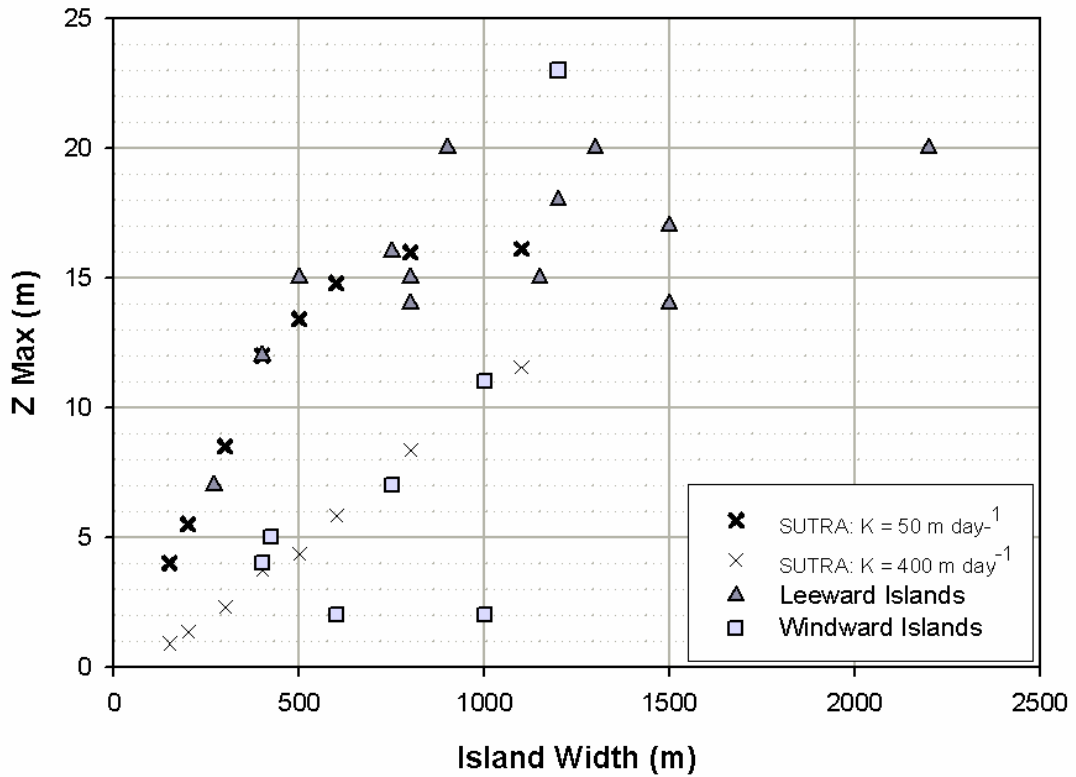


Figure 22. Observed depths compared to depths found from the hydraulic conductivity study. Using hydraulic conductivity values of 50 m day⁻¹ and 400 m day⁻¹ for the Holocene deposits produced lens depths which closely match the observed values on leeward islands and windward islands, respectively.

Depth to Thurber Discontinuity

The boundary between the Holocene deposits and the Pleistocene limestone was specified at six different depths (8, 10, 12, 14, 16, and 18 meters) to predict the influence of the boundary depth on the geometry of the freshwater lens. The objective behind the set-up of the simulations was to determine more precisely the effect of the Thurber Discontinuity (TD) on the bottom of the freshwater lens. Five island widths (150, 200, 300, 500, and 800 meters) were used, for a total of 30 simulations. Figure 24 shows the geometry of the lens for three different TD depths for an island width of 800 m. Each of the images shows the truncation of the lens at the Thurber Discontinuity, no matter at which depth the TD was set.

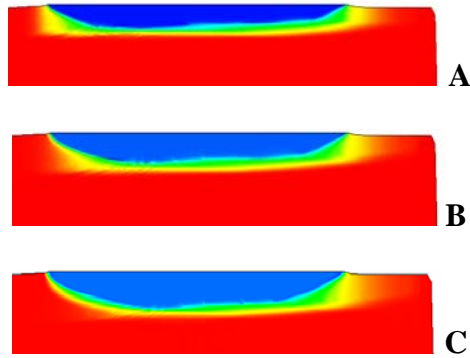


Figure 23. Lens geometries for a Thurber Discontinuity depth of (a) 10 m, (b) 14 m, and (c) 18 m

Figure 25 shows the thickness of the lens vs. the depth to the Thurber Discontinuity set in the simulation. A linear relationship between the two parameters, i.e., a TD depth of 12 m results in a lens thickness of 12 m, signifies that the Thurber Discontinuity does in fact limit the depth to which the lens can grow. This relationship is seen in Figure 25 for island widths of 500 and 800 m. For smaller islands wherein the maximum depth of the lens does not reach 8 m, the shallowest depth of the discontinuity in the simulations, there is no association between the depth of the lens and the Thurber Discontinuity.

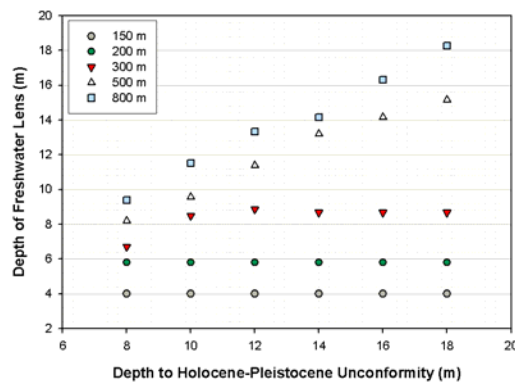


Figure 24. Results from the Thurber Discontinuity experiment, showing the lens thickness vs. the depth to the unconformity for 5 different island widths. Notice that the smaller islands are not affected by the unconformity.

Reef Flat Plate

Presence of the Reef Flat Plate

Twelve simulations were run to analyze the influence of the reef flat plate on the thickness of the freshwater lens. Two simulations were run for each of six island widths, one with the reef flat plate and one without. Table 8 summarizes the results of the simulations, which are plotted in Figure 26. Notice that the influence of the reef flat plate, i.e. the difference in the thickness of the freshwater lens, diminishes as island width increases. In general, the presence of a reef flat plate does not have a large influence on the maximum depth of the lens. The largest influence is felt for small islands, where the lens thickness increases from 4.00 m to 4.75 m, with and without the reef flat plate, respectively, for an island 150 m across.

Table 8. Influence of Reef Plate on Lens Thickness, for varying island widths

| Island Width (m) | No Reef Plate Lens Thickness (m) | Reef Plate Halfway Across Lens Thickness (m) | Without / With |
|------------------|----------------------------------|--|----------------|
| 150 | 4.00 | 4.75 | 0.84 |
| 200 | 5.80 | 6.56 | 0.88 |
| 300 | 8.60 | 9.60 | 0.90 |
| 400 | 12.00 | 13.00 | 0.92 |
| 500 | 13.41 | 13.94 | 0.96 |
| 1100 | 16.63 | 16.70 | 0.99 |

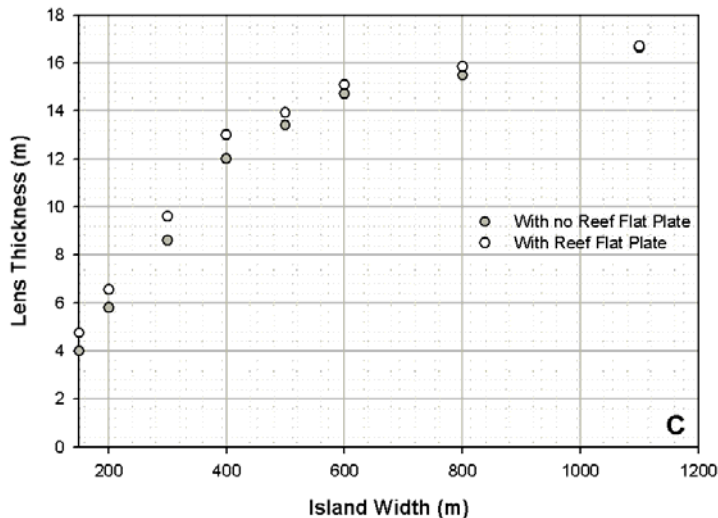


Figure 25. The lens thickness as the island width is varied, for simulations with and without a reef flat plate. Notice that the difference between the two simulations decreases as the island width

The presence of the reef flat plate does, however, have a significant influence on the volume of the lens on the ocean side of the island (see Figure 27). The lens extends further oceanward as the reef flat plate confines the freshwater, thus widening the lens and increasing its volume. Table 9 contains the cross-sectional areas of the lens for simulations with and without the reef flat plate for various island widths. The pattern of volume difference for a given island width is similar to that presented in Table 9: the

largest difference in volume occurs for small islands, whereas there is a negligible difference for islands with widths approaching 1000 meters.

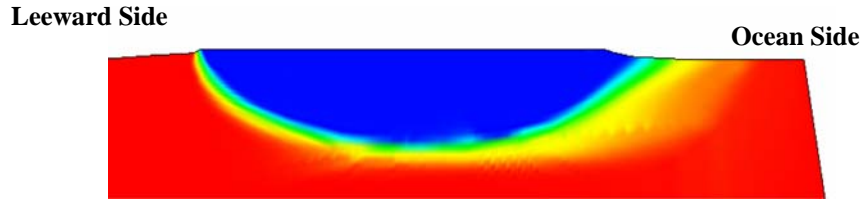


Figure 26. The freshwater lens configuration when a reef flat plate is present on the ocean side, for a 400 m wide island. Notice the thickness of the transition zone on the ocean side, as compared to the leeward side.

Table 9. Approximate cross-sectional area of the freshwater lens, comparing results from simulations with and without the reef flat plate. The difference in volume is greatest for small islands.

| Island Width | With RFP | Without RFP | Ratio |
|--------------|----------|-------------|-------|
| 150 | 450 | 560 | 1.24 |
| 200 | 800 | 1060 | 1.33 |
| 300 | 1930 | 2380 | 1.23 |
| 400 | 3560 | 4020 | 1.13 |
| 500 | 5020 | 5270 | 1.05 |
| 1100 | 13700 | 13759 | 1.00 |

The thickness of the mixing zone is also affected (Figure 27), as it extends along the length of the plate as water is forced under the confining layer to the reef, at which point it is discharged. This characteristic is seen in Figure 28, where the groundwater velocity vectors are shown for both the lagoon coast and the ocean coast. The groundwater discharges easily on the lagoon side, whereas the water is inhibited from discharging at the ocean coastline by the reef flat plate.

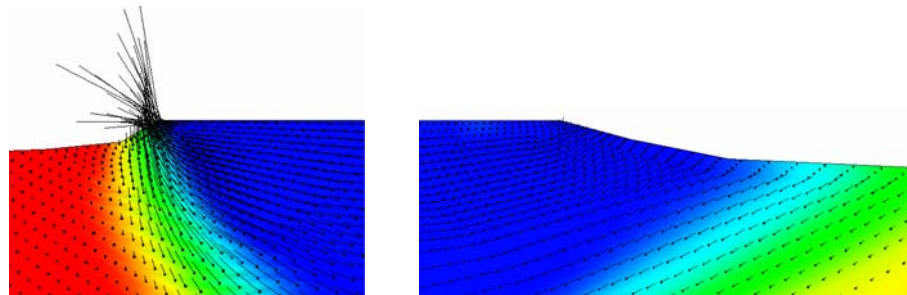


Figure 27. The direction and magnitude of the groundwater flow on (a) the lagoon side, where no reef flat plate exists, and (b) the ocean side.

Extent of the Reef Flat Plate

A second set of simulations was run to explore the change in the lens thickness for various spans of the reef flat plate. All simulations used an island width of 400 m. In the first simulation the reef plate only extended from the ocean reef to the island shoreline; subsequent configurations extended it lagoonward to varying lengths, as shown in Table 10.

Table 10. Extension of the reef flat plate under island

| Simulation | Extent of Plate (m) |
|------------|---------------------|
| 1 | 0 |
| 2 | 25 |
| 3 | 50 |
| 4 | 100 |
| 5 | 200 |
| 6 | 300 |
| 7 | 350 |

Figure 29 shows the results of these simulations, and illustrates that the extent of the reef flat plate has a minimal effect on the maximum depth of the freshwater lens. If the reef plate is present, the span of the plate underneath the island has no perceptible influence on the depth of the freshwater lens.

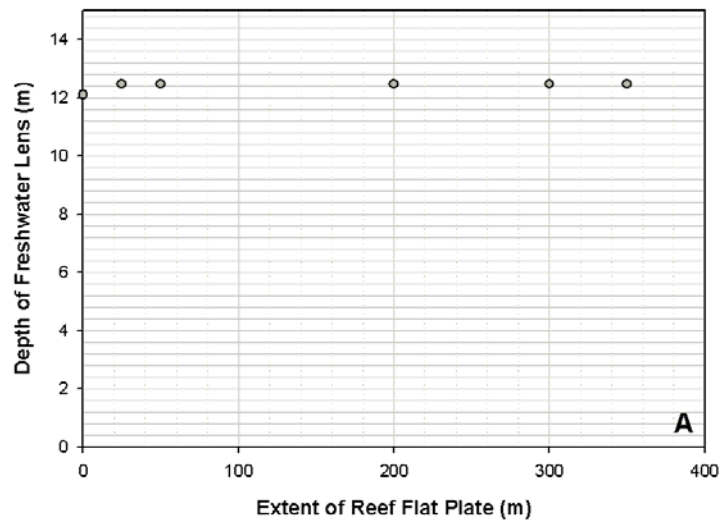


Figure 28. The thickness of the lens as the reef flat plate is extended to various distances across the atoll islands. The thickness is minimally affected.

Hydraulic Conductivity of the Reef Flat Plate

Thirteen simulations were run to observe the influence of the reef flat plate hydraulic conductivity on the maximum thickness of the freshwater lens. All simulations used an island width of 400 meters, with a reef flat plate extending halfway across the island. The hydraulic conductivity of the reef plate was varied from 0.050 m day^{-1} to 50 m day^{-1} . The hydraulic conductivity of the reef flat plate has an insignificant effect on the thickness of the freshwater lens (Figure 30), with the thickness of the lens only increasing about 0.1 meter when hydraulic conductivity is reduced from 50 m day^{-1} to 0.05 m day^{-1} .

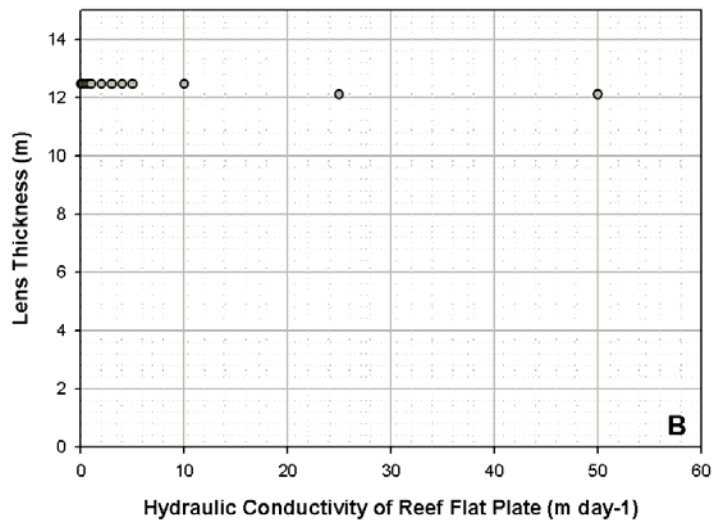


Figure 29. The thickness of the lens as the reef flat plate hydraulic conductivity is varied. The thickness is minimally affected.

Sensitivity Analysis

The results from the preceding simulations were analyzed to produce a sensitivity analysis of the parameter values, calculating the change in the thickness of the lens per the change in the parameter value (Figure 31). The depth to the Thurber Discontinuity and the hydraulic conductivity of the Holocene deposits has the greatest influence on the thickness of the freshwater lens, followed by the width of the island and the annual recharge rate.

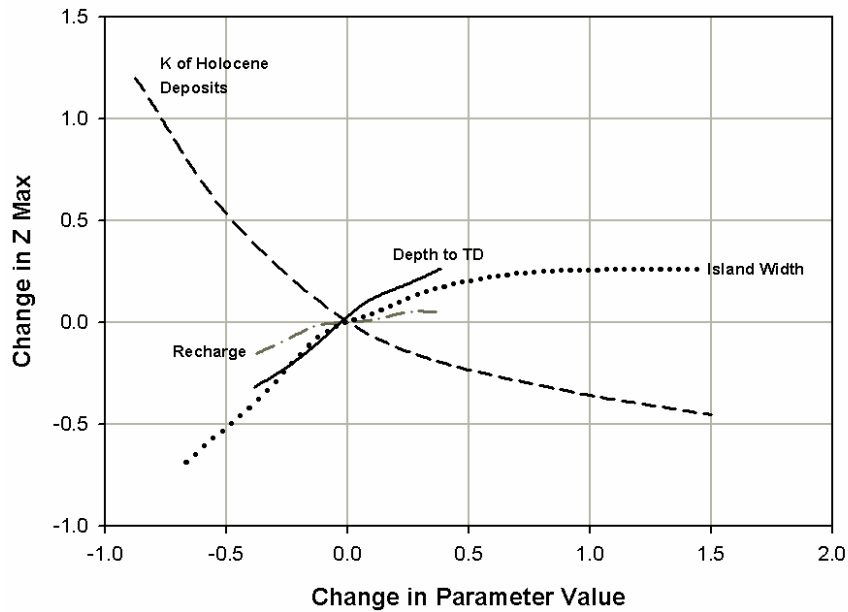


Figure 30. Sensitivity analysis of the parameters analyzed in the steady-state simulations. The depth to the Thurber Discontinuity has the greatest change in lens thickness per change in parameter value, followed by the hydraulic conductivity, the width of the island, and the recharge rate.

TRANSIENT SIMULATIONS

Transient Conditions

The freshwater lens is rarely at steady-state. Daily and seasonal weather conditions and tidal fluctuations each have an important influence on the thickness and geometry of the freshwater lens. Accordingly, transient simulations were run using SUTRA in order to model the behavior of the lens through time. Long-term transient observation data of the freshwater lens on atoll islands is not available. However, the matching of the steady-state simulation results with observed lens depths provides confidence that the physics and parameters used in the steady-state model are an acceptable approximation of the actual system.

Most parameters of the transient simulations are identical to the steady-state simulations (Table 5). The boundary conditions, however, were varied through time to simulate changing daily recharge at the water table and tides on both the lagoon and ocean sides. These transient simulations were tailored to the weather and tide data from the regions of Yap and Pohnpei, as they provide representations of the weather patterns experienced in the Western and Eastern Caroline Islands, respectively. Daily weather data and hourly tide data were taken from these two islands, since such data are not available for individual atoll islands. It is assumed that the temperatures, precipitation events and tidal fluctuations experienced on Yap and Pohnpei extend to their neighboring outer islands.

Time-Variable Boundary Conditions

Time-Variable Recharge and Recharge Model

The SUTRA code was modified to handle time-variable recharge. The subroutine retrieves a recharge value [M/T] for each timestep and distributes it evenly across the source nodes, taking into account the number of nodes contained within the fluid source boundary. This enables the same input file to be used for simulations of various island widths. Daily recharge was calculated using the method described by Falkland (1994). Table 11 contains the parameter values of the model.

Table 11. Parameter Values for Daily Recharge Model (after Falkland 1994)

| Parameter | Value |
|-------------------------|------------|
| Vegetation Interception | 1 mm day-1 |
| Soil Zone Thickness | 500 mm |
| Soil Field Capacity | 75 mm |
| Soil Wilting Point | 25 mm |

Daily temperature values were taken from Pohnpei and Yap for the years 1994-2004, as recorded by the National Oceanic and Atmospheric Administration (NOAA). Coconut root transpiration from the lens was included by assuming that the maximum value of the daily evapotranspiration rate, as calculated by the Thornwaite (1948) method, was extracted from the lens on days of no recharge. The maximum value was chosen to provide a conservative estimate of recharge. Table 12 contains a spreadsheet example of

Table 12. Daily recharge calculations for May 2000, using Yap daily rainfall and weather data, and the Thornwaite evapotranspiration calculation

| Day | Rainfall (mm) | Interception Storage (mm) | Effective Rainfall (mm) | Potential ET (mm) | Excess Moisture (mm) | Moisture (mm) | Moisture Deficit (mm) | Recharge (mm) |
|--------------|---------------|---------------------------|-------------------------|-------------------|----------------------|---------------|-----------------------|---------------|
| 1 | 0.00 | 1.00 | 0.00 | 5.04 | -5.04 | 73.83 | 1.17 | -5.04 |
| 2 | 2.29 | 1.00 | 1.29 | 4.53 | -3.24 | 75.63 | -0.63 | 0.63 |
| 3 | 49.78 | 1.00 | 48.78 | 3.99 | 44.79 | 119.79 | -44.79 | 44.79 |
| 4 | 66.80 | 1.00 | 65.80 | 3.78 | 62.02 | 137.02 | -62.02 | 62.02 |
| 5 | 0.76 | 1.00 | 0.00 | 4.51 | -4.51 | 70.49 | 4.51 | -4.51 |
| 6 | 6.35 | 1.00 | 5.35 | 4.39 | 0.96 | 75.96 | -0.96 | 0.96 |
| 7 | 4.06 | 1.00 | 3.06 | 4.53 | -1.47 | 73.53 | 1.47 | -4.53 |
| 8 | 6.35 | 1.00 | 5.35 | 4.39 | 0.96 | 79.02 | -4.02 | 4.02 |
| 9 | 2.79 | 1.00 | 1.79 | 4.45 | -2.66 | 72.34 | 2.66 | -4.45 |
| 10 | 28.96 | 1.00 | 27.96 | 4.12 | 23.84 | 100.63 | -25.63 | 25.63 |
| 11 | 25.40 | 1.00 | 24.40 | 3.86 | 20.54 | 95.54 | -20.54 | 20.54 |
| 12 | 6.60 | 1.00 | 5.60 | 4.12 | 1.48 | 76.48 | -1.48 | 1.48 |
| 13 | 11.43 | 1.00 | 10.43 | 4.70 | 5.73 | 80.73 | -5.73 | 5.73 |
| 14 | 6.35 | 1.00 | 5.35 | 4.51 | 0.84 | 75.84 | -0.84 | 0.84 |
| 15 | 4.06 | 1.00 | 3.06 | 4.51 | -1.45 | 73.55 | 1.45 | -4.51 |
| 16 | 80.77 | 1.00 | 79.77 | 4.53 | 75.24 | 153.30 | -78.30 | 78.30 |
| 17 | 0.76 | 1.00 | 0.00 | 4.93 | -4.93 | 70.07 | 4.93 | -4.93 |
| 18 | 1.02 | 1.00 | 0.02 | 4.63 | -4.61 | 70.39 | 4.61 | -4.63 |
| 19 | 7.11 | 1.00 | 6.11 | 4.20 | 1.91 | 76.93 | -1.93 | 1.93 |
| 20 | 9.14 | 1.00 | 8.14 | 4.58 | 3.56 | 78.56 | -3.56 | 3.56 |
| 21 | 0.00 | 1.00 | 0.00 | 4.45 | -4.45 | 70.55 | 4.45 | -4.45 |
| 22 | 9.91 | 1.00 | 8.91 | 4.51 | 4.40 | 79.40 | -4.40 | 4.40 |
| 23 | 1.27 | 1.00 | 0.27 | 4.51 | -4.24 | 70.76 | 4.24 | -4.51 |
| 24 | 48.77 | 1.00 | 47.77 | 4.39 | 43.38 | 118.65 | -43.65 | 43.65 |
| 25 | 12.45 | 1.00 | 11.45 | 4.21 | 7.24 | 82.24 | -7.24 | 7.24 |
| 26 | 7.87 | 1.00 | 6.87 | 4.28 | 2.59 | 77.59 | -2.59 | 2.59 |
| 27 | 143.76 | 1.00 | 142.76 | 3.92 | 138.84 | 213.84 | -138.84 | 138.84 |
| 28 | 1.02 | 1.00 | 0.02 | 4.53 | -4.51 | 70.49 | 4.51 | -4.53 |
| 29 | 5.33 | 1.00 | 4.33 | 4.32 | 0.01 | 75.03 | -0.03 | 0.03 |
| 30 | 5.08 | 1.00 | 4.08 | 4.44 | -0.36 | 74.64 | 0.36 | -4.44 |
| 31 | 0.00 | 1.00 | 0.00 | 4.63 | -4.63 | 74.45 | 0.55 | -4.63 |
| TOTAL | 556.24 | | | | | | | 392.03 |

the model, showing daily recharge calculations for the Yap region for May 2000. Figure 32 shows the calculated recharge for the year 2000 on Yap.

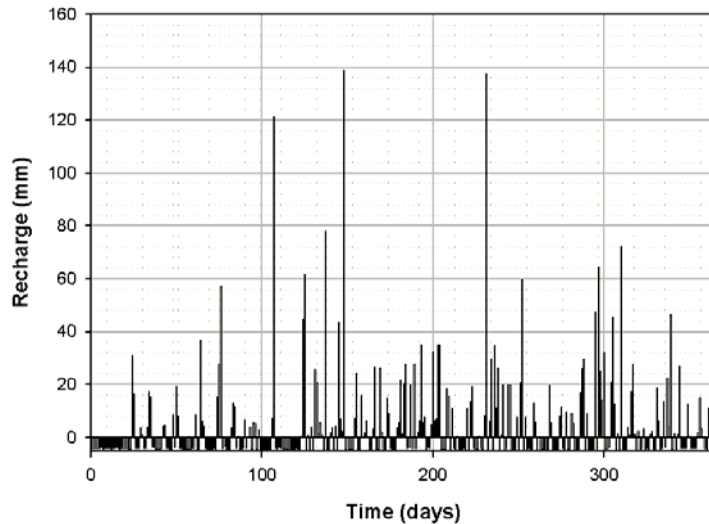


Figure 31. Daily recharge for Yap, 2000

Time-Variable Pressure

Hourly tide data were provided by the University of Hawaii Sea Level Center for the islands of Yap and Pohnpei for 1994-2004. These data were added to the static specified pressure values given to the modified SUTRA code.

Influence of the Reef Flat Plate on Simulation Results

Two simulations were run to observe the difference in the lens with and without a reef flat plate. A 400-m wide island was also simulated for this experiment. The results (Figure 35) for the years 1997-2000 show that the reef flat plate causes a consistently deeper lens than would be present if there were no confining layer, with the difference in freshwater lens depth of about 1.0 to 1.5 m. The reef flat plate was included in all transient simulations.

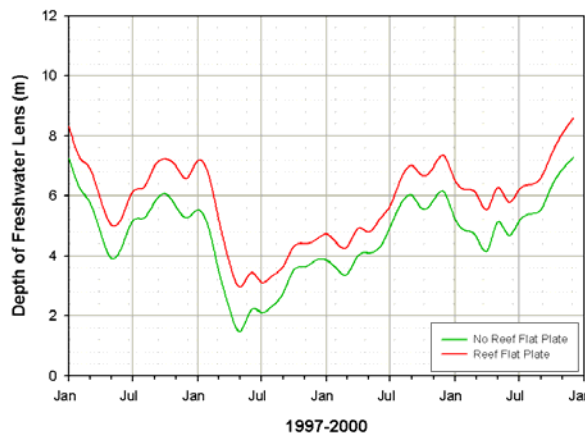


Figure 32. Effect of including the reef flat plate on the freshwater lens

Simulations and Results

Table 13 summarizes the transient simulations. A reef flat plate, extending from the ocean reef to halfway under the island, was included in every simulation. Two different sets of simulations were run, one for rainfall rates similar to those experienced in the region of Yap, in western FSM, and another for rainfall rates similar to those experienced in the region of Pohnpei, in eastern FSM, with hourly tidal values from each island used for their respective simulations. Two different subsets of simulations were run at various island widths (200, 400, and 600 meters) within each of these main sets, one for hydraulic conductivity rates found on leeward islands and another for hydraulic conductivity rates found on windward islands. In the steady-state simulations (Figure 23), these values were found to be 50 and 400 m day⁻¹, respectively. For each island model one simulation was run to replicate average annual seasonal variation, and another simulation used rainfall and tide data for the El Niño event of 1997-1998.

For each simulation the depth of the freshwater lens was defined as the point at which the concentration of the water was equivalent to the potable limit of freshwater, 0.00089 kg salt / kg water, equivalent to a chloride concentration of 500 mg L⁻¹ (Lloyd et al., 1980).

Table 13. Summary of transient simulations

| Simulation | Region | Island Width | Island Type | Type |
|-------------------|---------------|---------------------|--------------------|----------------------|
| 1 | East | 200 | Leeward | Seasonal Fluctuation |
| 2 | East | 200 | Leeward | El Niño |
| 3 | East | 200 | Windward | Seasonal Fluctuation |
| 4 | East | 200 | Windward | El Niño |
| 5 | East | 400 | Leeward | Seasonal Fluctuation |
| 6 | East | 400 | Leeward | El Niño |
| 7 | East | 400 | Windward | Seasonal Fluctuation |
| 8 | East | 400 | Windward | El Niño |
| 9 | East | 600 | Leeward | Seasonal Fluctuation |
| 10 | East | 600 | Leeward | El Niño |
| 11 | East | 600 | Windward | Seasonal Fluctuation |
| 12 | East | 600 | Windward | El Niño |
| 13 | West | 200 | Leeward | Seasonal Fluctuation |
| 14 | West | 200 | Leeward | El Niño |
| 15 | West | 200 | Windward | Seasonal Fluctuation |
| 16 | West | 200 | Windward | El Niño |
| 17 | West | 400 | Leeward | Seasonal Fluctuation |
| 18 | West | 400 | Leeward | El Niño |
| 19 | West | 400 | Windward | Seasonal Fluctuation |
| 20 | West | 400 | Windward | El Niño |
| 21 | West | 600 | Leeward | Seasonal Fluctuation |
| 22 | West | 600 | Leeward | El Niño |
| 23 | West | 600 | Windward | Seasonal Fluctuation |
| 24 | West | 600 | Windward | El Niño |

Average Seasonal Variation

Daily rainfall was averaged for each day over 1994-2005 to obtain the average rainfall value for each day. The same was done for hourly tide data. Simulations were run for various island widths, on both the leeward and windward side of the atoll. The model results show the fluctuation of the freshwater lens for a typical year in the Eastern Caroline region (Figure 36). Figure 37 compares the results of the Yap and Pohnpei regions.

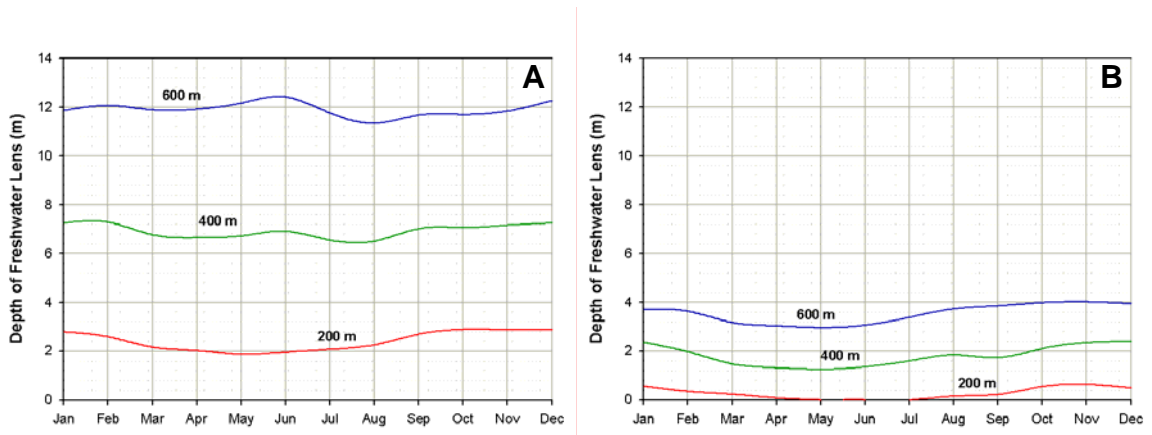


Figure 33. Thickness of the lens as it responds to regular seasonal rainfall variation, for (A) leeward islands and (B) windward islands located in the Western Caroline Islands. The windward islands, with a much higher hydraulic conductivity than leeward islands, have much thinner lenses. The lens of the 200 m wide windward island is altogether depleted during the dry summer months.

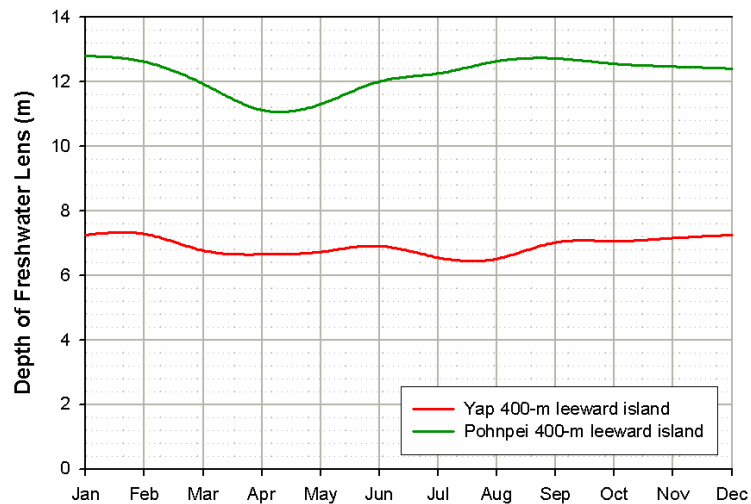


Figure 34. Comparison of lens behavior between leeward islands located in the Western Caroline region (Yap) and the Eastern Caroline region (Pohnpei).

El Niño Event

Daily recharge and hourly tide data were used from 1997-2000 in order to show the condition of the freshwater lens before, during, and after an El Niño event. Figure 38 shows the monthly rainfall values during 1997-1999. The letters A, B, C, D and E correspond to maximum and minimum thicknesses of the lens (Figures 39-40) at the following points in time:

- A.** January 1997 – Condition of the lens before the El Niño event.
- B.** May 1997 – Minimum lens thickness during the El Niño year.
- C.** January 1998 – Maximum lens thickness during 1997-1998.
- D.** June-July 1998 – Absolute minimum of the lens thickness during 1997-1998, corresponding to the peak of the drought.
- E.** December 1999 – Full recovery of the lens.

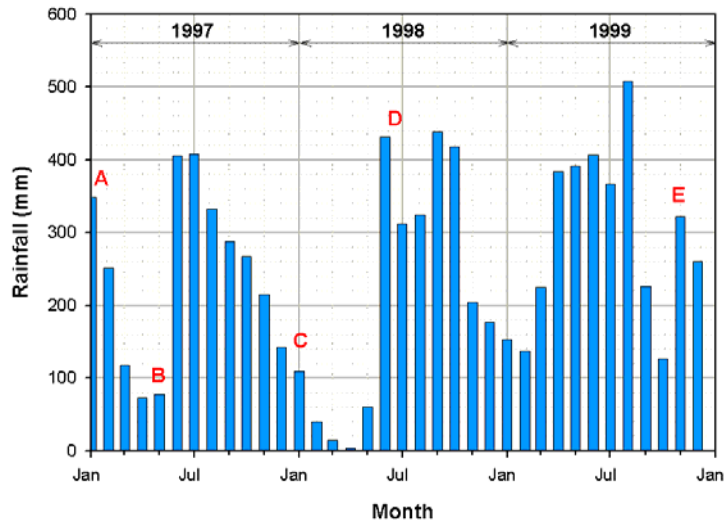


Figure 35. Monthly rainfall during the El Niño event of 1997-1999 in the Western Caroline region (using Yap rainfall and weather data). The points in time labeled A, B, C, D and E correspond to maxima and minima thicknesses experienced by the freshwater lens, as shown in Figure 39.

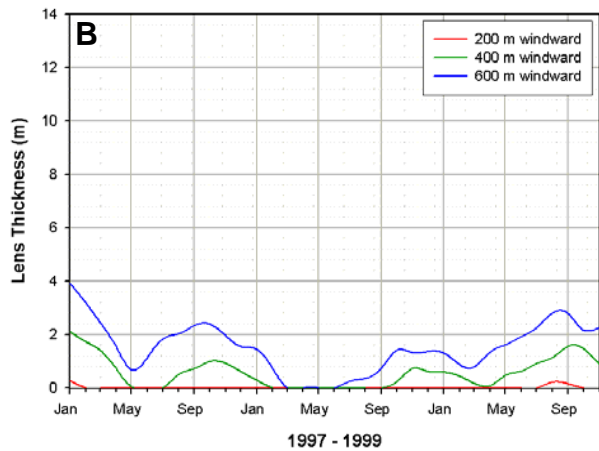
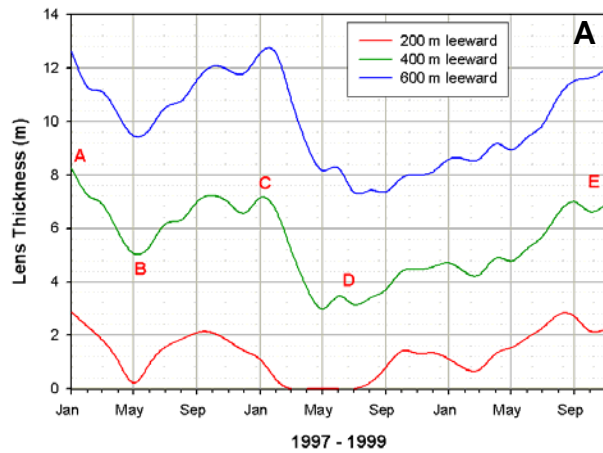


Figure 36. Thickness of the lens as it responds to an El Niño event, for (A) leeward islands and (B) windward islands located in the Western Caroline Islands. The windward islands, with a much higher hydraulic conductivity than leeward islands, have much thinner lenses.

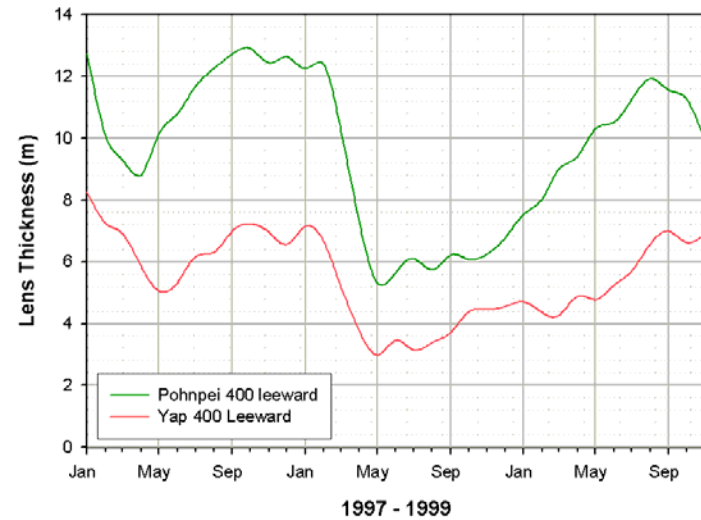


Figure 37. Comparison of lens thickness during the 1997-1998 El Niño event between Western Caroline islands (using Yap data) and Eastern Caroline islands (using Pohnpei data).

The results of the El Niño simulations demonstrate the following:

- The lens experiences a dramatic decrease in lens thickness during time of drought, and about one and a half years of normal weather conditions are required to bring the freshwater lens back into its average state.
- The amount of rainfall and the location of the island on the atoll ring exert a strong influence on the behavior of the lens. Atolls in the Eastern Caroline region, due to higher total rainfall throughout the year, will generally have lenses that are much thicker than those found in the Western Caroline region. Also, the freshwater lens on a windward island will be depleted much more rapidly than those on leeward islands, and will in some cases be completely contaminated. Figure 41 compares the average seasonal lens fluctuation with that of 1997-1999 for the Western Caroline region.

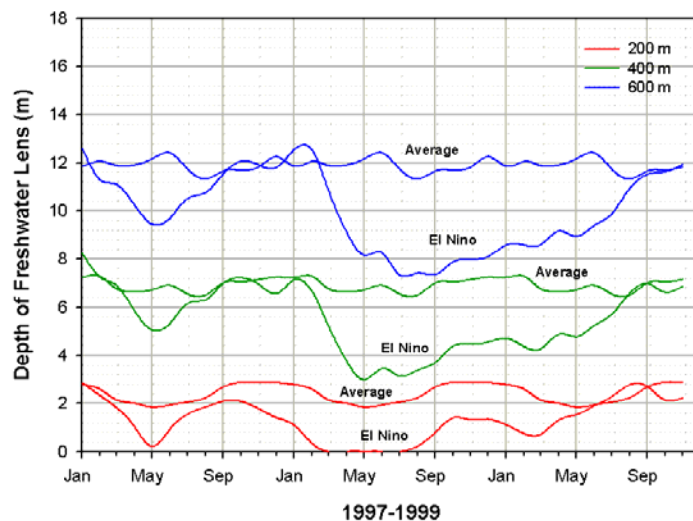


Figure 38. Comparison of the lens depth through time for average seasonal weather patterns and an El Niño event, in the Western Caroline region, for island widths of 200, 400, and 600 m. The upper and lower curves for each island width correspond to average and El Niño conditions, respectively.

Washover Event

A washover event was simulated by placing 0.328 m (1 foot) of standing seawater across the width of the island for two days, after which normal rainfall conditions occurred. The shape and maximum depth of the freshwater lens were monitored throughout the simulation to view the progress of the lens. The level and pattern of contamination and recovery are spatially dependent due to the presence of the reef flat plate. During the first 48 hours the unconfined portion of the freshwater lens becomes contaminated (Figure 43 a-c) while the confined region, under the reef flat plate, is able to maintain a nucleus of freshwater throughout the entire simulation, although a thin layer of the lens immediately underneath the plate is contaminated. Freshwater begins to accumulate in the unconfined portion after 2 months (Figure 43e), but one year is required for the full recovery of the lens in the unconfined region (Figures 43g) after which the expected seasonal fluctuation of the lens commences. The lens recovery for the unconfined portion is also presented in Figure 44.

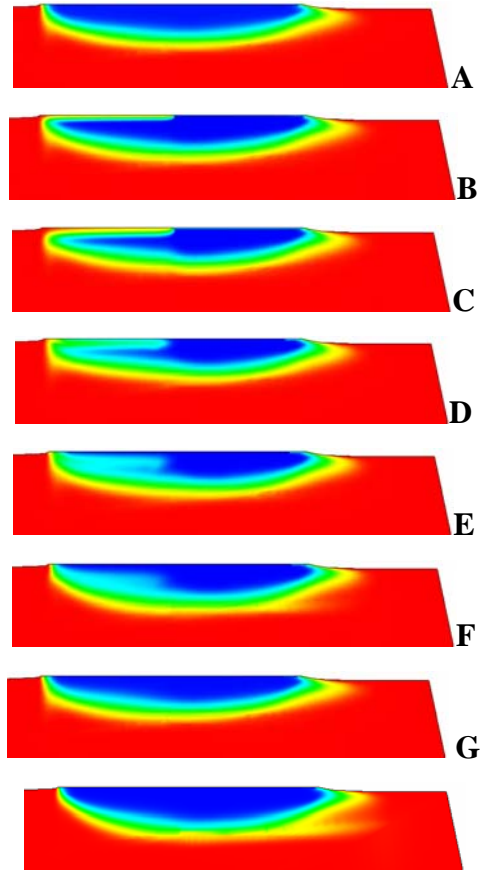


Figure 39. Contamination and recovery of the freshwater lens from a 48-hour washover event, at (A) initial conditions, (B) 16 hours, (C) 48 hours, (D) 1 month, (E) 2 months, (F) 4 months, (G) 1 year, (H) and 1 ½ years. The portion of the lens on the ocean side, underneath the reef flat plate, is protected from contamination.

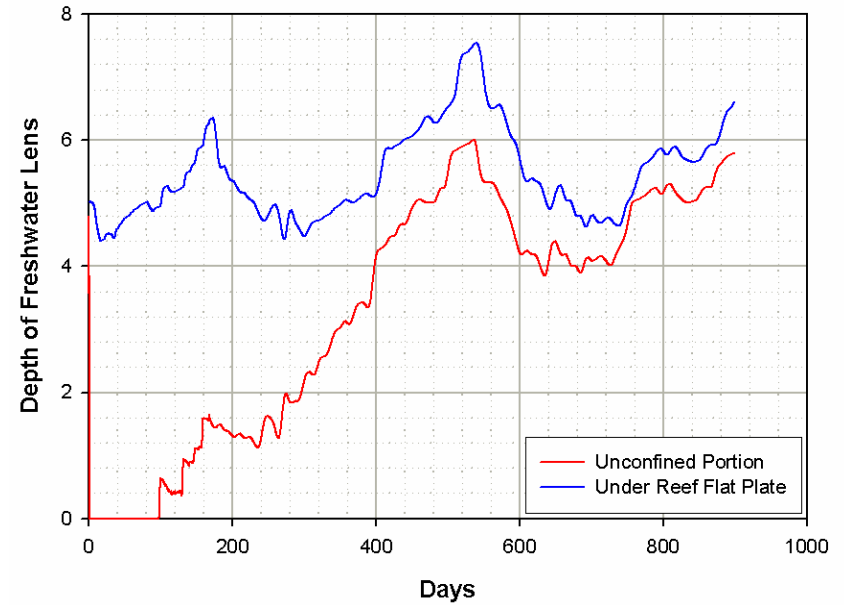


Figure 40. Recovery of the freshwater lens after a two-day washover event, (blue) underneath the reef flat plate, on the ocean side, and (red) in the unconfined region on the leeward side

APPLICATIONS

The main purpose of this study is to provide water resources managers of atoll islands with an accurate method to estimate the quantity of available groundwater for an atoll island. This chapter outlines the development of such a method.

Algebraic Model for Steady-State Conditions

The results of the numerical simulations were used to develop the following algebraic model. The model relates the maximum thickness of the freshwater lens to the parameters analyzed in the simulations. The underlying assumptions of the model are that the lens thickens with increasing recharge and island width, thins with increasing hydraulic conductivity, and is limited by the Thurber Discontinuity.

$$Z_{MAX} = \left[Y + \frac{(Z_{TD} - Y)R}{B + R} \right] (K)(C) \quad (6)$$

where

| | | |
|-------------|---|---|
| Z_{MAX} | = | Maximum depth of the freshwater lens for the island, in m [L] |
| R | = | Annual recharge rate, in $m\ yr^{-1}$ [$L\ T^{-1}$] |
| $Y\ and\ B$ | = | Parameters dependent on the width of the island [-] |
| Z_{TD} | = | Depth to the Thurber Discontinuity, in m [L] |
| K | = | Hydraulic Conductivity parameter [-] |
| C | = | Confining (reef flat plate) parameter [-] |

The above model can be divided into two main parts: first, a hyperbolic curve that determines the thickness of the lens according to the recharge rate, island width, and the Thurber Discontinuity; and second, a set of factors which either dampen or enhance the thickness provided by the hyperbolic curve.

Hyperbolic Curve

The hyperbolic curve describes the increase in lens thickness due to recharge and island width, and the limit of that increase due to the Thurber Discontinuity (Figure 45). Initially, when the lens is very shallow, an increase in the recharge rate brings about a proportional increase in the thickness of the lens. As the lens thickens, however, the rate of increase diminished, eventually ceasing altogether. This phenomenon has two principal parts: the initial decrease in the slope of the lens thickness/recharge relationship, followed by a truncation of the lens at the Thurber Discontinuity. The cause of the initial decrease in the slope of the lens thickness/recharge relationship occurs on any island containing a freshwater lens. Water mounding in the middle of the island is directed towards the coast according to the hydraulic gradient. As more rainfall infiltrates the soil and recharges the lens, more water is piled up, and the hydraulic head increases. However, with increasing head there is also an increase in hydraulic gradient, and thus an increase in specific discharge (Table 14).

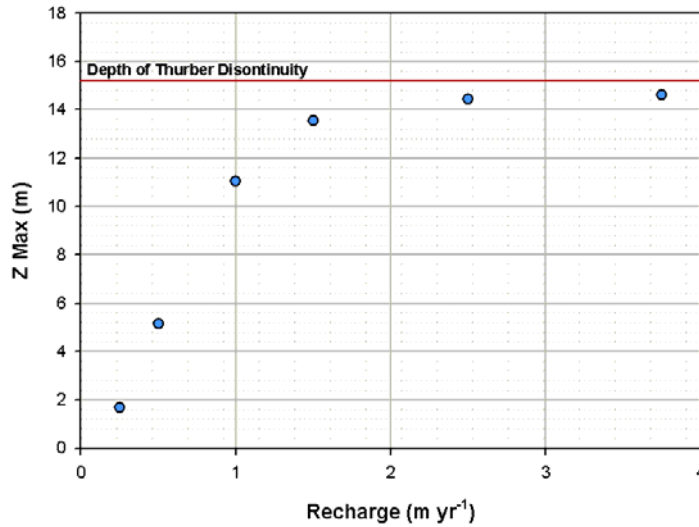


Figure 41. Relationship between the recharge rate and the corresponding maximum depth of the lens. Island width = 600 m. The relationship is relatively linear at low recharge rates. At higher recharge the rate of increase diminishes until it ceases altogether, at which point the lens has reached the Thurber Discontinuity.

Table 14. Hydraulic head at the middle of the island and the associated discharge velocity of the water at the coast, for varying recharge rates (Island width = 600 m). The discharge velocity increases with the recharge rate, thus conducting freshwater out of the system at a higher rate and slowing down the thickening of the lens.

| Recharge Rate (m yr ⁻¹) | Hydraulic Head (cm) | Discharge Velocity (cm s ⁻¹) |
|--|------------------------|---|
| 0.25 | 15.99 | 0.00228 |
| 0.5 | 25.59 | 0.00379 |
| 1 | 37.80 | 0.00582 |
| 1.5 | 42.50 | 0.00706 |
| 2.5 | 46.33 | 0.00830 |
| 3.75 | 48.82 | 0.00908 |

This increase in discharge slows down the rate of increase in the hydraulic head with respect to the increase in recharge. The hydraulic head, based on density differences between freshwater and seawater, dictates the depth of the lens to the freshwater/seawater interface. Thus, the thickness of the lens also increases at a slower rate.

The following hyperbolic curve was superimposed on the numerically calculated lens thickness values (Figure 46). The parameter values for Y_0 , a , and b were -11.5849, 29.2361, and 0.3175, respectively.

$$Y = Y_o + \frac{aX}{b + X} \quad (7)$$

Where:

- X = Input to the system (recharge to the freshwater lens)
- Y = Variable measured (thickness of the lens), and
- Y_o , a, and b are fitting terms.

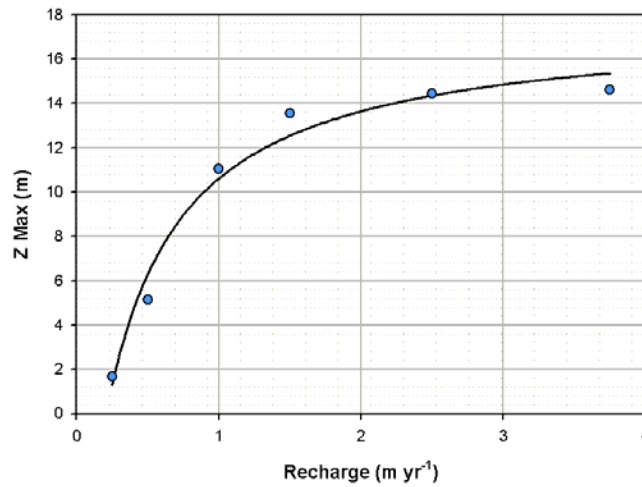


Figure 42 Hyperbolic fit to recharge/maximum lens depth relationship

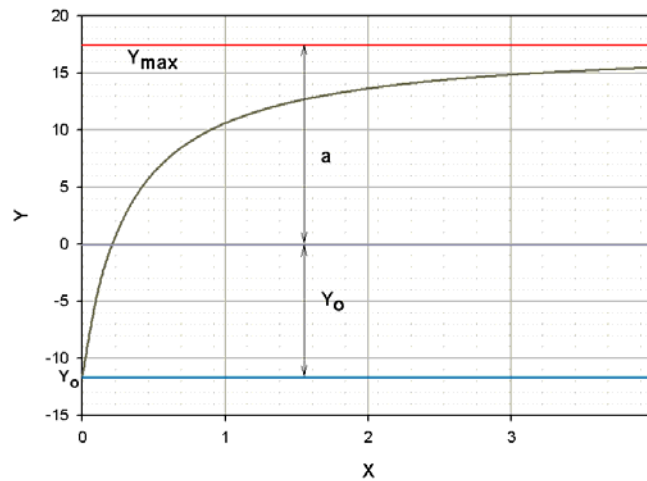


Figure 43 Graphical definition of terms in hyperbolic equation. Note that the limiting value of Y is $Y_o + a$.

Note that the limit of Y , as X approaches infinite, is $Y_o + a$ (Figure 47); thus

$$Y_{MAX} = Y_o + a \quad (8)$$

where Y_{MAX} is the limiting value of Y . Similarly, the limiting thickness of the freshwater lens is the depth to the Thurber Discontinuity. The lens can only be as thick as the depth to the discontinuity, regardless of recharge or island width. Thus:

$$Z_{TD} = Y_{MAX} = a + Y_o \quad (9)$$

where Z_{TD} is the depth to the Thurber Discontinuity. And by rearrangement of (9):

$$a = Z_{TD} - Y_o \quad (10)$$

and by substitution into equation (7):

$$Y = Y_o + \frac{(Z_{TD} - Y_o)X}{b + X} \quad (11)$$

and replacing the parameters with the terms common to hydrological studies:

$$Z_{MAX} = Y + \frac{(Z_{TD} - Y)R}{B + R} \quad (12)$$

where:

| | | |
|-------------|---|--|
| Z_{MAX} | = | Maximum thickness of the lens, in m |
| R | = | Recharge to the freshwater lens, in $m\ yr^{-1}$ |
| Z_{TD} | = | Depth to the Thurber Discontinuity, in m |
| Y and B | = | Constants, dependent on island width |

Using the fit of the hyperbolic equation to recharge/lens thickness relationships for various island widths, trends for the B and Y terms were established, thus generalizing the trend to a range of islands widths. For example, a power function was fit to the values of B (Figure 48A). The use of this curve, however, over-estimated the lens thickness for islands with widths less than 400 m. From equation 12 we know that an increase in the value of B will decrease Y (the estimated value of the thickness of the lens). The curve was thus changed to produce higher values of B for small island widths (Figure 48A). Similarly, a logarithmic function was fit to the Y term values (Figure 48B). The curves (Figure 49) for the B and Y terms allow the lens thickness to be calculated for any island width.

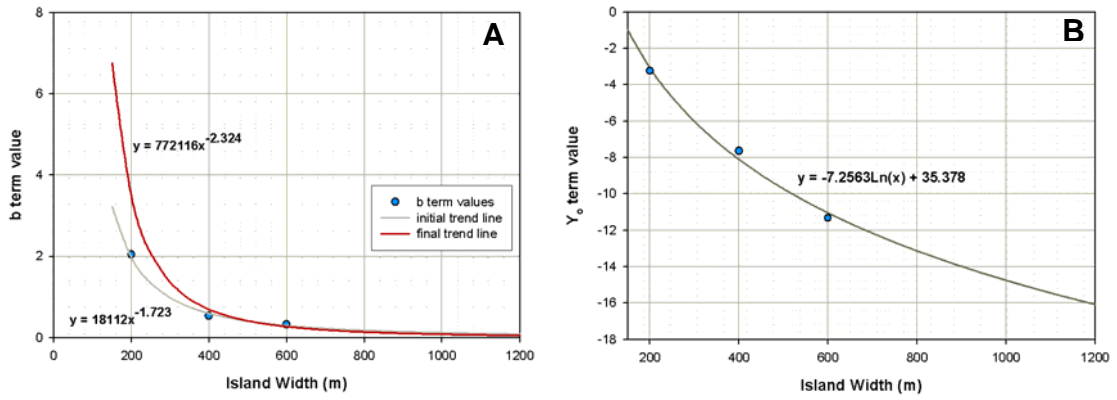


Figure 44. Curve-fitting to produce trends of (A) B parameter and (B) Y parameter

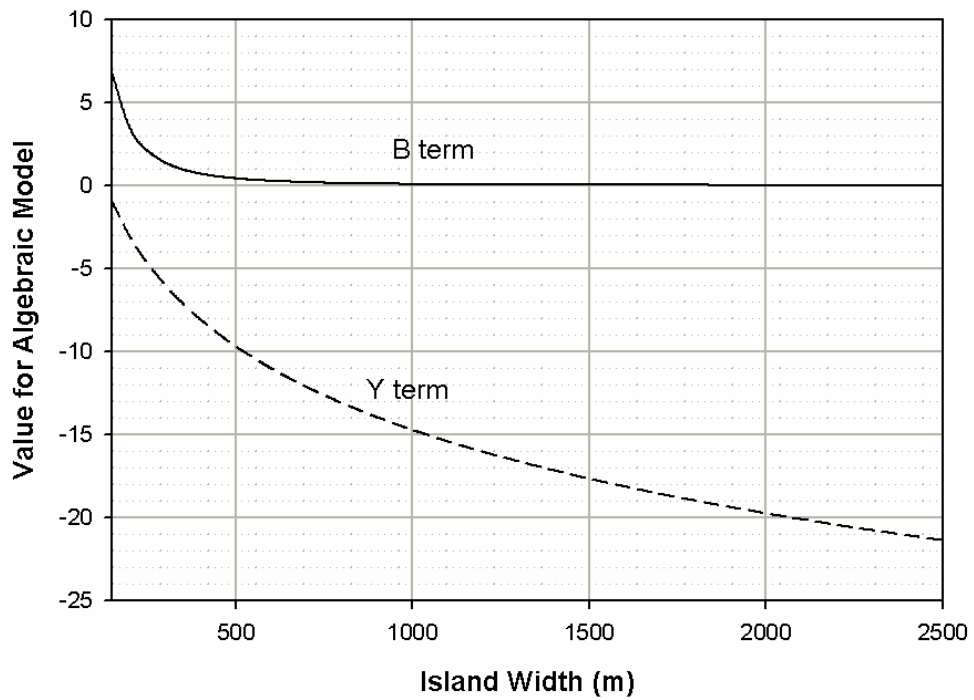


Figure 45. Curves for B and Y parameters of the Algebraic Model

Hydraulic Conductivity Factor

As noted previously, the hydraulic conductivity of the Holocene deposits has a large influence on the development of the freshwater lens. An equation which estimates the thickness of the lens must also include this variable. To do so the results from the steady-state simulation involving the variation of hydraulic conductivity were used to create values for a hydraulic conductivity term which could be included in equation (12):

$$Z_{MAX} = \left[Y + \frac{(Z_{TD} - Y)R}{B + R} \right] (K) \quad (13)$$

where:

K = Hydraulic Conductivity factor [-], with the rest of the terms as defined previously.

In the *Steady-State Simulations* it was shown that the hydraulic conductivity of the Holocene deposits is 50 m day⁻¹ on leeward islands, and 400 m day⁻¹ on windward islands. Ideally, however, values for any hydraulic conductivity would be available. Table 15 contains the results from the simulations for an island width of 500 m.

Table 15. Hydraulic Conductivity of Holocene Deposits and associated Depth to the Freshwater/Seawater Interface (Island Width = 500 m).

| Hydraulic Conductivity m day ⁻¹ | Maximum Depth to Interface m | Factor |
|---|------------------------------------|-------------|
| 25 | 15.0 | 1.1 |
| 50 | 13.4 | 1.00 |
| 100 | 10.5 | 0.78 |
| 200 | 6.8 | 0.51 |
| 300 | 5.2 | 0.39 |
| 400 | 4.4 | 0.32 |
| 500 | 3.7 | 0.27 |

The results in the table show that the thickness of the lens decreases significantly with increasing hydraulic conductivity. The hydraulic conductivity factor to be placed in equation (13) is presented in the third column of Table 15. The factor values were normalized to a hydraulic conductivity value of 50 m day⁻¹ since this value represents leeward islands. As an example calculation, the factor for the fourth row, with $K = 200$ m day⁻¹, was calculated by taking the lens thickness from the simulation, 6.818 m, and dividing it by the lens thickness from the simulation wherein $K = 50$ m day⁻¹ was used, 13.410 m, to give a value 0.51. This value is used in equation 14, and thus estimates the maximum depth of the lens on an island wherein the hydraulic conductivity of the Holocene sediments is 200 m day⁻¹.

As performed for the B and Y factors (see previous section), a curve is fit to the factor values in Table 15 (Figure 50A). This curve is then used to determine the

hydraulic conductivity factor for any value of hydraulic conductivity. This process was performed for all simulation island widths (150, 200, 300, 400, 500, 600, 800, and 100 m), with the results summarized in Figure 50B. These relationships are also shown in Figure 51, with the width of the island as the independent variable.

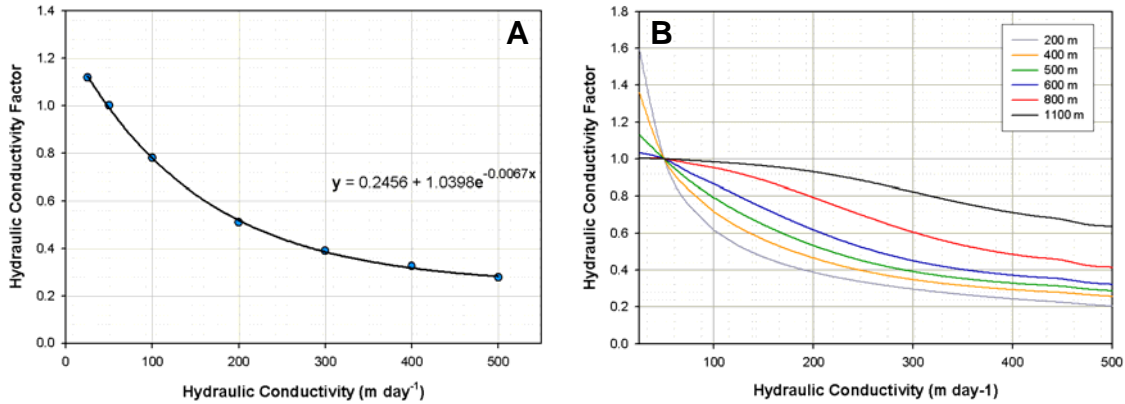


Figure 46. (A) Trend between the hydraulic conductivity of the Holocene sediments and the associated hydraulic conductivity factor, for an island width of 500 m, and (B) for each island width

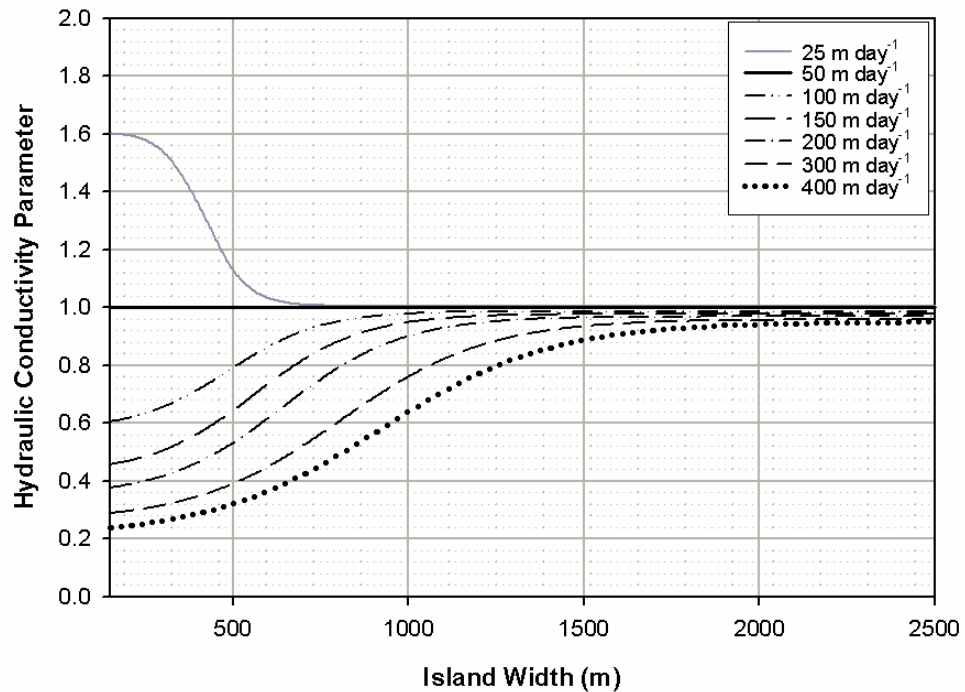


Figure 47. Relationship between the width of the island and the hydraulic conductivity factor, for various values of hydraulic conductivity

Reef Flat Plate Parameter

The presence of the reef flat plate has a small influence on the maximum depth of the freshwater lens (see *Steady-State Simulations* section). For small islands, such as the 150 m islands (see Table 16), the maximum depth of the lens increases from 4.0 m to 4.8 m with the presence of the confining reef flat plate, an increase of 18.75%. However, for large islands, such as the 1100 m islands, the effect is subdued, with an increase of only 1.00%, from 16.6 m to 16.7 m, an increase of only 0.60%. This trend is seen in the values of the fourth column of Table 16, which are calculated by dividing column 2 by column 3. As the width of the island increases, the factor approaches 1.000, meaning that there is a decreasing influence of the reef flat plate.

Table 16. Results of simulations, showing the maximum depth of the lens for conditions with and without a reef flat plate

| Island Width m | Max. Depth without RFP m | Max. Depth with RFP m | Factor |
|-------------------|--------------------------------|-----------------------------|--------|
| 150 | 4.000 | 4.750 | 0.842 |
| 200 | 5.800 | 6.560 | 0.884 |
| 300 | 8.600 | 9.600 | 0.896 |
| 400 | 12.000 | 13.000 | 0.923 |
| 500 | 13.410 | 13.940 | 0.962 |
| 600 | 14.722 | 14.251 | 0.968 |
| 800 | 15.488 | 15.256 | 0.985 |
| 1100 | 16.627 | 16.700 | 0.996 |

This curve is shown in Figure 52, which is a plot of the relationship between the reef flat plate factor and the width of the island.

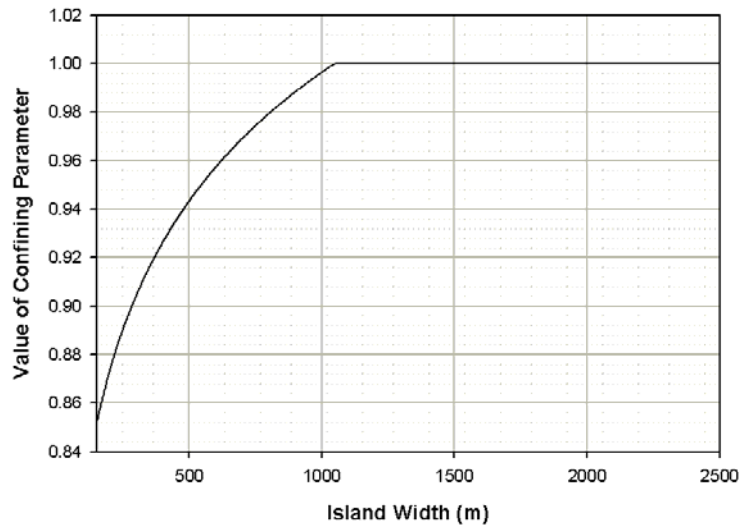


Figure 48. Relationship between the width of the island and the reef flat plate factor, which is the ratio of the lens thickness for islands with reef flat plates and those without. The influence of the reef flat plate in increasing the thickness of the lens decreases as the island width increases.

This relationship can be used to include a reef flat plate, or confining term, to equation (13):

$$Z_{MAX} = \left[Y + \frac{(Z_{TD} - Y)R}{B + R} \right] (K)(C) \quad (14)$$

where C is the confining term [-]. If the reef flat plate is present, the parameter receives a value of 1. If the plate is not present, the parameter value is determined by the curve presented in Figure 52.

Sensitivity Analysis

A sensitivity analysis of the parameters in the algebraic model (Figure 53) demonstrates the close fit between the results of the algebraic model and numerical simulations.

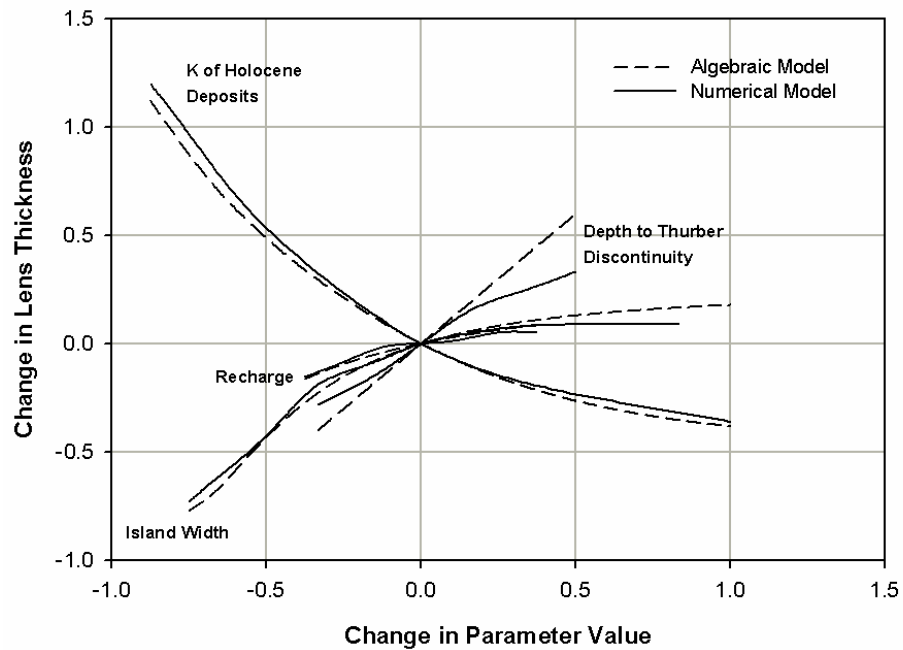


Figure 49. Comparison between the sensitivity of the parameters in the algebraic and numerical models. Only the derivative of the depth to Thurber Discontinuity parameter shows a deviation from the numerical results.

Comparison of Algebraic Model with numerical results

A comparison was made between the results from SUTRA and those from the algebraic model for both leeward and windward islands (Figure 54), using the hydraulic conductivity values of 50 and 400 m day⁻¹, respectively. The algebraic model was used repeatedly to calculate the maximum depth of the lens for island widths ranging from 150 m to 1200 m. Table 17 contains the values used in the algebraic model.

Table 17. Values of the terms used in the algebraic model, for both leeward and windward islands.

| Term | Leeward | Windward |
|-------------------------|--|---|
| R (m yr ⁻¹) | 2 | 2 |
| Z _{TD} (m) | 17.5 | 17.5 |
| B | Dependent on island size. | Use graph 48, using B curve. |
| Y | Dependent on island size. | Use graph 48, using Y curve. |
| K | Dependent on island size. Use graph 51, using 50 m day ⁻¹ curve | Dependent on island size. Use graph 51, using 400 m day ⁻¹ curve |
| C | 1 | 1 |

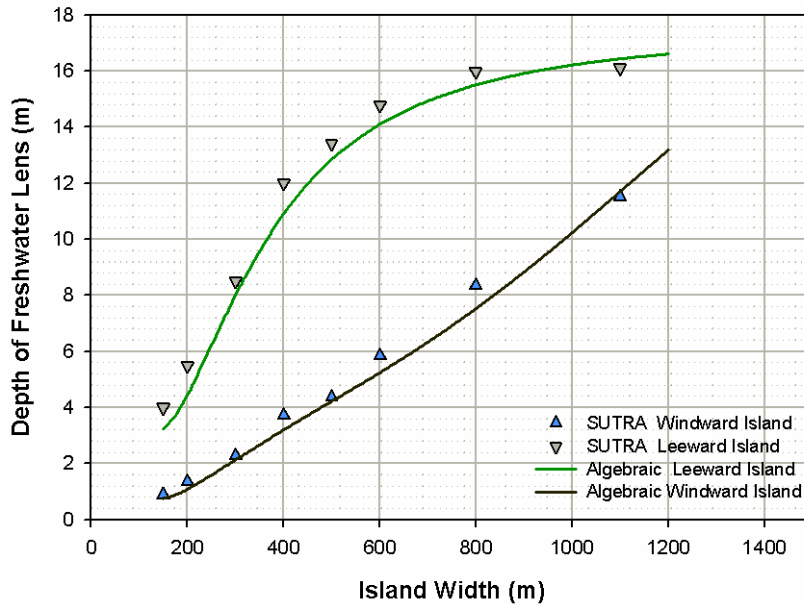


Figure 50. Comparison of SUTRA simulation results with the Algebraic model results. The SUTRA Leeward island simulations used a hydraulic conductivity value of 50 m day⁻¹, and the algebraic model used a K factor for a hydraulic conductivity value of 50 m day⁻¹. Similarly, the SUTRA Windward island simulations used a K hydraulic conductivity value of 400 m day⁻¹, and the algebraic model used K factors corresponding to a hydraulic conductivity value of 400 m day⁻¹.

Comparison of Algebraic Model Results to Observations

Figure 55 shows the affinity between the observed lens depths and the algebraic model results for leeward islands, using Thurber Discontinuity depths of 15, 17.5, and 20 m, which are typical depths, a recharge rate of 2 m yr^{-1} , and assuming that the reef flat plate is present. The curves passing through the observed depths of the leeward islands were created using a K factor corresponding to a hydraulic conductivity of 50 m day^{-1} (see Figure 23), while the curves passing through the observed depths of the windward islands use 400 m day^{-1} . As explained previously, however, the windward trend does not espouse as much confidence as the leeward trend, since several large windward islands do not contain a permanent freshwater lens. With all the inherent variability of atoll island geology, the model performs well. Curves using such as those presented in Figure 55 are a valuable tool in predicting the maximum lens thickness for leeward islands.

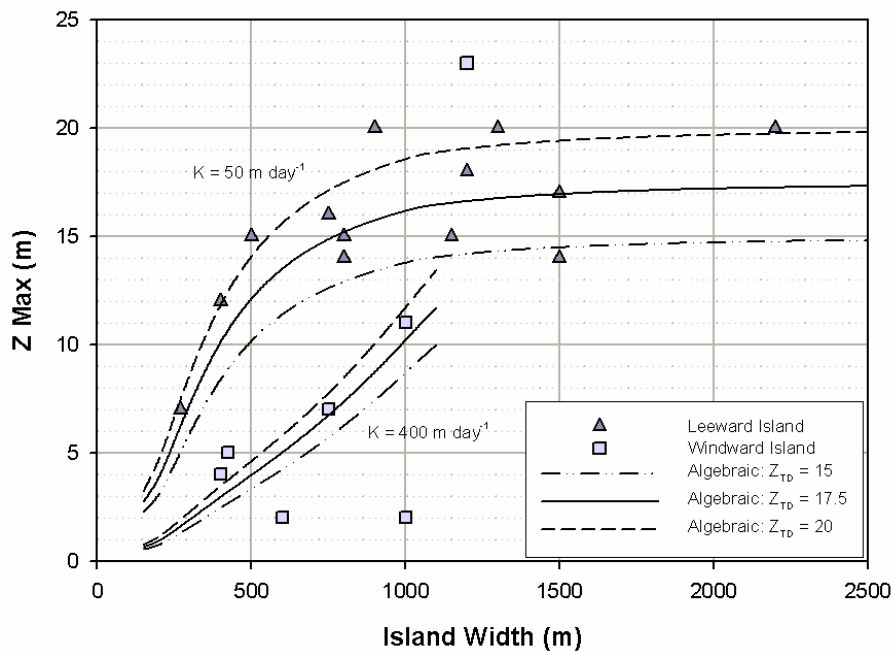
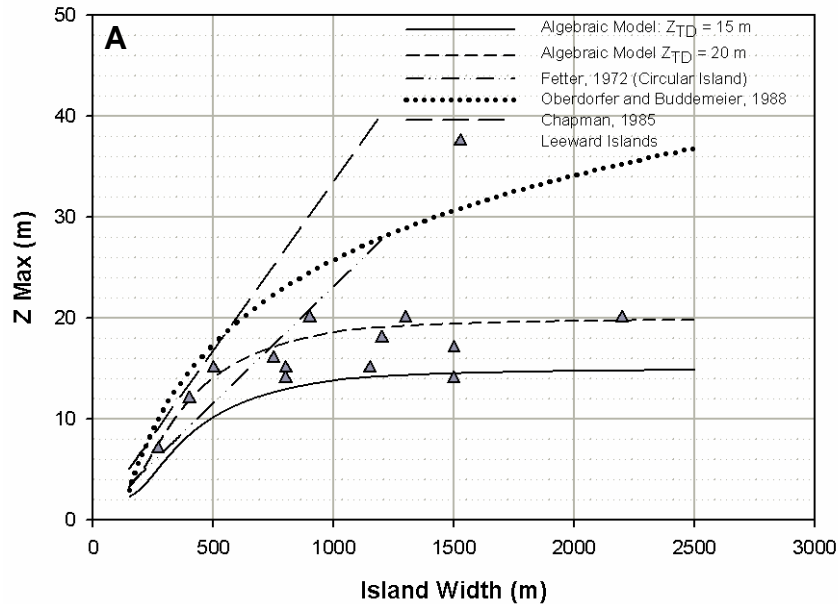


Figure 51. Comparison between observed lens maximum depths and results from the algebraic model. One curves used Thurber Discontinuity depths of 15, 17.5, and 20 m, which are typical depths. The curves passing through the leeward islands were created using a K factor corresponding to a hydraulic conductivity of 50 m day^{-1} , while the curves passing through the windward islands used 400 m day^{-1} .

Comparison of Algebraic Model with Analytical and Empirical Solutions

Figure 56 demonstrates the accuracy of the algebraic model in estimating the maximum thickness of the lens as compared to the analytical solutions of Fetter (1972) and Chapman (1985), and the empirical model of Oberdorfer and Buddemeier (1988). The solution for circular islands was used in the case for Fetter, since his infinite strip solution yields identical results to the solution of Chapman. For all the calculations the recharge rate was set at 2 m yr^{-1} (the depth of rainfall in the Oberdorfer and Buddemeier model was held at 4 m yr^{-1}), and the hydraulic conductivity value was held at 50 m day^{-1} and 400 m day^{-1} for the curves which pass through the leeward and windward islands, respectively. As seen in Figure 56A, the analytical and empirical models match the observed depths relatively well for small leeward islands. However, the match does not hold for large leeward atoll islands, wherein the Thurber Discontinuity limits the growth of the lens. This limiting feature is a key component of the algebraic model. Every model except for the Oberdorfer and Buddemeier model yields accurate results for windward islands (Figure 56B), since there is no provision in the model for hydraulic conductivity. Hence, the analytical solutions of Fetter and Chapman can be used for windward atoll islands.



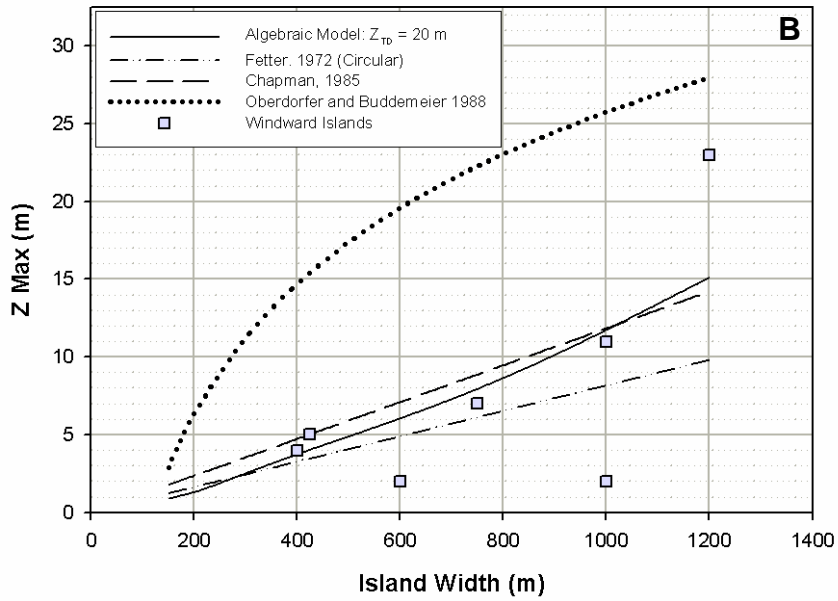


Figure 52. Comparison of observed lens depths on atoll islands, results from the algebraic model, the analytical modes proposed by Fetter (1972) and Chapman (1985) for oceanic islands, and the empirical model proposed by Oberdorfer and Buddemeier (1988), for (A) leeward islands, using a K factor corresponding to a hydraulic conductivity of 50 m day⁻¹, and (B) windward islands, using 400 m day⁻¹.

Algebraic Model for Transient Conditions

Determining the steady-state condition of the lens, by using equation (8), is an important first step in water resources management of atoll islands. However, the lens is always in a transient condition as it increases and decreases in thickness due to seasonal variation and drought. In order to incorporate the time-dependency of the lens thickness, the results from the transient simulations were used to add a time factor to equation (14):

$$Z_{MAX} = \left[Y + \frac{(Z_{TD} - Y)R}{B + R} \right] (K)(C)(T_{(r,s,w,y,m)}) \quad (15)$$

where T is the time factor [-], and the subscripts are as follows:

- **r** (Region). Either *W* for Western Caroline region (Yap data) or *E* for Eastern Caroline region (Pohnpei data)
- **s** (Side). Either *L* for Leeward or *W* for Windward.
- **w** (Weather Pattern). Either *S* for Seasonal Variation or *E* for El Niño.
- **y** (Year). For seasonal variation this term is always *1*. For an El Niño event it is *1*, *2*, or *3*; *1* being the year of the El Niño, *2* being the year following the El Niño, during which Micronesia normally experiences a severe drought, and *3* being the year of recovery following the drought.
- **m** (Month). There is a time factor value for every month of the year. This allows the fluctuation of the lens thickness to be observed throughout the year.

For example, if a water resources manager wanted to predict the thickness of the lens for a leeward atoll island located in Pohnpei state for the month of April during the year of drought following an El Niño, the subscript terms would be *E* (for Eastern Caroline region), *L* (for Leeward), *E* (for El Niño), *2* (for the 2nd year of the El Niño event), and *April*. The manager would locate the table labeled *ELE* and look up the time factor value for April in year 2. If the manager wanted to know the lens thickness for a windward atoll island located near Yap during the month of September for a regular year of rainfall, the subscript terms would be *W* (for Western Caroline region), *W* (for Windward), *S* (for Seasonal Variation), *1*, and *September*. The manager would locate the table labeled *WWS* and look up the time factor value for September. These tables are found in Appendix D. The rest of the chapter describes how these tables were constructed.

Seasonal Variation Time Parameter

The results of the seasonal variation simulation results were presented earlier. During the simulation the lens thickness was determined at the end of each month. The second column in Table 18 contains these monthly values for a 400-m wide leeward island in the West Caroline region.

Table 18. Monthly outputs for a 400-m leeward island within the West Caroline region

| Month | Thickness (m) | Factor |
|--------------|----------------------|---------------|
| Jan | 7.25 | 0.77 |
| Feb | 7.28 | 0.77 |
| Mar | 6.76 | 0.72 |
| Apr | 6.65 | 0.71 |
| May | 6.72 | 0.71 |
| Jun | 6.91 | 0.73 |
| Jul | 6.55 | 0.70 |
| Aug | 6.50 | 0.69 |
| Sep | 7.02 | 0.75 |
| Oct | 7.05 | 0.75 |
| Nov | 7.16 | 0.76 |
| Dec | 7.25 | 0.77 |

The maximum thickness in steady-state is 9.41 m. The time factor for each month was calculated by dividing the monthly lens thickness by the steady-state thickness of 9.41 m. Thus, the January time factor is $7.25 \text{ m} / 9.41 \text{ m} = 0.77$. By using this factor in equation (11), the lens thickness for a typical January can be calculated. The process is repeated for each month to estimate the fluctuation of the lens throughout the year. The same procedure was performed for all of the regular seasonal variation transient results for both the Eastern Caroline and Western Caroline regions (Appendix C).

El Niño Event Time Parameter

Time factors during an El Niño event were created using the same process explained in the previous section, but for boundary conditions from the El Niño event experienced during 1997-1999. The maximum thickness of the lens was determined at the end of each month during the 3-year simulation, and these were scaled to the steady-state thickness. Table 19 contains these results, which are displayed in Figure 57. Appendix C contains the tables of time factors for varying island width, island location, and geographic region. The tables are divided into three chronological parts: the year of the El Niño, the year following the El Niño, during which Micronesia normally experiences a severe drought, and the year of recovery following the drought. The fluctuation of the lens during these three time periods is reflected in Figure 57, which shows the rapid decrease of the lens thickness followed by a steady increase, as the lens returns to its normal condition following the drought.

Table 19. Monthly lens thickness during an El Niño event for a 400-m leeward island within the Yap region

| Month | Thickness | Factor |
|--------------|------------------|---------------|
| Jan-97 | 8.0894 | 0.8596 |
| Feb-97 | 8.2617 | 0.8779 |
| Mar-97 | 7.2422 | 0.7696 |
| Apr-97 | 6.9116 | 0.7344 |
| May-97 | 5.8688 | 0.6236 |
| Jun-97 | 5.0540 | 0.5371 |
| Jul-97 | 5.3252 | 0.5659 |
| Aug-97 | 6.1604 | 0.6546 |
| Sep-97 | 6.3071 | 0.6702 |
| Oct-97 | 7.0122 | 0.7451 |
| Nov-97 | 7.2185 | 0.7671 |
| Dec-97 | 6.9654 | 0.7402 |
| Jan-98 | 6.5671 | 0.6978 |
| Feb-98 | 7.1543 | 0.7602 |
| Mar-98 | 6.6627 | 0.7080 |
| Apr-98 | 5.2337 | 0.5561 |
| May-98 | 3.7917 | 0.4029 |
| Jun-98 | 2.9810 | 0.3168 |
| Jul-98 | 3.4613 | 0.3678 |
| Aug-98 | 3.1361 | 0.3332 |
| Sep-98 | 3.3970 | 0.3610 |
| Oct-98 | 3.7116 | 0.3944 |
| Nov-98 | 4.3887 | 0.4664 |
| Dec-98 | 4.4670 | 0.4747 |
| Jan-99 | 4.5601 | 0.4846 |
| Feb-99 | 4.6981 | 0.4992 |
| Mar-99 | 4.3600 | 0.4633 |
| Apr-99 | 4.2714 | 0.4539 |
| May-99 | 4.8830 | 0.5189 |
| Jun-99 | 4.7702 | 0.5069 |
| Jul-99 | 5.2478 | 0.5576 |
| Aug-99 | 5.7073 | 0.6065 |
| Sep-99 | 6.5824 | 0.6995 |
| Oct-99 | 6.9888 | 0.7427 |
| Nov-99 | 6.6175 | 0.7032 |
| Dec-99 | 6.8964 | 0.7328 |

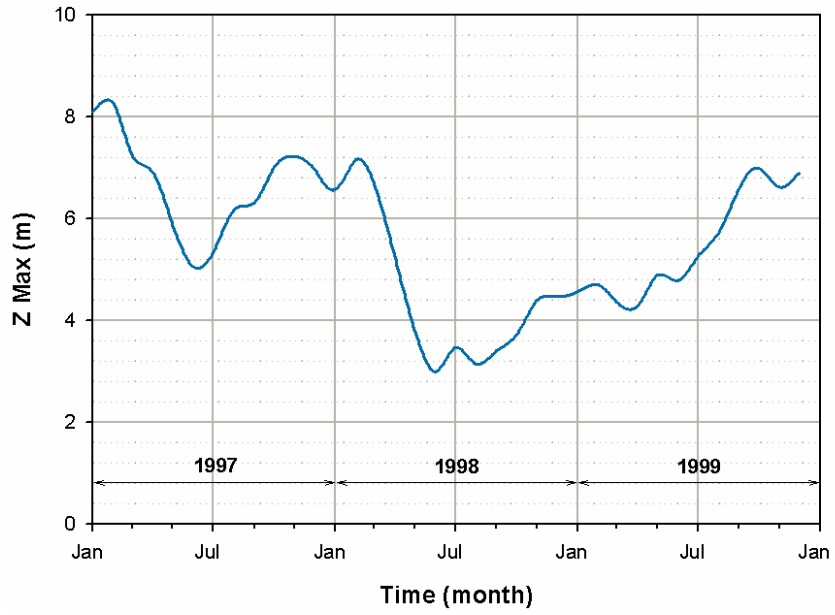


Figure 53. Fluctuation of the lens during an El Niño event for a 400-m island within the Yap region

Practical Applications

The algebraic model presented in equation 15 includes the variability of the hydraulic conductivity and the depth to the Thurber Discontinuity. These features, however, are rarely known for atoll islands, and thus a more practical solution is needed. The curves in Figure 58 are proposed as a tool for water resources to use when the specific geological characteristics of the atoll island are unknown. These curves were produced by holding the depth to the Thurber Discontinuity constant at 17.5 m, thought to be the average depth for atoll islands, and the hydraulic conductivity was set at 50 m day⁻¹ for leeward islands, and 400 m day⁻¹ for windward islands. Figure 58 shows the matching between the use of these values in the algebraic model and the observed values. The following procedure is followed to use the curves:

- (1) Determine the width of the island, the recharge to the lens (usually assumed to be half of rainfall), and the location of the island on the atoll ring (leeward or windward).
- (2) Beginning on the x-axis at the desired island width, draw a vertical line to the appropriate recharge rate curve, within the appropriate family of curves (leeward or windward).
- (3) From this point, draw a horizontal line to the y-axis to determine the maximum depth of the freshwater lens. This is the steady-state depth.
- (4) If the island is located between the leeward and windward portions of the atoll, interpolate between the two family of curves. It is assumed that such islands have a hydraulic conductivity varying between 50 and 400 m day⁻¹, with values approaching 400 m day⁻¹ the closer the island is to the leeward portion of the atoll.
- (5) Use the tables in Appendix D to determine the monthly fluctuation of the lens through the year. In practical applications these values can be determined using look-up tables from a spreadsheet. If the island in question resides in the Central Caroline region, such as islands in Chuuk state, the time factor term can be found by averaging the terms from the Western and Eastern regions. If the island in question is wider than 600 m, use the data for the 600 m wide islands.

For further methods and instructions on using the algebraic model, please refer to WERI Technical Report No. 120.

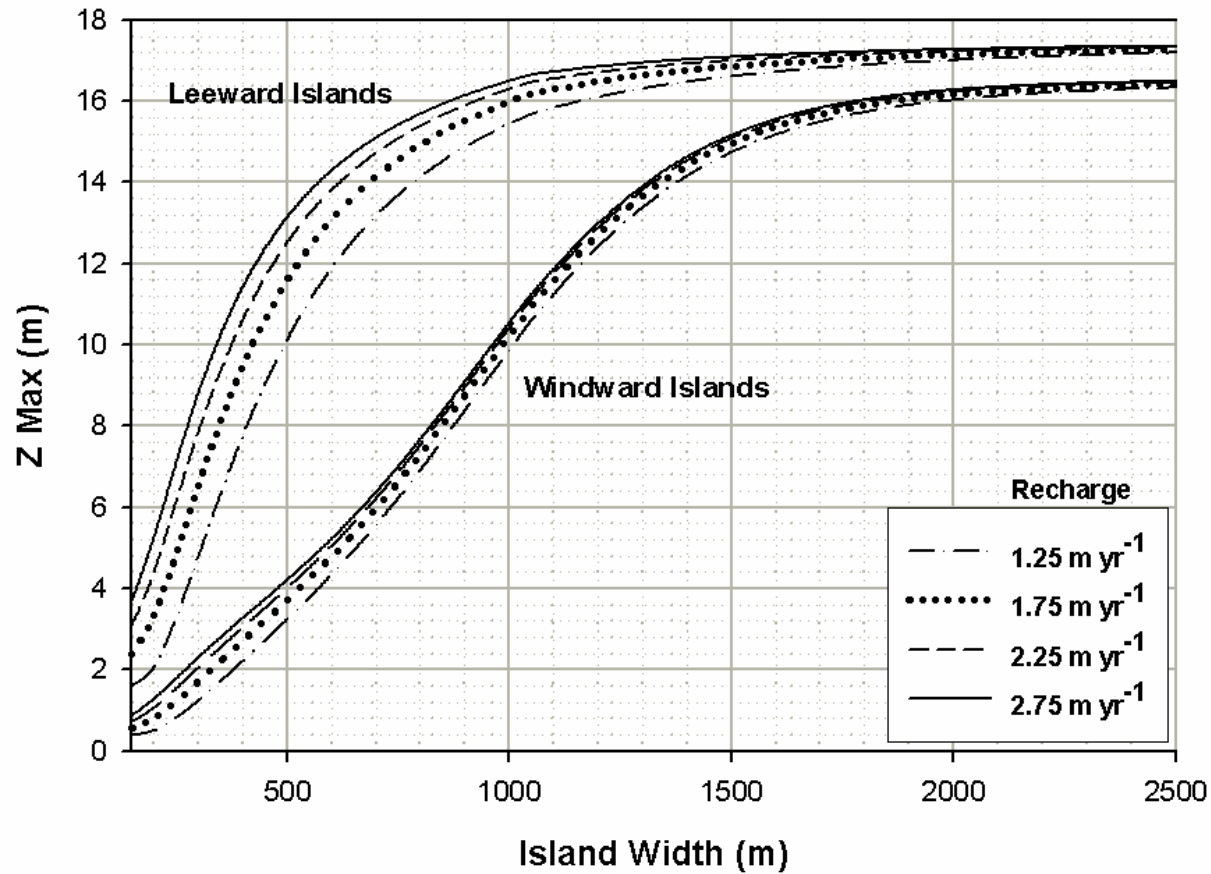


Figure 54. Freshwater Lens Tool for Water Resource Managers to determine the maximum thickness of the lens based on island width, rainfall rate, and the position (leeward or windward) of the island on the atoll. Interpolation between the two family of curves should be performed if the island is located between the leeward and windward portions of the atoll. These curves are to be used when the subsurface geology of the island has not been studied and documented.

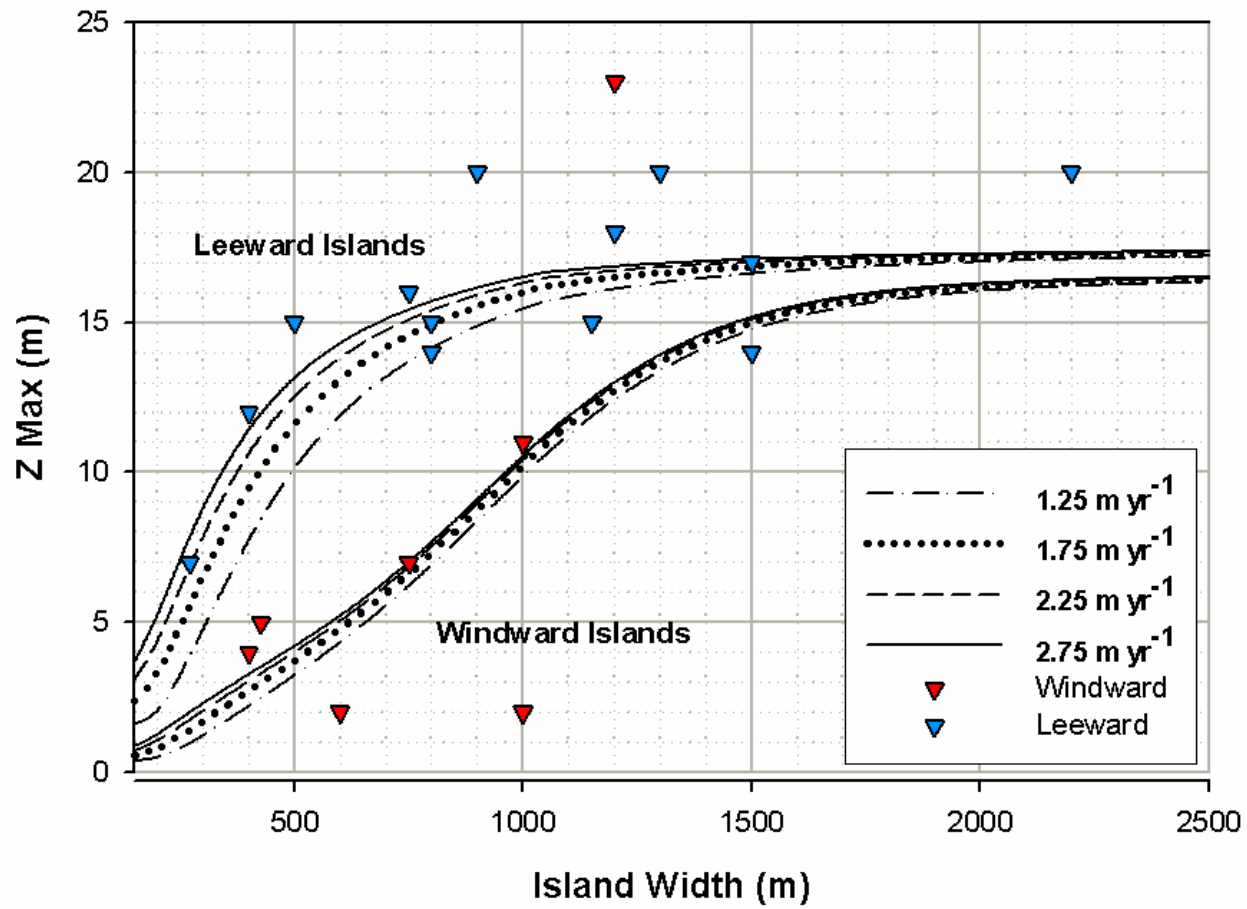


Figure 55. Comparison of recharge rates curves to the observed lens depths for leeward and windward islands.

CONCLUSIONS AND RECOMMENDATIONS

Insights into Atoll Island Hydrogeology

The recharge rate, island width, depth to the Thurber Discontinuity, hydraulic conductivity of the Holocene sediments, and the reef flat plate all affect the thickness and volume of the freshwater lens on atoll islands. The Thurber Discontinuity acts as the limiting growth factor of the lens. Increasing the width of the island and the recharge rate and decreasing the hydraulic conductivity serve to thicken the lens until it is truncated by the Thurber Discontinuity. A comparison between the results of the hydraulic conductivity simulations and observed lens depths shows that the hydraulic conductivity of the upper aquifer on leeward islands is 50 m day^{-1} , and that of windward islands is 400 m day^{-1} . The reef flat plate is a confining layer to the groundwater and serves to slightly thicken the lens and increase its volume.

Algebraic Model

An algebraic model (equation 15), based on the results of the steady-state and transient simulations, was formulated to estimate the depth of the freshwater lens under varying climatic and geological conditions.

$$Z_{MAX} = \left[Y + \frac{(Z_{TD} - Y)R}{B + R} \right] (K)(C)(T_{(r,s,w,y,m)})$$

where

| | | |
|-------------|---|--|
| Z_{MAX} | = | Maximum depth of the freshwater lens (m) |
| R | = | Recharge to the freshwater lens (m yr^{-1}) |
| Z_{TD} | = | Depth to the Thurber Discontinuity (m) |
| K | = | Hydraulic conductivity factor |
| C | = | Reef flat plate factor |
| Y | = | Constant, dependent on island width |
| B | = | Constant, dependent on island width |
| T_{rswym} | = | Time factor |

The subscripts for the time factor T denote **r**egion (Western or Eastern Caroline region), **s**ide (Leeward or Windward), **w**eahter Pattern (regular seasonal variation or El Niño event), **y**ear (1, 2, or 3 for the El Niño event and recovery period) and **m**onth. The algebraic model is hyperbolic to account for the limiting growth factor of the Thurber Discontinuity. The time factor accounts for the fluctuation of the lens thickness through varying weather patterns such as seasonal variation of rainfall and periods of drought during El Niño events.

Cautions

The steady-state version of the algebraic model (equation 14) is applicable to any atoll islands which exhibit typical geological characteristics (i.e., dual aquifer system and reef flat plate). The transient version (equation 15), however, is tailored specifically to the weather and tidal patterns experienced across the geographic region occupied by the

Federated State of Micronesia. Application of the model to any other region may or may not yield accurate results. Furthermore, absolute confidence in lens depths can only come through intensive field studies on individual atoll islands to analyze hydraulic conductivity and depth to the Thurber Discontinuity, along with any aquifer heterogeneities. Such field investigations have been performed on only a few atolls. In the absence of such information, the algebraic model should provide reasonable estimates.

Future Studies

This study dealt solely with the availability of freshwater. The quality of the freshwater is another matter altogether, and must be studied in order to provide full water resources service to inhabitants of atoll islands. Three-dimensional models will also provide a better estimate of the available freshwater, and will have the capability of accurately simulating pumping scenarios.

REFERENCES

- Anthony, S.S., 1987. Hydrogeochemistry of a small limestone-island: Laura, Majuru Atoll, Marshall Islands [M.S. thesis]: Honolulu, Hawaii, University of Hawaii, 114 p.
- Anthony, S.S., 1996a. Hydrogeology and Ground-water Resources of Ngatik Island, Sapwuahfik Atoll, State of Pohnpei, Federated States of Micronesia. U.S. Geol. Survey Water Resources Investigation Report 92-4005.
- Anthony, S.S., 1996b. Hydrogeology and Ground-water Resources of Kahlap Island, Mwoakilloa Atoll, State of Pohnpei, Federated States of Micronesia. U.S. Geol. Survey Water Resources Investigation Report 92-4005.
- Anthony, S.S., 1996c. Hydrogeology and Ground-water Resources of Pingelap Island, Pingelap Atoll, State of Pohnpei, Federated States of Micronesia. U.S. Geol. Survey Water Resources Investigation Report 92-4005.
- Anthony, S.S., 1997. Geology and Hydrogeology of Carbonate Islands. Development in Sedimentology, pp. 693-706.
- Ayers, J.F., Vacher, H.L., 1986. Hydrogeology of an Atoll Island: A Conceptual Model from Detailed Study of a Micronesian Example. *Ground Water* v. 24, no. 2, pp. 2-15.
- Bryan, E.H., Jr., 1953. Check list of atolls. *Atoll Res. Bull.*, 19:1-38
- Buddemeier, R.W. and Holladay, G., 1977. Atoll hydrology: island groundwater characteristics and their relationship to diagenesis. *Proc. 2nd Int. Coral Reef Symp.*, Miami, v.2, pp. 167-173.
- Chapman, T.G. 1985. The use of water balances for water resource estimation with special reference to small islands. *Bulleting No. 4. Pacific Regional Team. Australian Development Assistance Bureau, Canberra, Australia.*, pp 34.
- Chidley, T.R. and Lloyd, J.W., 1977. A mathematical model study of fresh-water lenses. *Ground Water* v. 15, pp. 215-222.
- Cox, D.C., 1951. The hydrology of Arno Atoll, Marshall Islands. *Atoll Res. Bull.*, 8: 1-29.
- Emery, K.O., Tracey, J.I., Ladd, H.S. 1954. Bikini and Nearby Atolls. U.S. Geological Survey Professional paper No. 260 (a) by U.S. Geological Survey.
- Falkland, A.C., 1983. Christmas Island (Kiritimati) Water Resources Study. V. 1. Australian Dept. Housing and Construction. 425 pp.

- Falkland, A. C., 1991. Hydrology and water resources of small islands: a practical guide. A contribution to the International Hydrological Programme, IHP-III, Project 4.6
- Falkland, A.C., 1992. Review of Tarawa Freshwater Lenses. ACT Electricity and Water, Canberra. Prepared for AIDAB, Canberra.
- Falkland, A.C., 1994. Climate, Hydrology and Water Resources of the Cocos (Keeling) Islands. Atoll Research Bulletin No. 400, Smithsonian Institute, Washington, D.C., 23 pp.
- Falkland, A.C., Woodroffe, C.D., 1997. Geology and Hydrogeology of Carbonate Islands. Development in Sedimentology, pp. 577-610.
- Falkland, T. 2003. Kiribati Water Resources Assessment Report. Promotion of Effective Water Management Policies and Practices TAR: 35494-01. Sinclair Knight Merz in association with Brisbane City Enterprises.
- Fetter, C.W., 1972. Position of the saline water interface beneath oceanic islands. Water Resour. Res. V. 8, pp. 1307-1315.
- Freeze, R.A., Cherry, J.A., 1979. Groundwater. Prentice-Hall, Inc., Englewood Cliffs, NJ. 604 pp.
- Ghassemi, F., Molson, J.W., Falkland, A. and Alam, K., 1998. Three-dimensional simulation of the Home Island freshwater lens: preliminary results. Environmental Modeling & Software 14(1999) 181-190.
- Gingerich, S.B., Numerical simulation of the freshwater lens on Roi-Namur Island, Kwajalein Atoll, Republic of the Marshall Islands, M.S. thesis, Dept. of Geology & Geophysics, Univ. of Hawaii, Honolulu, 1992.
- Griggs, J.E. 1989. Numerical simulation of groundwater development schemes for the Laura area of Majuro Atoll, Marshall Islands. Ph.D. dissertation (Geology/Geophysics), Univ. of Hawaii and Manoa, Honolulu.
- Griggs, J.E. and Peterson, F.L., 1993. Ground-Water flow dynamics and development strategies at the atoll scale. Ground Water, v. 31, no. 2, pp. 209-220.
- Hamlin, S.N., and Anthony, S.S., 1987. Ground-water resources of the Laura area, Majuro Atoll, Marshall Islands. U.S. Geol. Survey Water Resources Investigatio Report 87-4047.
- Herman, M.E. and S.W. Wheatcraft. 1984. Groundwater dynamics investigation of Enjebi Island, Enewetak Atoll: an interpretive computer model simulation, Finite Elements in Water Resources, Springer-Verlag, New York. pp. 133-142.

- Hogan, P.J., 1988. Modeling of fresh water-saltwater interaction on Enjebi Island, Enewetak Atoll, M.S. Thesis, San Jose State University, San Jose, CA, 141 pp.
- Hunt, C.D., Jr. 1997. Geology and Hydrogeology of Carbonate Islands. Development in Sedimentology, pp. 909-931.
- Hunt, C.D., Jr. and Peterson, F.L., 1980. Groundwater resources of Kwajalein Island, Marshall Islands. Technical Report No. 126. Water Resources Research Center, Univ. of Hawaii. 91 pp.
- Jacobson, G. and F.J. Taylor, 1981. Hydrogeology of Tarawa Atoll, Kiribati. Record 1981/31. Bureau of Mineral Resources, Geology and Geophysics, Australian Government.
- Lam, R.K., 1974. Atoll permeability calculated from tidal diffusion. J. Geophys. Res. V. 79, pp. 3073-3081.
- Lee, A.G., 2003. 3-D Numerical Modeling of Freshwater Lens on Atoll Islands. Proceedings, TOUGH Symposium, 2003. Lawrence Berkeley National Laboratory, Berkeley, California, May 12-14, 2003.
- Lessa, W.A., 1964. The Social Effects of Typhoon Ophelia (1960) on Ulithi. Micronesica, Vol. I Nos. 1 and 2, pp. 1-47.
- Lloyd, J.W., Drennen, D., Bennell, B.M., 1966. A Ground Water Recharge Study in North-Eastern Jordan. Proc. Instn. Civil Engrs. 35:615-631.
- Lloyd, J.W., Miles, J.C., Chessman, G.R., and Bugg, S.F., 1980. A Ground Water Resources Study of a Pacific Ocean Atoll – Tarawa, Gilbert Islands. Water Resources Bull. v. 16, No. 4, pp. 646-653.
- Mather, J.D. 1975. Development of the Groundwater Resources of Small Limestone Islands. Quarterly Journal of Engineering Geology 8:141-150.
- Oberdorfer, J.A. and R.W. Buddemeier. 1983. Hydrogeology of a Great Barrier Reef: implications for groundwater in reef and atoll islands. EOS. v. 64, p. 703
- Oberdorfer, J.A., Buddemeier, R.W., 1988. Climate change: effects on reef island resources. Proc. 6th Int. Coral Reef Symp. 3: 523-527.
- Oberdorfer, J.A., Hogan, P.J. and Buddemeier, R.W., 1990. Atoll island hydrogeology: flow and freshwater occurrence in a tidally dominated system. J. Hydrol., 120: 327-340.
- Penman, H.L. 1950. The Water Balance of the Stour Catchment Area. Jour. Instn. Water Engrs. 4:457-464.

- Peterson, F.L., 1997. Geology and Hydrogeology of Carbonate Islands. Development in Sedimentology, pp. 611-666.
- Peterson, F.L. and Gingerich, S.B., 1995. Groundwater Models for Resources Analysis and Management, pp. 275-292.
- PRC Toups, 1983. Engineering study to evaluate potable water supply alternatives and groundwater yield at Diego Garcia, BIOT. Unpublished report to the U.S. Navy: PRC Toups, 972 Town and Country Road, P.O. Box 5367, Orange, CA, 92688, USA.
- Purdy, E.G. and Winterer, E.L., 2001. Origin of atoll lagoons. GSA Bulletin; July 2001; v. 113; no. 7; p. 837-854
- Souza, W.R. and Voss, C.I., 1987. Analysis of an anisotropic coastal aquifer system using variable-density flow and solute transport simulation. J. Hydrol., 92: 17-41
- Spennemann, D., 2006. Non-traditional settlement patterns and typhoon hazard on contemporary Majuro Atoll, Republic of the Marshall Islands. Transforming Cultures eJournal Vol. 1 No. 2.
- Swartz, J.H., 1962. Some physical constants for the Marshall Island area. U.S. Geol. Survey Professional Paper 260-AA. Pp. 953-990.
- Thornwaite, C.W., 1948. An Approach Towards a Rational Classification of Climate. Geographical Review 38: 55-63.
- Thurber, D.L., Broecker, W.S., Blanchard, R.L. and Potratz, H.A., 1965. Uranium-series ages of Pacific atoll coral. Science, 149, 55-58.
- Underwood, M.R., Atoll island hydrogeology: Conceptual and numerical models, Ph.D. dissertation, Dept. of Geology & Geophysics, Univ. of Hawaii at Manoa, Honolulu, 1990.
- Underwood, M.R., Peterson, F.L. and Voss, C.I., 1992. Groundwater Lens Dynamics of Atoll Islands. Water Resources Bull. v. 28, no. 11, pp. 2889-2902.
- Vacher, H.L., 1997. Geology and Hydrogeology of Carbonate Islands. Development in Sedimentology, pp.1-33.
- Voss, C. 1984. A finite-element simulation model for saturated-unsaturated, fluid-density-dependent ground-water flow with energy transport of chemically-reactive single-species solute transport. U.S. Geol. Survey Water Resources Investigation Report 84-4369.

- Ward, R.C., 1971. Measuring Evapotranspiration: A Review. *Journal of Hydrology*. 13:1-21.
- Wheatcraft, S.W. and Buddemeier, R.W., 1981. Atoll Island Hydrology. *Ground Water*, v. 19, No. 3, pp. 311-320.
- White, I. 1996. Fresh groundwater lens recharge, Bonriki, Kiribati, preliminary report. International Hydrological Programme. IHP-V Project 6-1. UNESCO, Paris.
- WHO (World Health Organization), 1972. International standards for drinking-water, WHO (U.N.), Geneva.
- Woodroffe, C.D., Falkland, A.C., 1997. Geology and Hydrogeology of Carbonate Islands. *Development in Sedimentology*, pp. 885-908.

APPENDICES

Appendix A
Simulation Details for Experiments

Rainfall Experiment

Constants: HC = 50 m day-1
 HP boundary ~ 17.5 m

| Simulation | Rainfall Rate (m yr-1) | Island Width (m) | Max. Depth of Freshwater Lens (m) |
|-------------------|-------------------------------|-------------------------|--|
| 1 | 2.50 | 150 | 3.140 |
| 2 | 2.50 | 200 | 4.000 |
| 3 | 2.50 | 300 | 6.700 |
| 4 | 2.50 | 400 | 9.000 |
| 5 | 2.50 | 500 | 11.364 |
| 6 | 2.50 | 600 | 13.333 |
| 7 | 2.50 | 800 | 15.000 |
| 8 | 2.50 | 1100 | 15.833 |
| 9 | 3.00 | 150 | 3.30 |
| 10 | 3.00 | 200 | 4.60 |
| 11 | 3.00 | 300 | 7.60 |
| 12 | 3.00 | 400 | 10.000 |
| 13 | 3.00 | 500 | 12.273 |
| 14 | 3.00 | 600 | 14.167 |
| 15 | 3.00 | 800 | 15.000 |
| 16 | 3.00 | 1100 | 16.000 |
| 17 | 3.50 | 150 | 3.710 |
| 18 | 3.50 | 200 | 5.200 |
| 19 | 3.50 | 300 | 7.900 |
| 20 | 3.50 | 400 | 11.000 |
| 21 | 3.50 | 500 | 13.182 |
| 22 | 3.50 | 600 | 14.167 |
| 23 | 3.50 | 800 | 15.827 |
| 24 | 3.50 | 1100 | 16.000 |
| 25 | 4.00 | 150 | 4.000 |
| 26 | 4.00 | 200 | 5.500 |
| 27 | 4.00 | 300 | 8.500 |
| 28 | 4.00 | 400 | 12.000 |
| 29 | 4.00 | 500 | 13.410 |
| 30 | 4.00 | 600 | 14.792 |
| 31 | 4.00 | 800 | 15.978 |
| 32 | 4.00 | 1100 | 16.111 |
| 33 | 4.50 | 150 | 4.200 |
| 34 | 4.50 | 200 | 5.800 |
| 35 | 4.50 | 300 | 9.400 |
| 36 | 4.50 | 400 | 12.500 |
| 37 | 4.50 | 500 | 13.637 |
| 38 | 4.50 | 600 | 14.850 |
| 39 | 4.50 | 800 | 16.072 |
| 40 | 4.50 | 1100 | 16.400 |
| 41 | 5.00 | 150 | 4.600 |
| 42 | 5.00 | 200 | 6.400 |
| 43 | 5.00 | 300 | 9.850 |

| | | | |
|-----------|------|------|--------|
| 44 | 5.00 | 400 | 13.000 |
| 45 | 5.00 | 500 | 14.091 |
| 46 | 5.00 | 600 | 15.000 |
| 47 | 5.00 | 800 | 16.100 |
| 48 | 5.00 | 1100 | 16.667 |
| 49 | 5.50 | 150 | 4.800 |
| 50 | 5.50 | 200 | 6.600 |
| 51 | 5.50 | 300 | 10.300 |
| 52 | 5.50 | 400 | 13.000 |
| 53 | 5.50 | 500 | 14.091 |
| 54 | 5.50 | 600 | 15.400 |
| 55 | 5.50 | 800 | 16.562 |
| 56 | 5.50 | 1100 | 16.713 |

Hydraulic Conductivity Experiment

Constants: Rainfall = 4000 mm yr-1
 HP boundary = 17.5 m

| Simulation | Hydraulic Conductivity of Holocene Sediments (m day-1) | Island Width (m) | Max. Depth of Freshwater Lens (m) |
|------------|--|------------------|-----------------------------------|
| 1 | 25 | 150 | 5.800 |
| 2 | 25 | 200 | 8.200 |
| 3 | 25 | 300 | 12.325 |
| 4 | 25 | 400 | 15.000 |
| 5 | 25 | 500 | 15.000 |
| 6 | 25 | 600 | 15.000 |
| 7 | 25 | 800 | 15.769 |
| 8 | 25 | 1100 | 16.089 |
| 9 | 50 | 150 | 4.00 |
| 10 | 50 | 200 | 5.50 |
| 11 | 50 | 300 | 8.50 |
| 12 | 50 | 400 | 12.00 |
| 13 | 50 | 500 | 13.410 |
| 14 | 50 | 600 | 14.792 |
| 15 | 50 | 800 | 15.978 |
| 16 | 50 | 1100 | 16.111 |
| 17 | 100 | 150 | 2.666 |
| 18 | 100 | 200 | 3.714 |
| 19 | 100 | 300 | 5.900 |
| 20 | 100 | 400 | 8.000 |
| 21 | 100 | 500 | 10.455 |
| 22 | 100 | 600 | 13.333 |
| 23 | 100 | 800 | 15.583 |
| 24 | 100 | 1100 | 15.900 |
| 25 | 200 | 150 | 1.556 |
| 26 | 200 | 200 | 2.286 |
| 27 | 200 | 300 | 4.000 |
| 28 | 200 | 400 | 5.500 |
| 29 | 200 | 500 | 6.818 |
| 30 | 200 | 600 | 8.750 |
| 31 | 200 | 800 | 12.500 |
| 32 | 200 | 1100 | 15.000 |
| 33 | 300 | 150 | 1.111 |
| 34 | 300 | 200 | 1.778 |
| 35 | 300 | 300 | 3.143 |
| 36 | 300 | 400 | 4.000 |
| 37 | 300 | 500 | 5.227 |
| 38 | 300 | 600 | 6.834 |
| 39 | 300 | 800 | 9.583 |
| 40 | 300 | 1100 | 13.182 |
| 41 | 400 | 150 | 0.889 |
| 42 | 400 | 200 | 1.333 |
| 43 | 400 | 300 | 2.281 |
| 44 | 400 | 400 | 3.711 |
| 45 | 400 | 500 | 4.357 |
| 46 | 400 | 600 | 5.833 |
| 47 | 400 | 800 | 8.333 |

| | | | |
|-----------|-----|------|--------|
| 48 | 400 | 1100 | 11.516 |
| 49 | 500 | 150 | 0.667 |
| 50 | 500 | 200 | 1.000 |
| 51 | 500 | 300 | 2.000 |
| 52 | 500 | 400 | 2.854 |
| 53 | 500 | 500 | 3.714 |
| 54 | 500 | 600 | 4.657 |
| 55 | 500 | 800 | 6.683 |
| 56 | 500 | 1100 | 10.455 |

Thurber Discontinuity Experiment

Constants: HC = 50 m day⁻¹
Rainfall = 4000 mm yr⁻¹

| Simulation | Depth to Holocene-Pleistocene Unconformity (m) | Island Width (m) | Max. Depth of Freshwater Lens (m) |
|------------|--|------------------|-----------------------------------|
| 1 | 8 | 150 | 4.000 |
| 2 | 8 | 200 | 5.800 |
| 3 | 8 | 300 | 6.700 |
| 4 | 8 | 500 | 8.182 |
| 5 | 8 | 800 | 9.375 |
| 6 | 10 | 150 | 4.00 |
| 7 | 10 | 200 | 5.80 |
| 8 | 10 | 300 | 8.500 |
| 9 | 10 | 500 | 9.545 |
| 10 | 10 | 800 | 11.500 |
| 11 | 12 | 150 | 4.000 |
| 12 | 12 | 200 | 5.800 |
| 13 | 12 | 300 | 8.860 |
| 14 | 12 | 500 | 11.364 |
| 15 | 12 | 800 | 13.333 |
| 16 | 14 | 150 | 4.000 |
| 17 | 14 | 200 | 5.800 |
| 18 | 14 | 300 | 8.680 |
| 19 | 14 | 500 | 13.182 |
| 20 | 14 | 800 | 14.167 |
| 21 | 16 | 150 | 4.000 |
| 22 | 16 | 200 | 5.800 |
| 23 | 16 | 300 | 8.680 |
| 24 | 16 | 500 | 14.160 |
| 25 | 16 | 800 | 16.300 |
| 26 | 18 | 150 | 4.000 |
| 27 | 18 | 200 | 5.800 |
| 28 | 18 | 300 | 8.680 |
| 29 | 18 | 500 | 15.154 |
| 30 | 18 | 800 | 18.261 |

Reef Flat Plate Experiments

1. Extent of Reef Flat Plate

Constants: Island Width = 400 m
 HC = 50 m day-1
 Rainfall = 4000 mm yr-1
 HP boundary = 17.5 m

| Simulation | Extent of Reef Flat Plate (m) | Max. Depth of Freshwater Lens (m) |
|------------|-------------------------------|-----------------------------------|
| 1 | 0 | 12.100 |
| 2 | 25 | 12.467 |
| 3 | 50 | 12.467 |
| 4 | 200 | 12.467 |
| 5 | 300 | 12.467 |
| 6 | 350 | 12.467 |

2. Existence of Reef Flat Plate

Constants: Island Width = 400 m
 HC = 50 m day-1
 Rainfall = 4000 mm yr-1
 HP boundary = 17.5 m
 Extent of Reef Flat Plate when present = 200 m (halfway across the island)

| Simulation | Reef Flat Plate Present | Island Width (m) | Max. Depth of Freshwater Lens (m) |
|------------|-------------------------|------------------|-----------------------------------|
| 1 | TRUE | 150 | 4.750 |
| 2 | TRUE | 200 | 6.560 |
| 3 | TRUE | 300 | 9.600 |
| 4 | TRUE | 400 | 13.000 |
| 5 | TRUE | 500 | 13.940 |
| 6 | TRUE | 1100 | 16.700 |
| 7 | FALSE | 150 | 4.000 |
| 8 | FALSE | 200 | 5.800 |
| 9 | FALSE | 300 | 8.600 |
| 10 | FALSE | 400 | 12.000 |
| 11 | FALSE | 500 | 13.410 |
| 12 | FALSE | 1100 | 16.627 |

APPENDIX B
Term values for the steady-state, algebraic model

$$Z_{MAX} = \left[Y + \frac{(Z_{TD} - Y)R}{B + R} \right] (K)(C)$$

Values of the *B*, *Y*, and *C* terms in the hyperbolic equation, for various island widths

| Island Width | B Factor | Y Factor | C Factor |
|--------------|----------|----------|----------|
| 150 | 6.77 | -0.98 | 0.85 |
| 200 | 3.47 | -3.07 | 0.87 |
| 250 | 2.07 | -4.69 | 0.89 |
| 300 | 1.35 | -6.01 | 0.90 |
| 350 | 0.95 | -7.13 | 0.92 |
| 400 | 0.69 | -8.10 | 0.93 |
| 450 | 0.53 | -8.95 | 0.94 |
| 500 | 0.41 | -9.72 | 0.94 |
| 550 | 0.33 | -10.41 | 0.95 |
| 600 | 0.27 | -11.04 | 0.96 |
| 650 | 0.22 | -11.62 | 0.96 |
| 700 | 0.19 | -12.16 | 0.97 |
| 750 | 0.16 | -12.66 | 0.97 |
| 800 | 0.14 | -13.13 | 0.98 |
| 850 | 0.12 | -13.57 | 0.98 |
| 900 | 0.11 | -13.98 | 0.99 |
| 950 | 0.09 | -14.37 | 0.99 |
| 1000 | 0.08 | -14.75 | 1.00 |
| 1050 | 0.07 | -15.10 | 1.00 |
| 1100 | 0.07 | -15.44 | 1.00 |
| 1150 | 0.06 | -15.76 | 1.00 |
| 1200 | 0.05 | -16.07 | 1.00 |
| 1300 | 0.04 | -16.65 | 1.00 |
| 1400 | 0.04 | -17.19 | 1.00 |
| 1500 | 0.03 | -17.69 | 1.00 |
| 1600 | 0.03 | -18.16 | 1.00 |
| 1700 | 0.02 | -18.60 | 1.00 |
| 1800 | 0.02 | -19.01 | 1.00 |
| 1900 | 0.02 | -19.40 | 1.00 |
| 2000 | 0.02 | -19.78 | 1.00 |
| 2100 | 0.01 | -20.13 | 1.00 |
| 2200 | 0.01 | -20.47 | 1.00 |
| 2300 | 0.01 | -20.79 | 1.00 |
| 2400 | 0.01 | -21.10 | 1.00 |
| 2500 | 0.01 | -21.40 | 1.00 |

Values for the Hydraulic Conductivity term, K

| IslandWidth | 25 | 50 | 75 | 100 | 125 | 150 | 175 | 200 | 225 | 250 | 275 | 300 | 325 | 400 |
|--------------------|-----------|-----------|-----------|------------|------------|------------|------------|------------|------------|------------|------------|------------|------------|------------|
| 150 | 1.604 | 1.000 | 0.740 | 0.606 | 0.519 | 0.457 | 0.412 | 0.377 | 0.349 | 0.326 | 0.306 | 0.289 | 0.273 | 0.239 |
| 200 | 1.596 | 1.000 | 0.752 | 0.618 | 0.531 | 0.470 | 0.423 | 0.388 | 0.358 | 0.334 | 0.314 | 0.296 | 0.281 | 0.246 |
| 250 | 1.578 | 1.000 | 0.768 | 0.635 | 0.548 | 0.486 | 0.438 | 0.401 | 0.370 | 0.345 | 0.324 | 0.305 | 0.290 | 0.253 |
| 300 | 1.541 | 1.000 | 0.787 | 0.657 | 0.570 | 0.507 | 0.457 | 0.418 | 0.385 | 0.358 | 0.336 | 0.317 | 0.301 | 0.263 |
| 350 | 1.470 | 1.000 | 0.809 | 0.684 | 0.598 | 0.533 | 0.481 | 0.439 | 0.404 | 0.375 | 0.351 | 0.331 | 0.314 | 0.274 |
| 400 | 1.361 | 1.000 | 0.834 | 0.717 | 0.632 | 0.565 | 0.511 | 0.465 | 0.427 | 0.395 | 0.369 | 0.348 | 0.330 | 0.287 |
| 450 | 1.236 | 1.000 | 0.859 | 0.754 | 0.671 | 0.603 | 0.545 | 0.496 | 0.455 | 0.420 | 0.391 | 0.368 | 0.349 | 0.303 |
| 500 | 1.132 | 1.000 | 0.885 | 0.793 | 0.714 | 0.645 | 0.585 | 0.533 | 0.488 | 0.449 | 0.418 | 0.392 | 0.370 | 0.321 |
| 550 | 1.067 | 1.000 | 0.908 | 0.831 | 0.758 | 0.691 | 0.629 | 0.574 | 0.525 | 0.483 | 0.448 | 0.419 | 0.396 | 0.342 |
| 600 | 1.033 | 1.000 | 0.928 | 0.866 | 0.801 | 0.736 | 0.675 | 0.618 | 0.567 | 0.521 | 0.483 | 0.451 | 0.424 | 0.366 |
| 650 | 1.017 | 1.000 | 0.945 | 0.895 | 0.840 | 0.780 | 0.721 | 0.664 | 0.611 | 0.563 | 0.521 | 0.486 | 0.456 | 0.393 |
| 700 | 1.009 | 1.000 | 0.958 | 0.920 | 0.873 | 0.820 | 0.765 | 0.710 | 0.656 | 0.607 | 0.562 | 0.524 | 0.491 | 0.422 |
| 750 | 1.006 | 1.000 | 0.968 | 0.939 | 0.901 | 0.855 | 0.805 | 0.753 | 0.701 | 0.652 | 0.605 | 0.564 | 0.528 | 0.455 |
| 800 | 1.005 | 1.000 | 0.976 | 0.953 | 0.922 | 0.884 | 0.840 | 0.793 | 0.744 | 0.695 | 0.649 | 0.606 | 0.568 | 0.490 |
| 850 | 1.004 | 1.000 | 0.981 | 0.963 | 0.939 | 0.907 | 0.870 | 0.828 | 0.783 | 0.737 | 0.691 | 0.648 | 0.608 | 0.526 |
| 900 | 1.004 | 1.000 | 0.985 | 0.971 | 0.951 | 0.925 | 0.894 | 0.858 | 0.817 | 0.775 | 0.731 | 0.688 | 0.648 | 0.564 |
| 950 | 1.004 | 1.000 | 0.988 | 0.976 | 0.960 | 0.939 | 0.913 | 0.882 | 0.847 | 0.808 | 0.768 | 0.727 | 0.687 | 0.602 |
| 1000 | 1.004 | 1.000 | 0.990 | 0.980 | 0.967 | 0.950 | 0.928 | 0.902 | 0.872 | 0.838 | 0.801 | 0.763 | 0.725 | 0.640 |
| 1050 | 1.004 | 1.000 | 0.992 | 0.982 | 0.971 | 0.958 | 0.940 | 0.918 | 0.892 | 0.862 | 0.829 | 0.795 | 0.760 | 0.676 |
| 1100 | 1.004 | 1.000 | 0.993 | 0.984 | 0.975 | 0.963 | 0.949 | 0.931 | 0.908 | 0.882 | 0.853 | 0.823 | 0.792 | 0.710 |
| 1150 | 1.004 | 1.000 | 0.993 | 0.985 | 0.977 | 0.967 | 0.955 | 0.940 | 0.921 | 0.899 | 0.874 | 0.847 | 0.821 | 0.743 |
| 1200 | 1.004 | 1.000 | 0.994 | 0.986 | 0.979 | 0.971 | 0.960 | 0.947 | 0.931 | 0.912 | 0.890 | 0.868 | 0.846 | 0.772 |
| 1300 | 1.004 | 1.000 | 0.995 | 0.987 | 0.981 | 0.974 | 0.967 | 0.957 | 0.945 | 0.930 | 0.915 | 0.900 | 0.887 | 0.822 |
| 1400 | 1.004 | 1.000 | 0.995 | 0.988 | 0.982 | 0.976 | 0.970 | 0.963 | 0.953 | 0.942 | 0.931 | 0.921 | 0.917 | 0.860 |
| 1500 | 1.004 | 1.000 | 0.995 | 0.988 | 0.982 | 0.977 | 0.972 | 0.966 | 0.958 | 0.949 | 0.940 | 0.936 | 0.938 | 0.888 |
| 1600 | 1.004 | 1.000 | 0.995 | 0.988 | 0.982 | 0.978 | 0.973 | 0.968 | 0.960 | 0.953 | 0.946 | 0.944 | 0.952 | 0.908 |
| 1700 | 1.004 | 1.000 | 0.995 | 0.988 | 0.982 | 0.978 | 0.974 | 0.969 | 0.962 | 0.955 | 0.950 | 0.950 | 0.961 | 0.922 |
| 1800 | 1.004 | 1.000 | 0.995 | 0.988 | 0.982 | 0.978 | 0.974 | 0.969 | 0.963 | 0.956 | 0.952 | 0.954 | 0.967 | 0.932 |
| 1900 | 1.004 | 1.000 | 0.995 | 0.988 | 0.982 | 0.978 | 0.974 | 0.969 | 0.963 | 0.957 | 0.953 | 0.956 | 0.971 | 0.938 |
| 2000 | 1.004 | 1.000 | 0.995 | 0.988 | 0.982 | 0.978 | 0.974 | 0.969 | 0.963 | 0.958 | 0.954 | 0.957 | 0.974 | 0.943 |
| 2100 | 1.004 | 1.000 | 0.995 | 0.988 | 0.982 | 0.978 | 0.974 | 0.970 | 0.964 | 0.958 | 0.955 | 0.958 | 0.975 | 0.945 |
| 2200 | 1.004 | 1.000 | 0.995 | 0.988 | 0.982 | 0.978 | 0.974 | 0.970 | 0.964 | 0.958 | 0.955 | 0.959 | 0.976 | 0.947 |
| 2300 | 1.004 | 1.000 | 0.995 | 0.988 | 0.982 | 0.978 | 0.974 | 0.970 | 0.964 | 0.958 | 0.955 | 0.959 | 0.977 | 0.949 |
| 2400 | 1.004 | 1.000 | 0.995 | 0.988 | 0.982 | 0.978 | 0.974 | 0.970 | 0.964 | 0.958 | 0.955 | 0.959 | 0.977 | 0.950 |
| 2500 | 1.004 | 1.000 | 0.995 | 0.988 | 0.982 | 0.978 | 0.974 | 0.970 | 0.964 | 0.958 | 0.955 | 0.959 | 0.978 | 0.950 |

APPENDIX C

Term values for the time factor in the algebraic model

$$Z_{MAX} = \left[Y + \frac{(Z_{TD} - Y)R}{B + R} \right] (K)(C)(T_{(r,s,w,y,m)})$$

WLS

Western Caroline region, Leeward island, Normal seasonal fluctuations

| MONTH | ISLAND WIDTH | | |
|-------|--------------|--------|--------|
| | 200 | 400 | 600 |
| Jan | 0.8857 | 0.7699 | 0.9020 |
| Feb | 0.8246 | 0.7738 | 0.9174 |
| Mar | 0.6841 | 0.7188 | 0.9039 |
| Apr | 0.6402 | 0.7064 | 0.9063 |
| May | 0.5893 | 0.7139 | 0.9256 |
| Jun | 0.6178 | 0.7339 | 0.9447 |
| Jul | 0.6564 | 0.6959 | 0.8942 |
| Aug | 0.7164 | 0.6912 | 0.8616 |
| Sep | 0.8596 | 0.7459 | 0.8871 |
| Oct | 0.9173 | 0.7495 | 0.8887 |
| Nov | 0.9148 | 0.7603 | 0.9003 |
| Dec | 0.9135 | 0.7699 | 0.9327 |

ELS

East Caroline region, Leeward island, Normal seasonal fluctuations

| MONTH | ISLAND WIDTH | | |
|-------|--------------|--------|--------|
| | 200 | 400 | 600 |
| Jan | 1.0534 | 1.1152 | 0.9312 |
| Feb | 1.0384 | 1.0996 | 0.9263 |
| Mar | 0.9351 | 1.0397 | 0.9239 |
| Apr | 0.9289 | 0.9689 | 0.9238 |
| May | 0.9682 | 0.9842 | 0.9249 |
| Jun | 1.0377 | 1.0460 | 0.9257 |
| Jul | 1.0383 | 1.0678 | 0.9240 |
| Aug | 1.0439 | 1.1012 | 0.9250 |
| Sep | 1.0588 | 1.1088 | 0.9284 |
| Oct | 1.0488 | 1.0944 | 0.9331 |
| Nov | 1.0386 | 1.0869 | 0.9346 |
| Dec | 1.0294 | 1.0810 | 0.9358 |

WWS

Western Caroline region, Windward island, Normal seasonal fluctuations

| MONTH | ISLAND WIDTH | | |
|--------------|---------------------|------------|------------|
| | 200 | 400 | 600 |
| JAN | 0.7331 | 1.0261 | 0.7552 |
| FEB | 0.4470 | 0.8602 | 0.7419 |
| MAR | 0.2964 | 0.6396 | 0.6478 |
| APR | 0.0998 | 0.5707 | 0.6194 |
| MAY | 0.0000 | 0.5413 | 0.6048 |
| JUN | 0.0000 | 0.5895 | 0.6261 |
| JUL | 0.0000 | 0.6934 | 0.6922 |
| AUG | 0.1949 | 0.7987 | 0.7620 |
| SEP | 0.2867 | 0.7502 | 0.7874 |
| OCT | 0.7128 | 0.9192 | 0.8138 |
| NOV | 0.8289 | 1.0217 | 0.8200 |
| DEC | 0.6429 | 1.0458 | 0.8053 |

EWS

East Caroline region, Windward island, Normal seasonal fluctuations

| MONTH | ISLAND WIDTH | | |
|--------------|---------------------|------------|------------|
| | 200 | 400 | 600 |
| Jan | 0.6978 | 1.2256 | 1.1936 |
| Feb | 0.9247 | 1.2002 | 1.1960 |
| Mar | 0.9539 | 1.1082 | 1.1039 |
| Apr | 0.9236 | 1.0504 | 1.0938 |
| May | 0.5186 | 1.1172 | 1.0928 |
| Jun | 0.7927 | 1.2270 | 1.1499 |
| Jul | 1.1914 | 1.2537 | 1.1717 |
| Aug | 1.2363 | 1.2788 | 1.1883 |
| Sep | 1.2357 | 1.2877 | 1.2288 |
| Oct | 1.1936 | 1.2350 | 1.2282 |
| Nov | 1.1338 | 1.2134 | 1.2160 |
| Dec | 1.0383 | 1.1650 | 1.1863 |

WLE**West Caroline region, Leeward island, El Niño event**

| Year | MONTH | ISLAND WIDTH | | | |
|-------------|--------------|---------------------|------------|------------|--------|
| | | 200 | 400 | 600 | |
| 1 | El Niño | JAN | 0.9219 | 0.8596 | 0.9543 |
| | El Niño | FEB | 0.9144 | 0.8779 | 0.9606 |
| | El Niño | MAR | 0.7414 | 0.7696 | 0.8582 |
| | El Niño | APR | 0.5834 | 0.7344 | 0.8446 |
| | El Niño | MAY | 0.3351 | 0.6236 | 0.7801 |
| | El Niño | JUN | 0.0687 | 0.5371 | 0.7189 |
| | El Niño | JUL | 0.2991 | 0.5659 | 0.7381 |
| | El Niño | AUG | 0.4974 | 0.6546 | 0.7997 |
| | El Niño | SEP | 0.5923 | 0.6702 | 0.819 |
| | El Niño | OCT | 0.6697 | 0.7451 | 0.8796 |
| | El Niño | NOV | 0.6653 | 0.7671 | 0.9175 |
| | El Niño | DEC | 0.5694 | 0.7402 | 0.9064 |
| 2 | Post-El Niño | JAN | 0.4508 | 0.6978 | 0.8986 |
| | Post-El Niño | FEB | 0.3489 | 0.7602 | 0.9562 |
| | Post-El Niño | MAR | 0.1083 | 0.708 | 0.9537 |
| | Post-El Niño | APR | 0 | 0.5561 | 0.8272 |
| | Post-El Niño | MAY | 0 | 0.4029 | 0.6959 |
| | Post-El Niño | JUN | 0 | 0.3168 | 0.6207 |
| | Post-El Niño | JUL | 0 | 0.3678 | 0.6283 |
| | Post-El Niño | AUG | 0 | 0.3332 | 0.5582 |
| | Post-El Niño | SEP | 0.0745 | 0.361 | 0.5646 |
| | Post-El Niño | OCT | 0.2589 | 0.3944 | 0.5598 |
| | Post-El Niño | NOV | 0.4485 | 0.4664 | 0.6 |
| | Post-El Niño | DEC | 0.4209 | 0.4747 | 0.6077 |
| 3 | Recovery | JAN | 0.4276 | 0.4846 | 0.6177 |
| | Recovery | FEB | 0.3522 | 0.4992 | 0.6535 |
| | Recovery | MAR | 0.2379 | 0.4633 | 0.6526 |
| | Recovery | APR | 0.2297 | 0.4539 | 0.6542 |
| | Recovery | MAY | 0.4196 | 0.5189 | 0.6976 |
| | Recovery | JUN | 0.4884 | 0.5069 | 0.6791 |
| | Recovery | JUL | 0.6101 | 0.5576 | 0.7158 |
| | Recovery | AUG | 0.7295 | 0.6065 | 0.7508 |
| | Recovery | SEP | 0.886 | 0.6995 | 0.8319 |
| | Recovery | OCT | 0.8606 | 0.7427 | 0.8765 |
| | Recovery | NOV | 0.6834 | 0.7032 | 0.884 |
| | Recovery | DEC | 0.7111 | 0.7328 | 0.9093 |

*ELE***East Caroline region, Leeward island, El Niño event**

| Year | MONTH | ISLAND WIDTH | | | |
|-------------|--------------|---------------------|------------|------------|--------|
| | | 200 | 400 | 600 | |
| 1 | El Niño | JAN | 1.0529 | 1.109 | 0.8361 |
| | El Niño | FEB | 0.8252 | 0.8777 | 0.8252 |
| | El Niño | MAR | 0.7719 | 0.8103 | 0.7868 |
| | El Niño | APR | 0.7049 | 0.7661 | 0.8753 |
| | El Niño | MAY | 0.8799 | 0.8833 | 0.891 |
| | El Niño | JUN | 0.8781 | 0.9399 | 0.9011 |
| | El Niño | JUL | 0.8368 | 1.018 | 0.9151 |
| | El Niño | AUG | 0.8927 | 1.0689 | 0.9319 |
| | El Niño | SEP | 0.9592 | 1.1094 | 0.9353 |
| | El Niño | OCT | 0.9772 | 1.1242 | 0.9305 |
| | El Niño | NOV | 0.9139 | 1.0837 | 0.9302 |
| | El Niño | DEC | 0.8634 | 1.1017 | 0.9271 |
| 2 | Post-El Niño | JAN | 0.7354 | 1.0681 | 0.9245 |
| | Post-El Niño | FEB | 0.5759 | 1.0795 | 0.8627 |
| | Post-El Niño | MAR | 0.3131 | 0.8979 | 0.7092 |
| | Post-El Niño | APR | 0.0701 | 0.6395 | 0.5818 |
| | Post-El Niño | MAY | 0 | 0.4637 | 0.5999 |
| | Post-El Niño | JUN | 0.1189 | 0.4919 | 0.6347 |
| | Post-El Niño | JUL | 0.2747 | 0.5313 | 0.6254 |
| | Post-El Niño | AUG | 0.2295 | 0.5001 | 0.6578 |
| | Post-El Niño | SEP | 0.3165 | 0.5426 | 0.66 |
| | Post-El Niño | OCT | 0.3175 | 0.529 | 0.6818 |
| | Post-El Niño | NOV | 0.3822 | 0.5454 | 0.7191 |
| | Post-El Niño | DEC | 0.4863 | 0.5904 | 0.7847 |
| 3 | Recovery | JAN | 0.6239 | 0.6572 | 0.8241 |
| | Recovery | FEB | 0.6798 | 0.6998 | 0.877 |
| | Recovery | MAR | 0.8004 | 0.7846 | 0.8881 |
| | Recovery | APR | 0.9095 | 0.8202 | 0.9233 |
| | Recovery | MAY | 1.0107 | 0.8979 | 0.9159 |
| | Recovery | JUN | 0.9534 | 0.9168 | 0.9123 |
| | Recovery | JUL | 0.9428 | 0.9816 | 0.9164 |
| | Recovery | AUG | 0.9326 | 1.0397 | 0.9031 |
| | Recovery | SEP | 0.8143 | 1.0067 | 0.9066 |
| | Recovery | OCT | 0.8024 | 0.9819 | 0.8591 |
| | Recovery | NOV | 0.6834 | 0.865 | 0.818 |
| | Recovery | DEC | 0.6427 | 0.7879 | 0.8749 |

WWE**West Caroline region, Windward island, El Niño event**

| Year | MONTH | ISLAND WIDTH | | | |
|------|--------------|--------------|--------|--------|--------|
| | | 200 | 400 | 600 | |
| 1 | El Niño | JAN | 0.3454 | 0.9215 | 0.802 |
| | El Niño | FEB | 0 | 0.7508 | 0.6522 |
| | El Niño | MAR | 0 | 0.6126 | 0.5004 |
| | El Niño | APR | 0 | 0.3187 | 0.3177 |
| | El Niño | MAY | 0 | 0.0168 | 0.1348 |
| | El Niño | JUN | 0 | 0 | 0.2299 |
| | El Niño | JUL | 0 | 0 | 0.374 |
| | El Niño | AUG | 0 | 0.2177 | 0.4149 |
| | El Niño | SEP | 0 | 0.315 | 0.4786 |
| | El Niño | OCT | 0 | 0.4297 | 0.4876 |
| | El Niño | NOV | 0 | 0.398 | 0.4012 |
| | El Niño | DEC | 0 | 0.2598 | 0.3147 |
| 2 | Post-El Niño | JAN | 0 | 0.1222 | 0.2934 |
| | Post-El Niño | FEB | 0 | 0 | 0.148 |
| | Post-El Niño | MAR | 0 | 0 | 0 |
| | Post-El Niño | APR | 0 | 0 | 0 |
| | Post-El Niño | MAY | 0 | 0 | 0 |
| | Post-El Niño | JUN | 0 | 0 | 0 |
| | Post-El Niño | JUL | 0 | 0 | 0.0493 |
| | Post-El Niño | AUG | 0 | 0 | 0.0716 |
| | Post-El Niño | SEP | 0 | 0 | 0.1492 |
| | Post-El Niño | OCT | 0 | 0.1009 | 0.2879 |
| | Post-El Niño | NOV | 0 | 0.3168 | 0.2681 |
| | Post-El Niño | DEC | 0 | 0.2616 | 0.278 |
| 3 | Recovery | JAN | 0 | 0.2522 | 0.2646 |
| | Recovery | FEB | 0 | 0.1871 | 0.1765 |
| | Recovery | MAR | 0 | 0.072 | 0.1583 |
| | Recovery | APR | 0 | 0.0336 | 0.2722 |
| | Recovery | MAY | 0 | 0.2027 | 0.3281 |
| | Recovery | JUN | 0 | 0.2689 | 0.3924 |
| | Recovery | JUL | 0 | 0.3966 | 0.4604 |
| | Recovery | AUG | 0.278 | 0.4959 | 0.5733 |
| | Recovery | SEP | 0.1903 | 0.6816 | 0.5686 |
| | Recovery | OCT | 0 | 0.6378 | 0.4405 |
| | Recovery | NOV | 0 | 0.384 | 0.4618 |
| | Recovery | DEC | 0 | 0.3419 | 0.4755 |

*EWE***Eastern Caroline region, Windward island, El Niño event**

| Year | MONTH | ISLAND WIDTH | | | |
|-------------|--------------|---------------------|------------|------------|-------|
| | | 200 | 400 | 600 | |
| 1 | El Niño | JAN | 0.700 | 1.167 | 1.191 |
| | El Niño | FEB | 0.075 | 0.796 | 0.943 |
| | El Niño | MAR | 0.162 | 0.724 | 0.851 |
| | El Niño | APR | 0.000 | 0.590 | 0.745 |
| | El Niño | MAY | 0.319 | 0.806 | 0.922 |
| | El Niño | JUN | 0.266 | 0.776 | 0.937 |
| | El Niño | JUL | 0.089 | 0.685 | 0.908 |
| | El Niño | AUG | 0.000 | 0.705 | 0.963 |
| | El Niño | SEP | 0.210 | 0.816 | 1.013 |
| | El Niño | OCT | 0.177 | 0.817 | 1.008 |
| | El Niño | NOV | 0.211 | 0.748 | 0.961 |
| | El Niño | DEC | 0.000 | 0.609 | 0.923 |
| 2 | Post-El Niño | JAN | 0.000 | 0.420 | 0.802 |
| | Post-El Niño | FEB | 0.000 | 0.208 | 0.679 |
| | Post-El Niño | MAR | 0.000 | 0.000 | 0.442 |
| | Post-El Niño | APR | 0.000 | 0.000 | 0.250 |
| | Post-El Niño | MAY | 0.000 | 0.000 | 0.149 |
| | Post-El Niño | JUN | 0.000 | 0.000 | 0.223 |
| | Post-El Niño | JUL | 0.000 | 0.122 | 0.314 |
| | Post-El Niño | AUG | 0.000 | 0.094 | 0.284 |
| | Post-El Niño | SEP | 0.000 | 0.169 | 0.363 |
| | Post-El Niño | OCT | 0.000 | 0.156 | 0.359 |
| | Post-El Niño | NOV | 0.000 | 0.229 | 0.412 |
| | Post-El Niño | DEC | 0.064 | 0.359 | 0.511 |
| 3 | Recovery | JAN | 0.286 | 0.556 | 0.649 |
| | Recovery | FEB | 0.142 | 0.624 | 0.718 |
| | Recovery | MAR | 0.380 | 0.753 | 0.830 |
| | Recovery | APR | 0.799 | 0.955 | 0.951 |
| | Recovery | MAY | 0.782 | 1.030 | 1.000 |
| | Recovery | JUN | 0.289 | 0.875 | 0.957 |
| | Recovery | JUL | 0.377 | 0.873 | 0.957 |
| | Recovery | AUG | 0.144 | 0.830 | 0.956 |
| | Recovery | SEP | 0.031 | 0.701 | 0.852 |
| | Recovery | OCT | 0.062 | 0.708 | 0.847 |
| | Recovery | NOV | 0.000 | 0.611 | 0.739 |
| | Recovery | DEC | 0.000 | 0.551 | 0.690 |

